Critical Design Report
24 Hours of Lemons – Pulp Friction Crew

COLORADO SCHOOL OF MINES

Client: Brad Stolz – Stolz Engineering

Project Advisor: Scott Cochran

Date: 2/3/2026

Andrew Nester | Ben Holowaty | Nolan Kelley | Sappho Buller | Jackson McCool

Bennett Subach | Dakota Johnson | Dalton Webb | Daniel Sandoval-Rosales

Jacob Rueter | Liam Yaconiello | Nicolas Alonso | Sterling Schrader

Executive Summary

The Colorado School of Mines 24 Hours of Lemons team (“The Pulp Friction Crew”) is developing a build-ready, rule-compliant Mazda Miata endurance race car for competition in Summer 2026 at High Plains Raceway. This Critical Design (CD) Report communicates the team’s finalized design direction across the Powertrain, Structures, Electronics, and Aerodynamics subsystems, documents how Preliminary Design Review (PDR) feedback was incorporated, and defines the remaining path to fabrication, integration, and verification.

The design strategy is driven by the primary reliability failures observed in the previous campaign: differential housing cracking, chronic overheating, wiring harness degradation, and roll-cage construction deficiencies. Powertrain work focuses on endurance reliability for the Ford 302 V8 through a cooling package sized for sustained load, improved radiator ducting and shrouding, and an intake/exhaust architecture selected using quantitative trade studies. Structures work centers on a Lemons-compliant roll cage developed from 3D scan data to improve fitment and inspection readiness, along with a reinforced differential housing strategy that preserves existing geometry while improving fatigue resistance. Electronics work establishes a robust baseline harness and verified sensor suite, then plans staged integration of a sponsored OneGauge display system to support real-time driver awareness and pit decision-making. Aerodynamics work integrates radiator ducting, splitter/diffuser geometry, and stability-focused elements validated through CFD and structural feasibility checks.

To complete the CD phase and enable Spring 2026 fabrication, the remaining deliverables are: (1) a signed analysis package covering critical load paths and thermal limits, (2) a verification and validation plan with explicit pass/fail criteria tied to subsystem requirements, and (3) a preliminary drawing set sufficient to fabricate, install, and inspect each subsystem. In addition to this report, the team will provide supplemental submissions consisting of a FMEA-based risk assessment, an updated project budget tracker, and an updated Gantt chart reflecting the critical path and build/test schedule. Collectively, these outputs support an aggressive but realistic integration timeline and early track validation plan ahead of the Summer 2026 event.

Table of Contents

Design Narrative

This section provides a brief introduction to the proposed solution and the logic used to justify major design selections. It is intended to help the client and advisors navigate the report by explaining why included requirements, schedules, and drawings are relevant to achieving a safe, reliable, and competitive endurance race entry.

Background and Problem Statement

Following the prior campaign, the vehicle exhibited multiple critical failure modes, including differential housing cracking, cooling system underperformance, degraded wiring harness reliability, and roll-cage inspection nonconformances. The project objective is to deliver a build-ready design package that eliminates these deficiencies while improving endurance performance within the 24 Hours of Lemons ruleset and Senior Design constraints.

Design Approach and Justification Method

The team applied a structured, subsystem-based design process: (1) define requirements and verification methods, (2) generate and screen concepts using decision matrices, (3) develop integration-aware CAD, and (4) validate critical performance claims using appropriate analysis and test plans. PDR feedback was incorporated through added quantitative success criteria, improved decision matrix structure, explicit cooling-aero integration planning, strengthened compliance and inspection readiness for the roll cage, more realistic differential loading and weld/geometry documentation, and a harness-first reliability baseline prior to upgrades.

Design Requirements Tables

Tables 1-5 summarize the system-level and subsystem-level design requirements and verification methods carried forward from the PDR. These requirements will be used as the basis for verification and validation activities in Spring 2026.

System-level requirements (Table 1)

ID	Requirement	Verification Method
G-1	Vehicle systems should be capable of surviving subsystem-specific race loadings for 24 hours.	FEA / benchtop testing
G-2	All designs shall meet all specifications set out by Lemon's rulebook.	Dimensional check and mock inspection
G-3	Subsystem CAD models and analyses shall be completed	Client sign-off

	and approved by the client prior to fabrication/purchase.	
G-4	All modifications shall remain within project budget.	Final budget audit

Powertrain requirements (Table 2)

ID	Requirement	Verification Method
P-1	Engine compression shall meet OEM tolerance range (~10% variation).	Leak-down and compression testing
P-2	Cooling system shall maintain fluid temperatures below 225°F ± 10°F.	Coolant temperature sensor
P-3	Intake/exhaust redesign shall increase engine horsepower by 10%.	Flow simulation and bench airflow test, dynamometer
P-4	Subsystem design documentation finalized for client approval.	Client sign-off

Structures requirements (Table 3)

ID	Requirement	Verification Method
S-1	Factor of Safety: Differential ≥ 2.5	FEA
S-2	Fatigue analysis shows differential capable of surviving 24 hr. race	Mathematical estimation
S-3	Factor of Safety: Roll cage ≥ 3.0	FEA
S-4	Roll cage shall conform to SCCA/Lemons specification (1.5 in DOM; 0.095 in wall or better).	Dimensional check and mock inspection. Purchased 1.5 in x 0.120 in wall tubing

Electronics requirements (Table 4)

ID	Requirement	Verification Method
E-1	Wiring harness shall be fully labeled, characterized, and tested.	Physical documentation and test results
E-2	ECU upgrade viability shall be assessed and decided upon.	Design and risk mitigation documentation
E-3	Alternate accessory switching method will be determined and testing plan created	Documentation and supporting information

Aerodynamics requirements (Table 5)

ID	Requirement	Verification Method
A-1	Front splitter, rear diffusers, and rear wing shall induce capable of achieving a 50/50 front to rear percentage at or above 60 mph while not increasing drag by more than 250 N at or below 100 mph.	CFD aerodynamic validation
A-2	Aero package must prove to require 50% less energy compared to adding mass to the rear for equivalent downforce effects on rear axle.	CFD and relevant road load and energy calculations
A-3	All aerodynamic mounts shall be designed with FoS ≥ 2 based on estimated loading conditions.	FEA structural analysis and static bench test
A-4	All aerodynamic components shall comply with Lemons visibility, clearance, and safety regulations.	Dimensional inspection and rule check
A-5	Final aerodynamic design package shall be approved prior to fabrication.	Client sign-off

Proposed Solution Summary by Subsystem

Powertrain

The Powertrain design prioritizes reliable thermal management and simplified, manufacturable airflow and exhaust routing. Trade studies completed in the PDR selected short-tube exhaust headers and a headlight-based intake concept to improve flow without introducing excessive fabrication complexity. The cooling strategy centers on a radiator sized for the V8 application and a sealed duct/shroud strategy integrated with the front aero package; belt drive improvements (tensioner/idler) are included to eliminate water-pump slip. Final component selection and packaging will be validated against the coolant temperature requirement (P-2) using the analysis and test plan placeholders in later sections.

Structures

Structures work addresses safety and driveline durability. The roll cage is a ground-up design built from 3D scans of the vehicle tub to ensure fitment, ergonomics, and inspection readiness. For the drivetrain, the baseline is a donated, reinforced Miata 7-inch A356-T6 differential, using welded 1/8-in plates on the arms to remove the known weak point while preserving OEM geometry. FEA loads are derived from driveline torque (engine torque scaled by representative gearing), converted to ring-and-pinion bearing forces, and checked under both nominal and conservative amplified cases to bound clutch shock and wheel hop. A worst-case fatigue check then includes torque reversal during braking with a modified Goodman correction and conservative A356-T6 S–N input, translating predicted life into a lap-count at High Plains Raceway to confirm durability requirements are met.

Electronics

Electronics work follows a harness-first reliability approach: document and remediate failure modes, verify baseline sensor operation, and only then integrate upgrades. The sponsored OneGauge system is the baseline display and sensor hub, enabling direct sensor inputs without requiring full system Electronic Control Unit (ECU)/CAN modernization. ECU upgrade feasibility remains a controlled decision dependent on harness stability, integration effort, and verified benefit to endurance reliability.

Aerodynamics

Aerodynamics work integrates cooling and stability objectives by combining radiator ducting with front and rear aero devices (splitter, diffuser, and rear wing/spoiler). Designs will be validated with CFD and supported by structural checks of mounts to meet aero performance and safety requirements (A-1 through A-5).

Engineering Calculations & Analysis

Aerodynamics

Computational Fluid Dynamics

To achieve a front to rear percentage of 50/50 downforce must be applied to the rear axle as the balance was shifted due to the addition of the upgraded powertrain assembly. Calculations were performed to estimate the required downforce applied near the rear bumper to achieve the desired balance. It was estimated that 330 Newtons of downforce would be required, Appendix D. Restoring the front to rear percentage to 50/50 will improve vehicle handling and help balance brake and tire wear over the course of an endurance race.

An alternative option to an aerodynamic package is adding mass to the rear of the vehicle, likely in the trunk. An estimated 75.9 lb. would need to be added. This addition would require an additional 9588 ft*lbf of energy to accelerate from 0-60 mph while the estimated drag created from the aerodynamic package traveling at 60 mph for an equivalent time only requires an additional 3985 ft*lbf of energy, satisfying requirement A-2. Since the car is expected to perform repeated heavy braking and acceleration zones during the planned race the additional mass solution is not recommended, Appendix D.

Redistribution of mass throughout the vehicle was considered but deemed not to be feasible as very few components could feasibly be rearranged and those that could, such as parts of the fire suppression assembly, do not have the needed mass to provide any meaningful balance improvements.

Initial calculations were done to estimate downforce potential from only the rear wing assembly; the wing was assumed to act as a flat plate at an angle of attack of 10° for peak performance prior to the stall condition. At 60 mph the wing would be capable of producing 173.96 N of downforce, full calculations in Appendix D. From these initial calculations, it has been shown that a wing alone will meet requirements and budget constraints, so a CFD analysis was performed using SolidWorks Flow Simulation to obtain drag and downforce data for a variety of aero package layouts. The full aero model can be seen in Figure 1.

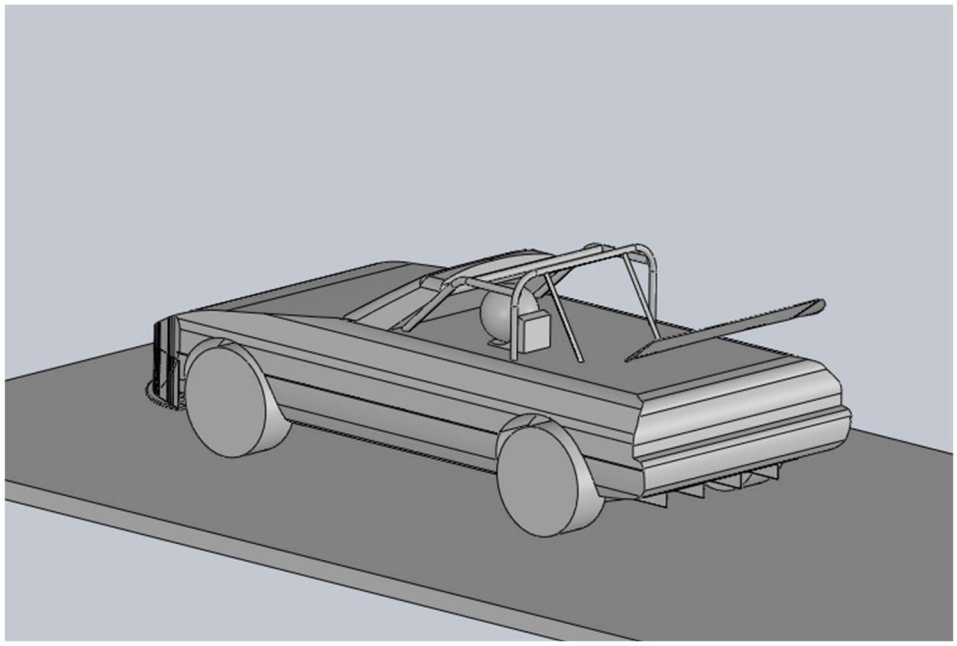

Figure 1 - Full Aero Model for CFD

Analysis was performed on a stock model, the model with a wing, splitter, and diffuser, a model with only a wing, a model with only the splitter and diffuser, and lastly a model with the wing, splitter, diffuser, and a roof. Both the movement of the ground and wheels have been simulated to improve accuracy of airflow under the vehicle. This analysis is not free of error, the roll cage used is not current, the vehicle shape is simplified, mounting assemblies for components are not included, and components like side mirrors are not present. Despite this, the drag data on the stock model matches the reported drag coefficient from the manufacturer, improving confidence in the simulation.

Analysis was done for speeds between 10 and 120 mph yielding the following drag and downforce plots, Figures 2 & 3. Full data in Appendix D.

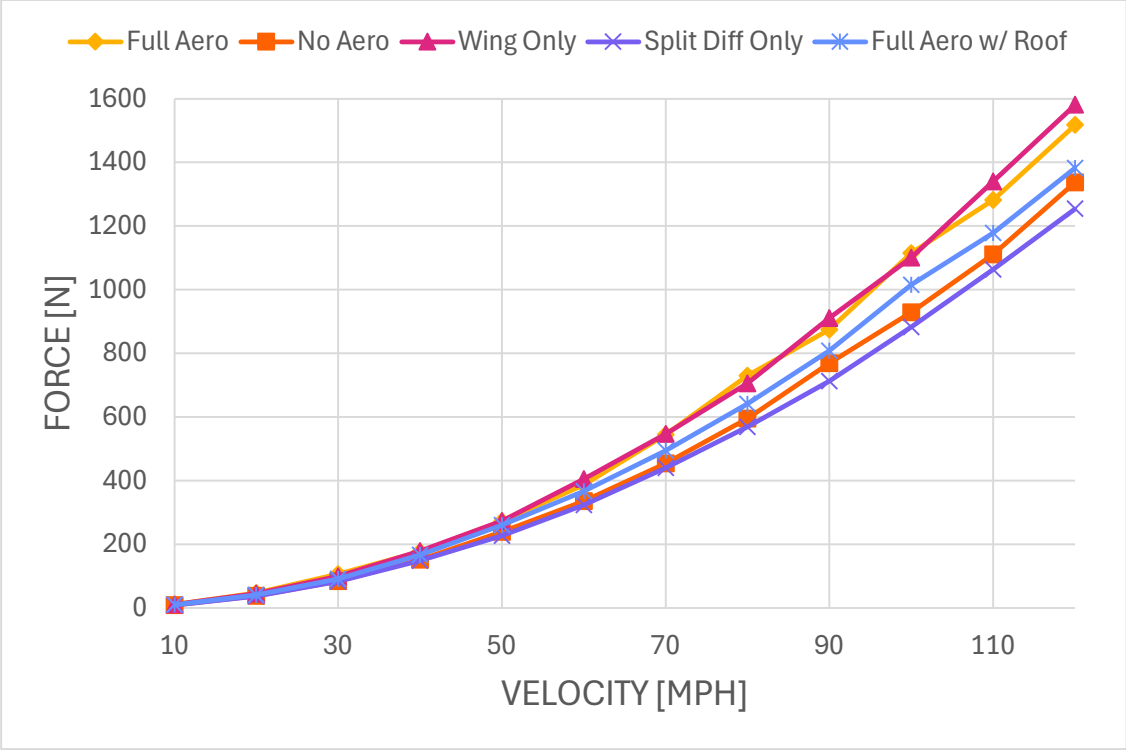

Figure 2 - CFD Drag Analysis

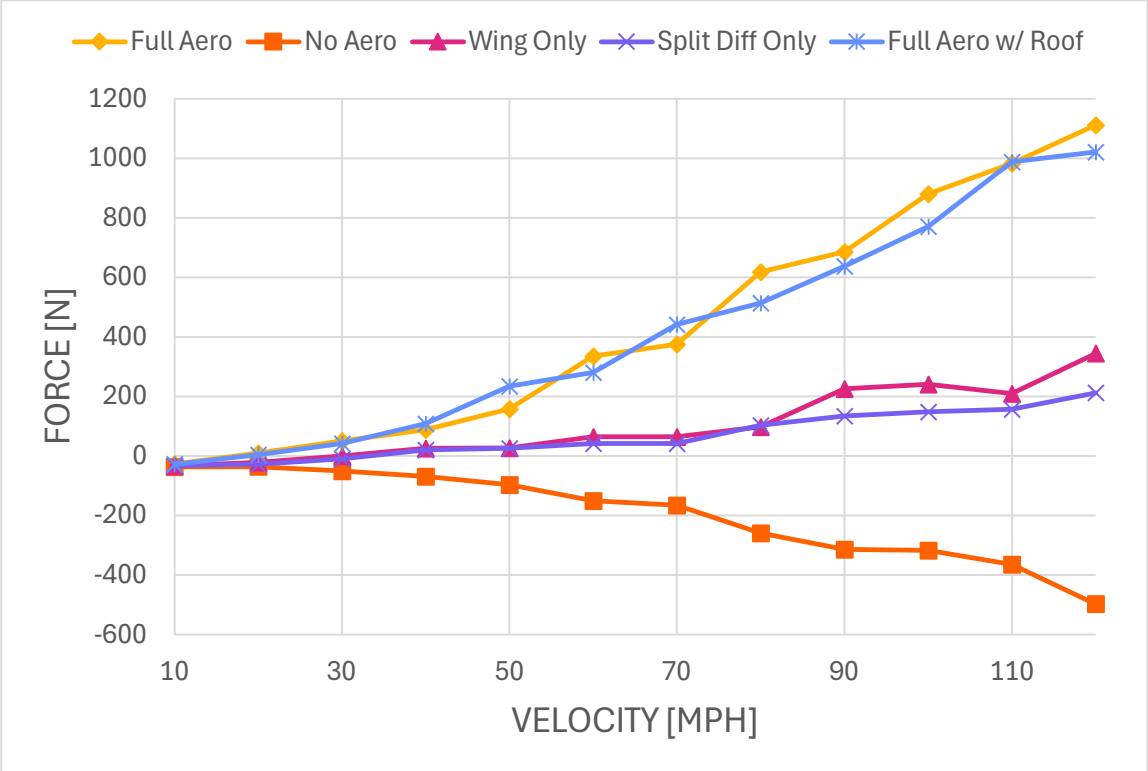

Figure 3 - CFD Downforce Analysis

At 60 mph both the full aero package with and without the roof show similar downforce data where the full aero package without the roof produces 335.9 Newtons of downforce, reaching the initial requirement. The full aero package without the roof produces 180.6 more newtons of drag at 120 mph, fully meeting requirement A-1. Figure 4 shows flow trajectories of the full aero configuration at 60 mph. Figures 4, 5, 6 and 7 show the pressure and velocity cut plots for the full aero and no aero configurations at 60 mph. Note the low-pressure zones that from when the splitter and diffuser are added along with the difference in the velocity under the vehicle. These effects demonstrate how the additional components are increasing downforce and reducing the drag effects under the vehicle. There are also notable low- and high-pressure zones on the wing along with drag effects. Cut plots of other configurations are located in Appendix D.

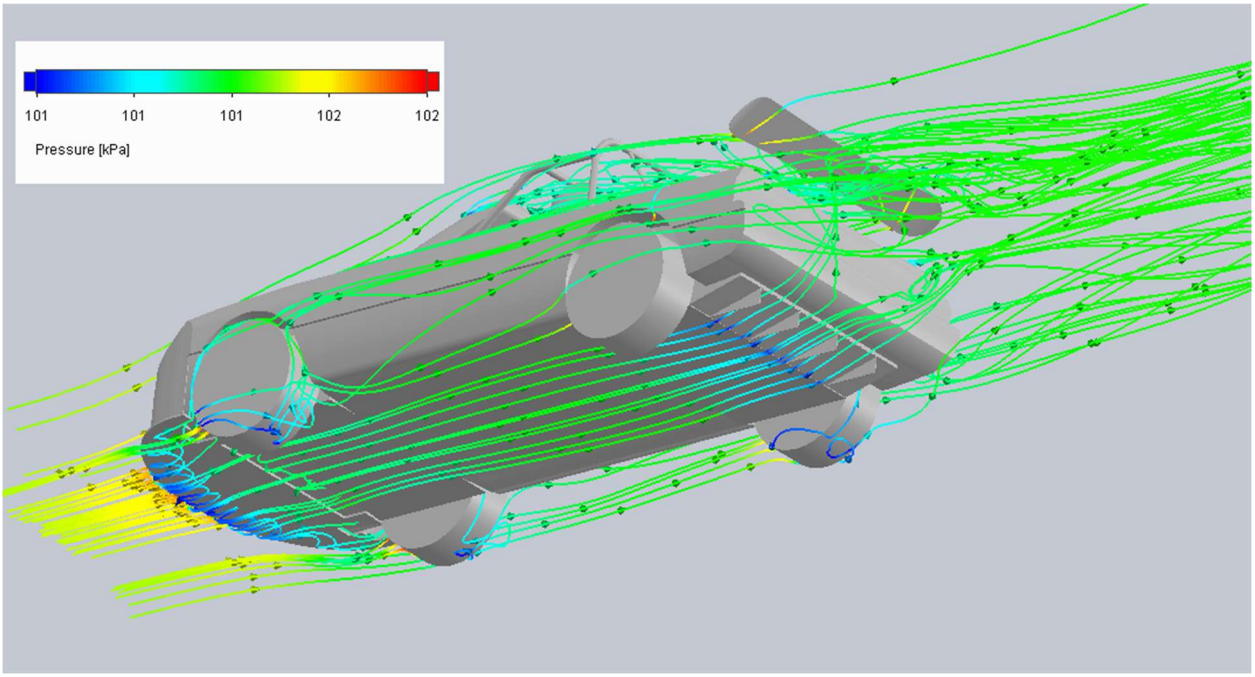

Figure 4 - Full aero flow trajectories-pressure plot-full aero

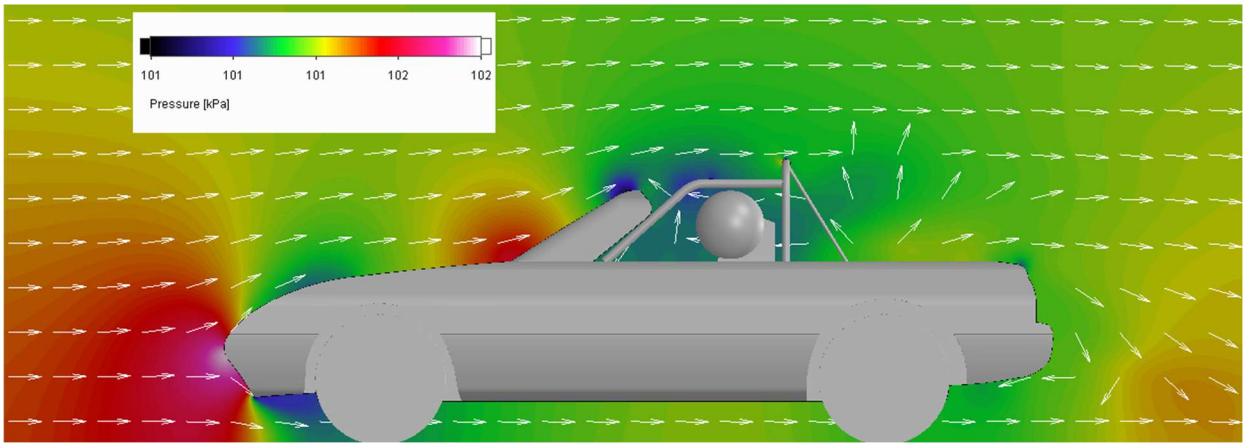

Figure 5 - Stock configuration pressure plot - 60 mph

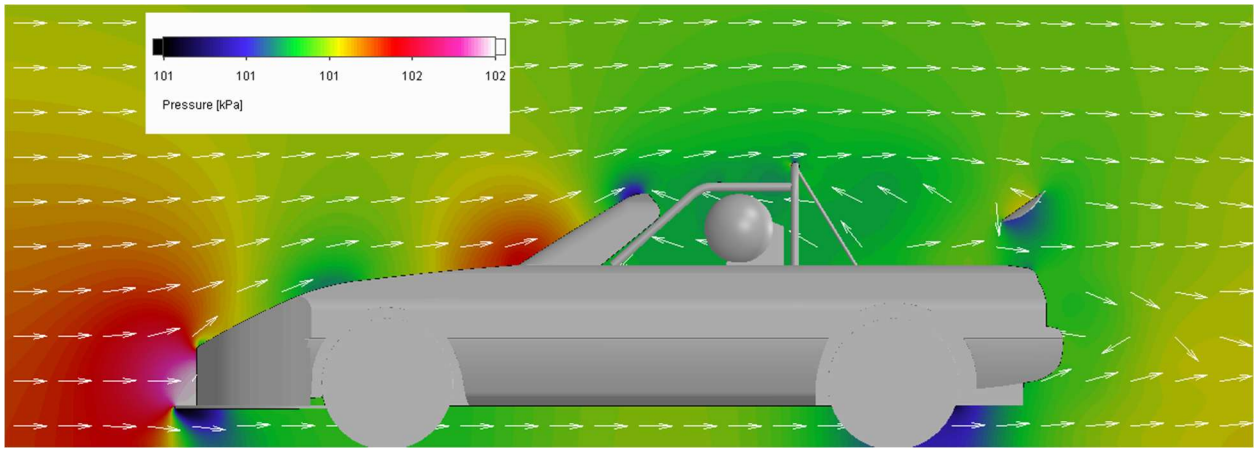

Figure 6 - Full aero configuration pressure plot - 60 mph

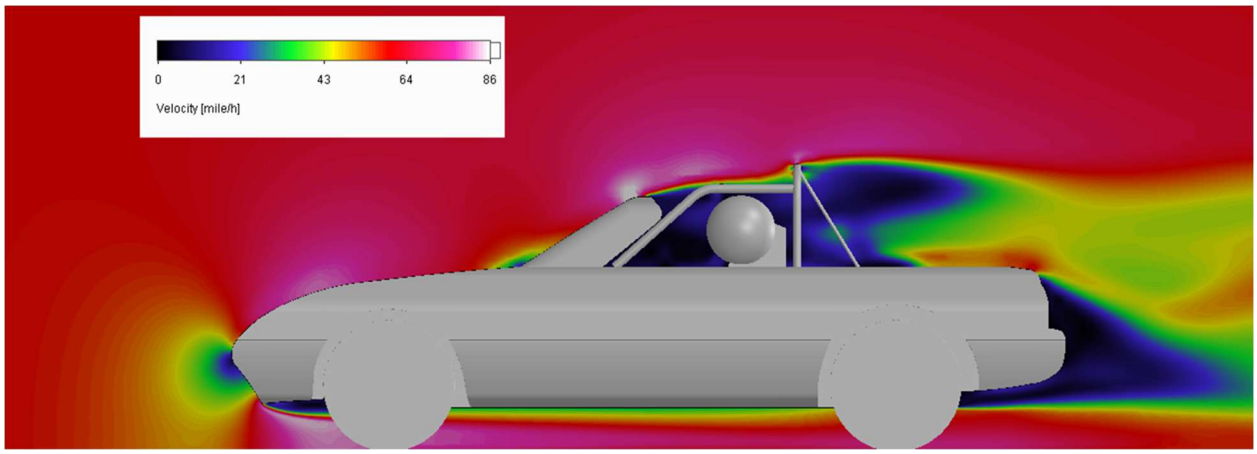

Figure 7 - Stock configuration velocity plot - 60 mph

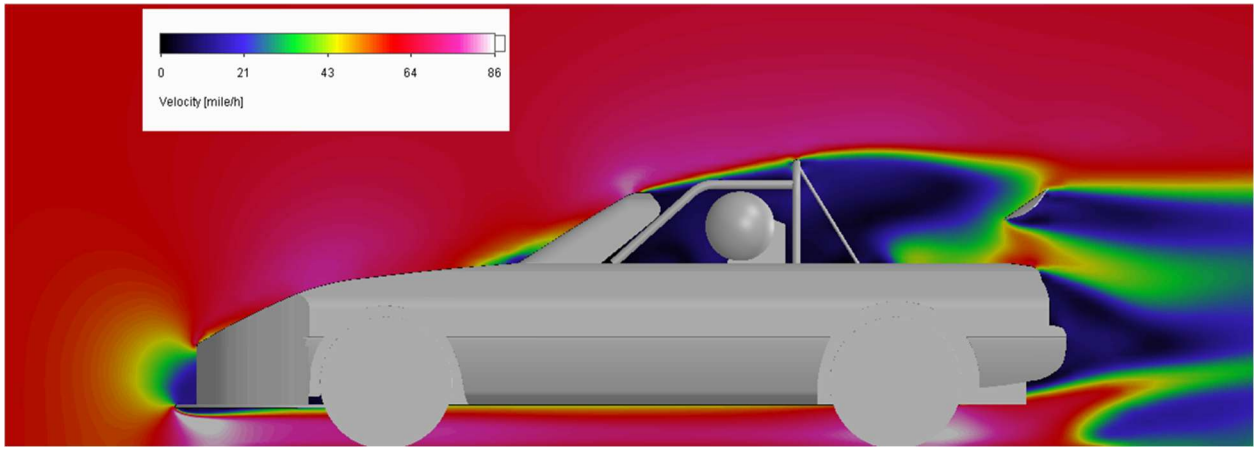

Figure 8 – Full aero configuration velocity plot - 60 mph

Despite the drag improvements shown by the CFD analysis subsystem budget does not allow for design or purchase of a roof assembly. As no structural components will be built outside the

vehicle frame that could act as crash bars and the tow straps will not be obscured, the full package will follow the Lemons rules, satisfying requirement A-4.

Air Dam

The air dam will act to minimize airflow through the engine bay while also optimizing the splitter, ensuring that there is a lower pressure zone beneath the splitter. The air dam itself will be made of a 1/8-inch-thick HDPE plastic sheet. Using HDPE plastic will allow for the air dam to be stiff enough to hold its shape under high speeds while also being flexible enough to bend to the contour of the front of the vehicle. The HDPE plastic will be riveted onto the bumper of the car as well as the side panels using 3/16 in. X 1 in. rivets. The basic dimensioned air dam is in the Figure 9 below.

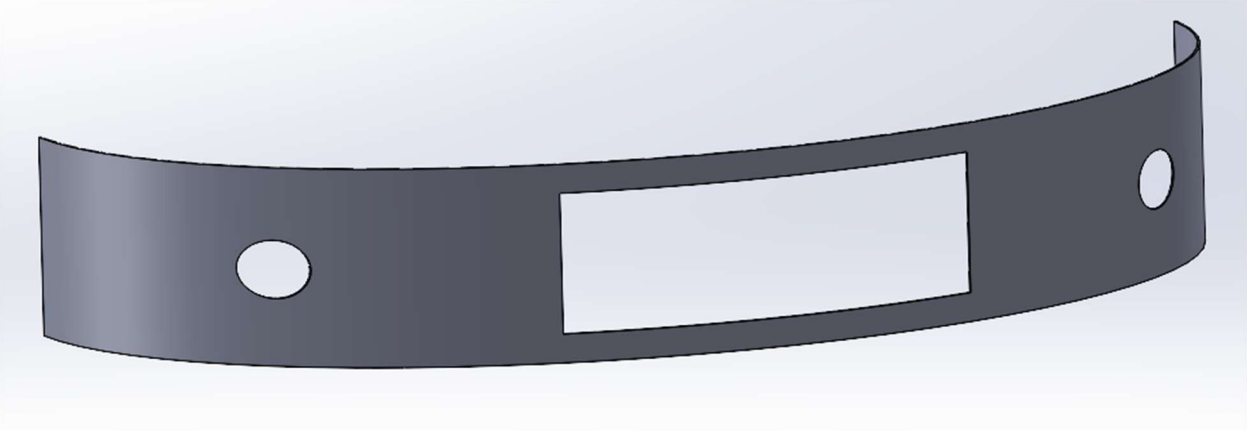

Figure 9 - Air Dam Model

Additionally, there is a rectangular cutout in the middle of the air dam; this will ensure that the radiator gets proper airflow through it. On either side of the rectangular cutout are two circular cutouts. These will be used to provide brake duct cooling.

Wing Mounting

A snowboard was chosen for the wing assembly to fit budget requirements, so a mounting assembly was designed to be plasma cut from 10-gauge steel sheet metal. Figures 10 & 11 show the full assembly.

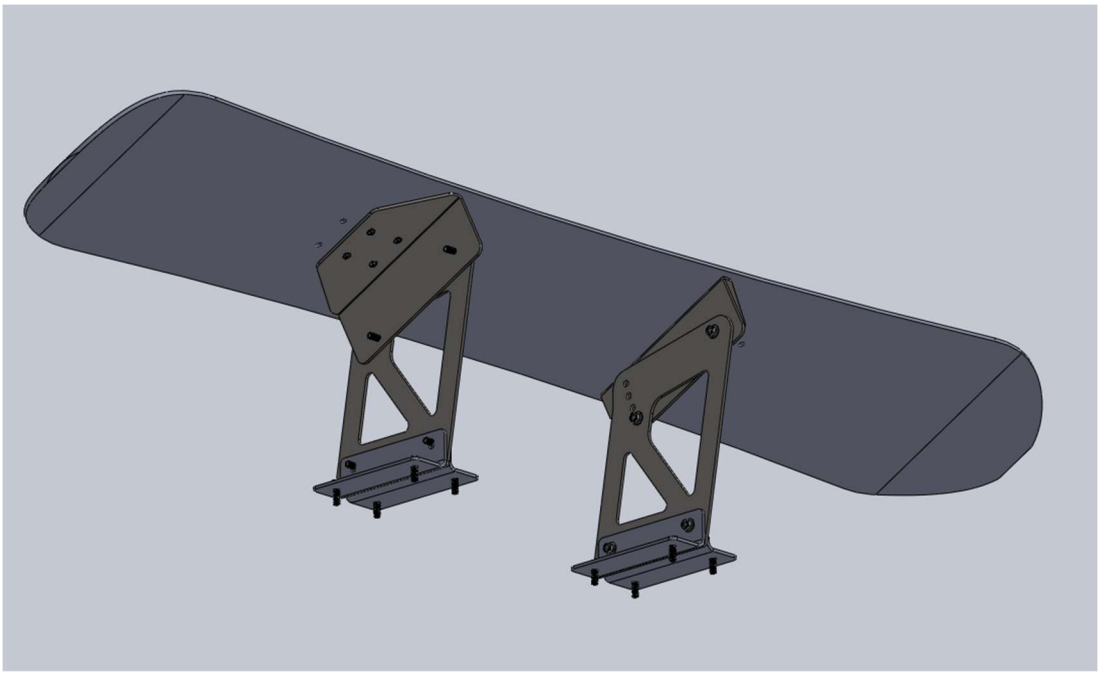

Figure 10 - Full Wing Assembly

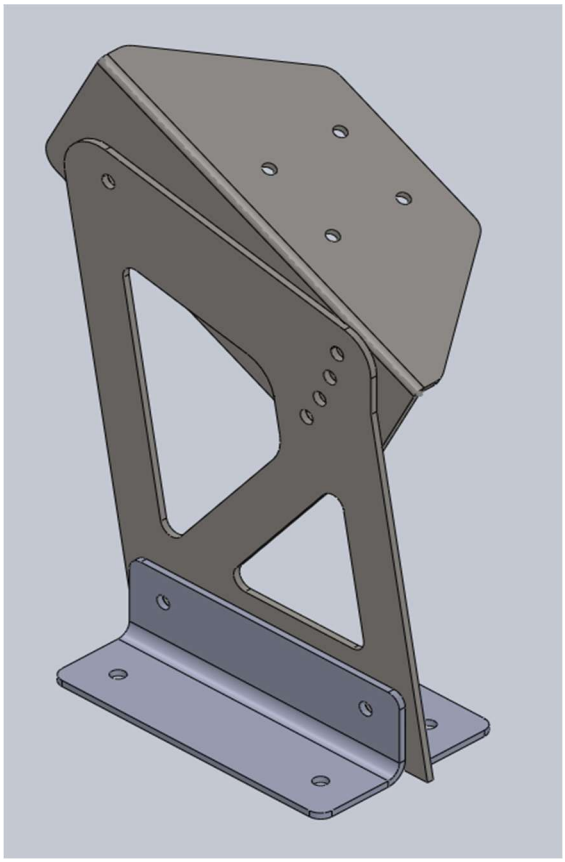

Figure 11 - Single Support of Wing Assembly

FEA was performed on the full wing assembly, the support assembly, and the vertical support structure alone. The full assembly used fixed hinges on the holes bolted to the trunk, roller sliders on the lower faces of the trunk brackets, and pin connectors on other holes. Full FEA system configuration figures can be found in Appendix D.

Based on estimations from the flat plate lift analysis, 700 Newtons of force was applied to the top of the wing and 350 Newtons on the single support assembly. Material properties can be seen in Table 6.

Table 6 - Material Properties

AISI 1020 Steel		
Elastic Modulus	200	GPa
Poisson's Ratio	0.29	N/A
Tensile Strength	420.5	MPa
Yield Strength	351.6	MPa

The results of the study indicated that the assembly experience maximum stress at the fillet at the lower front cutout with a factor of safety of 2.03 using the von Mises criterion, Figure 12. Bearing stress was analyzed in the holes, which yielded a factor of safety of 74, as seen in Appendix D.

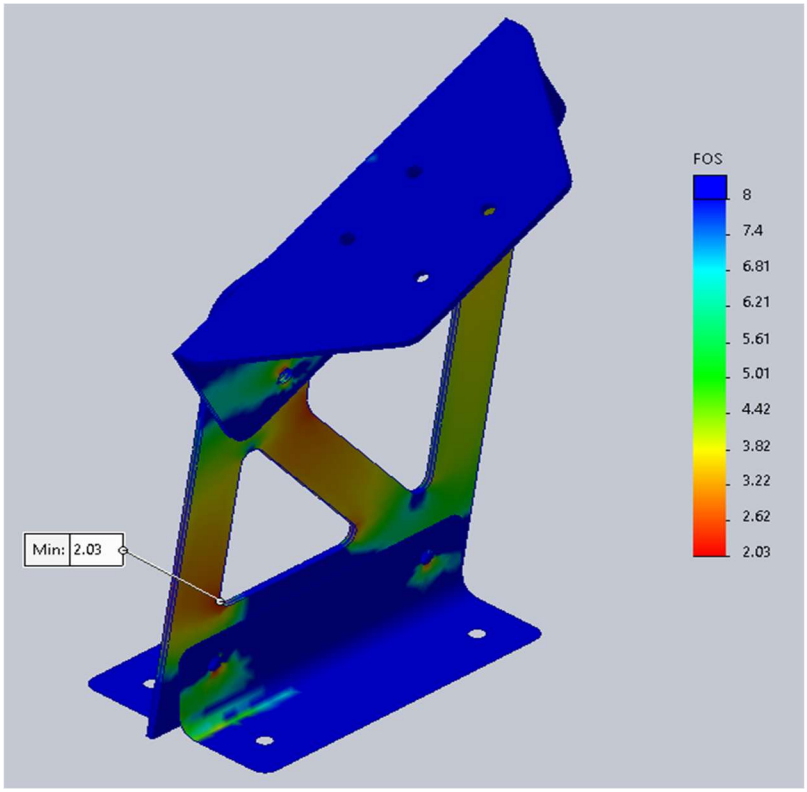

Figure 12 - FOS plot of single support assembly

To ensure the assembly was not at risk of excessive deformation, a study was run on the same assembly shown in figure 6 where 150 N was applied to the side of the upper mount. The full deformation can be seen in Figure 13.

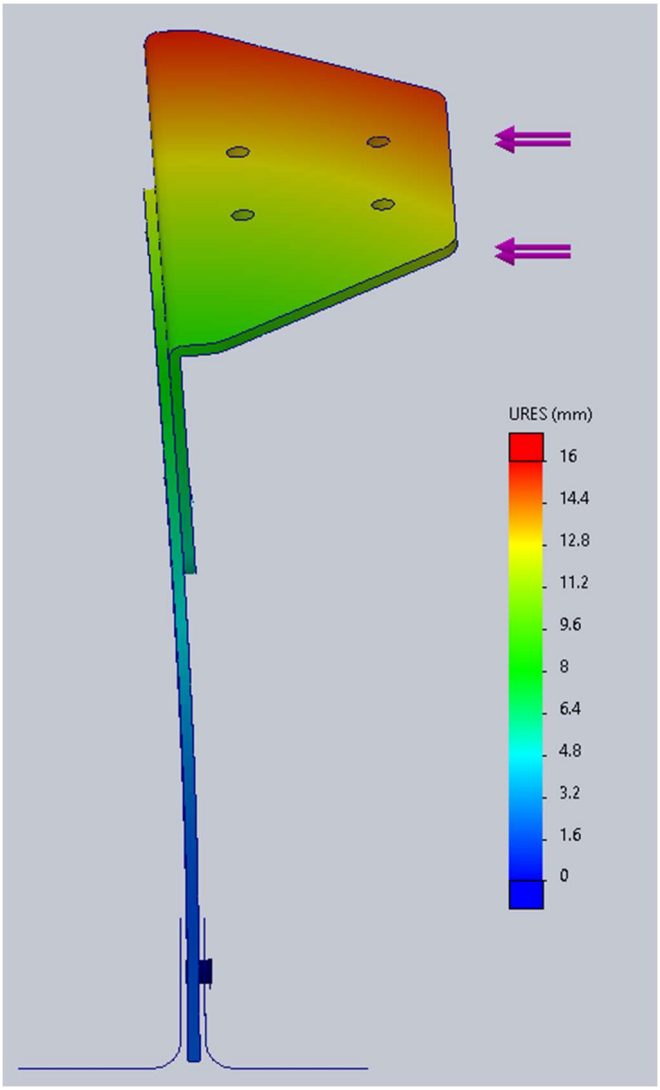

Figure 13 - Deformation of wing mount assembly, visual scale 1

Full results figures including von Mises stress, factory of safety, and deformation plots of all simulations can be found in Appendix D. These results satisfy requirement A-3.

Splitter Mounting

A FEA simulation was run for the mounting of the splitter. This FEA allowed the team to see whether mounting points and components such as brackets and turnbuckles will be able to withstand the anticipated load on the splitter. The FEA simulation was run with a downward load of 200 lbf. The 200 lbf is the anticipated maximum load the splitter will see [1]. SolidWorks Simulation bolts were used to connect each of the mounting components together and each point connecting directly to the car used fixtures to simulate the rigidity of the car. Additionally, the

material for the bolts was carbon steel with a yield strength of 60,000 psi. The brackets and turnbuckles were added modelled using galvanized steel with a yield strength of 75,000. Finally, the splitter was modelled using a custom material to resemble ½ inch birch plywood. This custom material had a yield strength of 6,500 psi. This is shown in Figure 14.

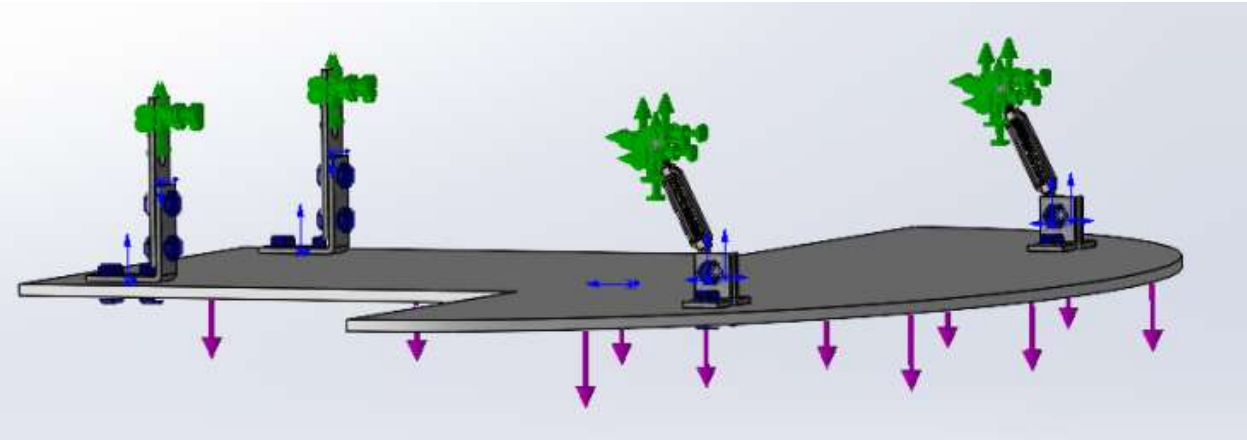

Figure 14 - Full Splitter Configuration

There are two points of interest when running the simulation where the factor of safety is lower than other places, showing where the mounting is most likely to fail. These two points are on the rear L-shaped brackets and the eye of the turnbuckles. The minimum factor of safety on the turnbuckle was found to be 2.53, and the minimum on the L-bracket was 2. These values meet the teams' mounting requirements, specifying that a minimum factor of safety to 2 to be maintained. Figures 15-18 depict this.

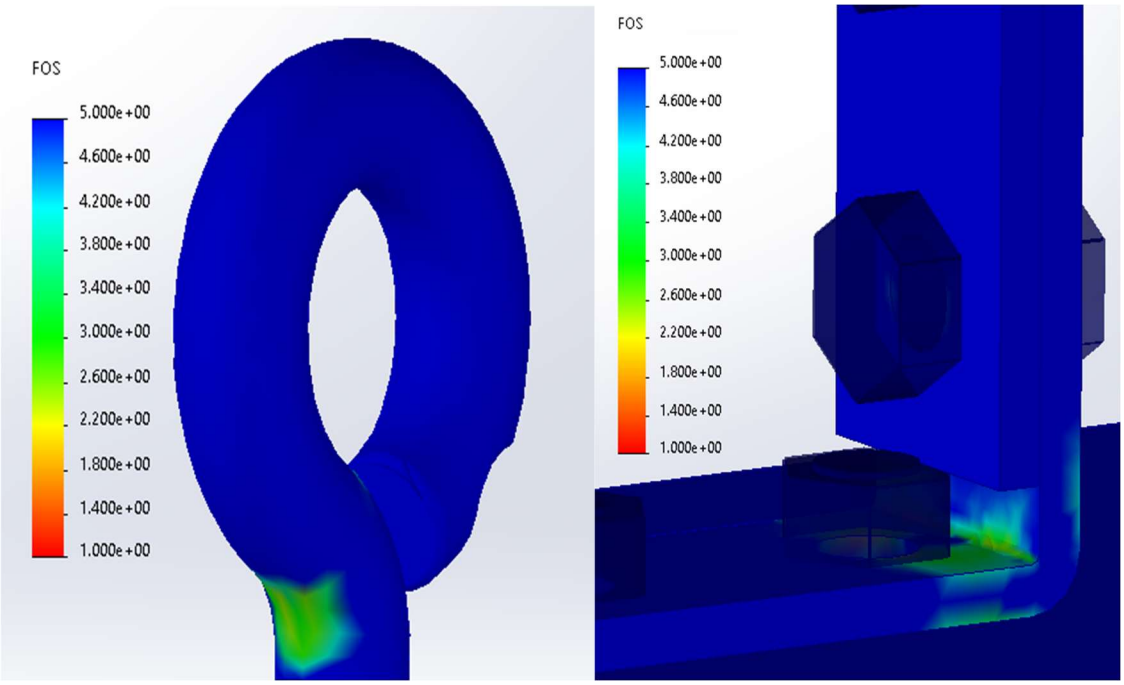

Figure 15 and 16 - Simulated FOS of turnbuckle eye (left) and L-bracket (right)

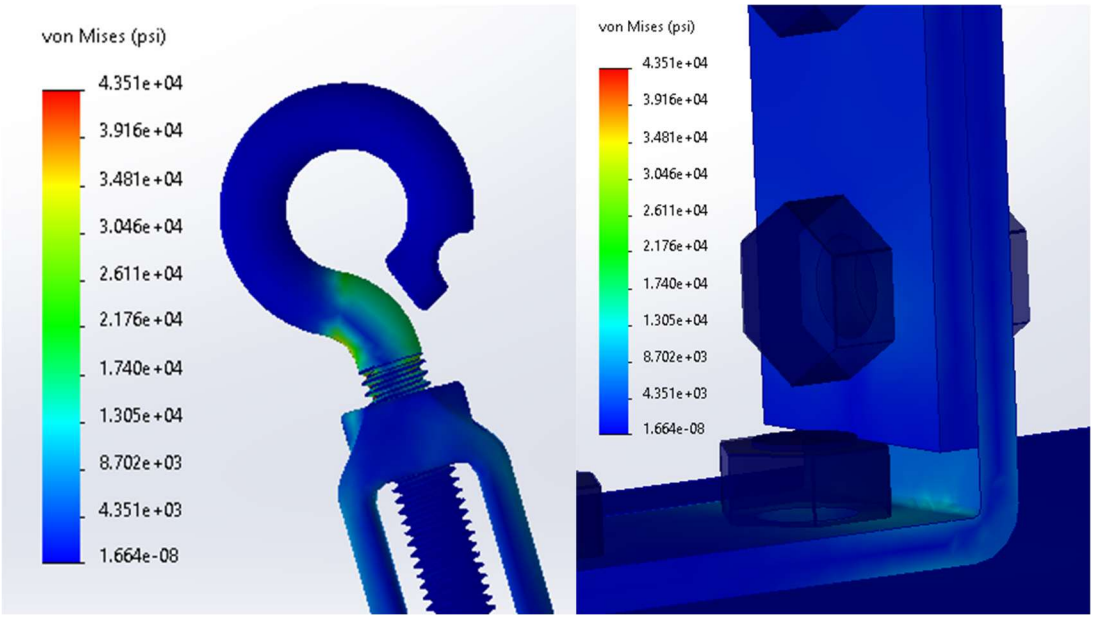

Figure 17 and 18 - Simulated von Mises of turnbuckle eye (left) and L-bracket (right)

Additionally, the max Von Mises values were found in the same locations within the turnbuckle eye and L-bracket. The max Von Mises stress is 36,100 psi in the turnbuckle eye and 14,800 psi in the L-bracket. The brackets and turnbuckles are made of galvanized steel having a yield

strength of 60,000 psi. This means that the anticipated max stresses within the brackets are safely below the material yield strength.

Diffuser Manufacturing

After testing the diffuser efficiency using CFD, the next concern to address is manufacturability. To save cost, the diffuser can be made with spare, 0.13 inch-thick, stainless steel sheet metal. The process uses a plasma cutter on hand and a brake press to bend the flanges. Then, the parts are welded together. To ensure the correct dimensions are used in the final diffuser, a cardstock prototype was made with a laser cutter. This is shown in Figure 19.

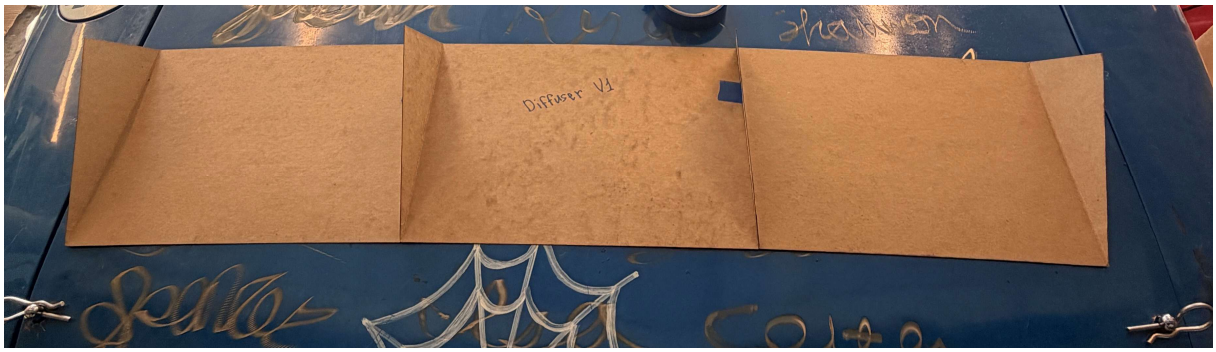

Figure 19: Splitter Mockup

This proved that the dimensions would physically fit between the wheel wells. The next step was to find a way to mount it underneath the rear end of the car.

Diffuser Mounting

The subframe of the Miata was the perfect place to mount the diffuser. Another sheet metal piece can be modeled to hold the diffuser in place. Two of these brackets will connect the subframe with the diffuser as shown in Figure 20 below.

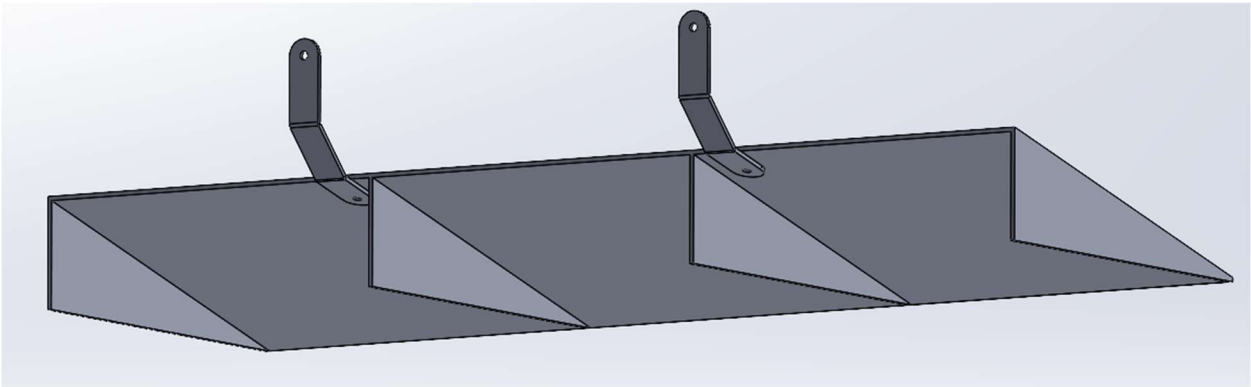

Figure 20: Diffuser mounts

Next, another finite element analysis was conducted on the diffuser and mounts to make sure that it fails when needed. This was done in SolidWorks' integrated features. The top holes on the brackets are modeled as a fixed geometry, and bolt connectors simulated the connection between the diffuser and the bracket. To simulate a clash between the ground and the diffuser, a 200 lbf,

external load was applied upward to the bottom of the flanges. After running the simulation, the following Factor of Safety plot was found (Figure 21).

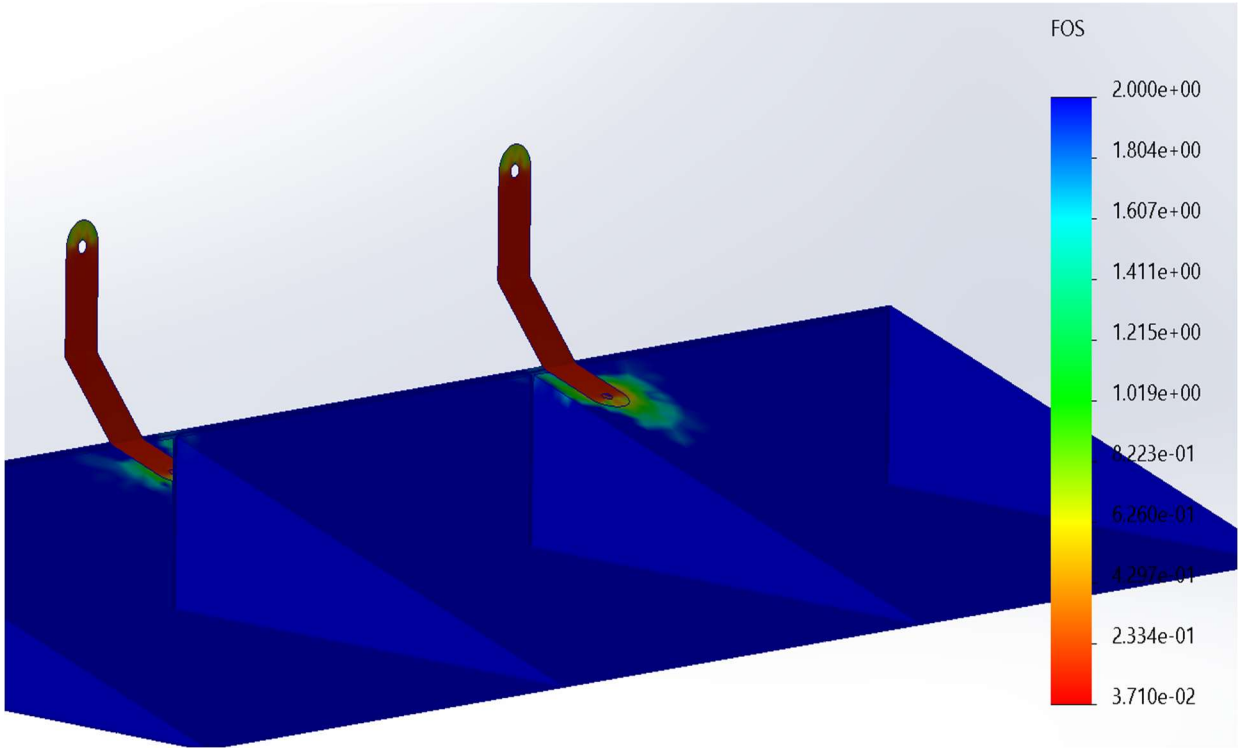

Figure 21: Diffuser mounting Factor of Safety plot in SolidWorks

The FoS of the bracket is much lower than that of the diffuser. This figure shows that the brackets will fail before the diffuser itself. In the event of an unpredictable crash, the brackets will break off before the diffuser. This is done to increase safety as this part is expendable. The team believes that making this part fail easily will be a good design feature to ensure safety during racing.

Electronics

Wiring Harness

The electrical team spent a significant amount of time fully removing the wiring harness from the body of the car. With the harness fully removed, full characterization of the system was achieved. The current state of the wiring harness is shown in a circuit diagram, Figure 22 below.

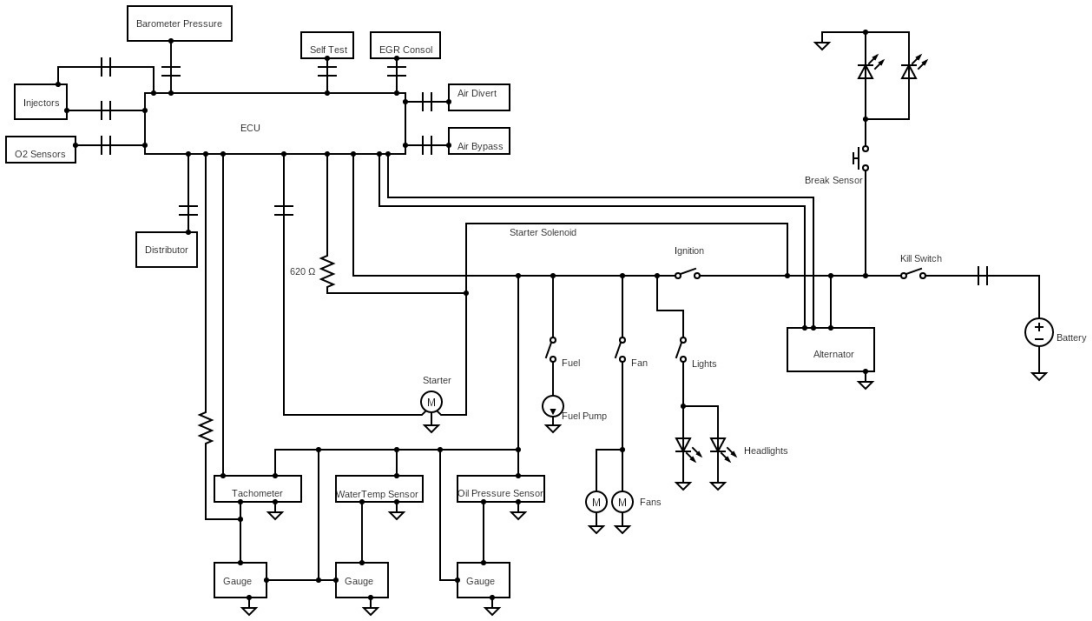

Figure 22: Circuit Diagram of Wiring Harness

Multiple wires with one termination location on each end of the run are considered bundles, and are shown as wires with two small lines crossing them near their origin. A few unimportant bundles are missing from the ECU block, namely the collection of unused connectors. It is noted that the current headlights and brake lights are not actually LED systems, and that the LED symbols shown are merely meant to represent a light. This diagram shows the important connections to be preserved. This diagram satisfies most of requirement G-1, with the rest addressed in the testing plan. As of writing, the OneGauge display system has just arrived, and as such hasn't been characterized and added to the wiring diagram. This will be the first thing addressed after the CDR presentation.

The switching schema, once seen from the perspective of the diagram, has problems arise. All of the current that runs the respective functions goes through the user's switches. Upon inspection, the switches used only have ratings for up to 20 A at 125 V AC. Since there is no DC current rating, a similarly AC rated switch was found, and its DC rating (15 A at 12 VDC) was used as an approximation [2]. The highest current draw of any component on the accessory switches is the fans, with a peak current draw of 25.4 A [3]. This massively exceeds the estimated rating of the switch, meaning problems will arise. This information is summarized in the circuit diagram of the current switching schema shown in Figure 23 below.

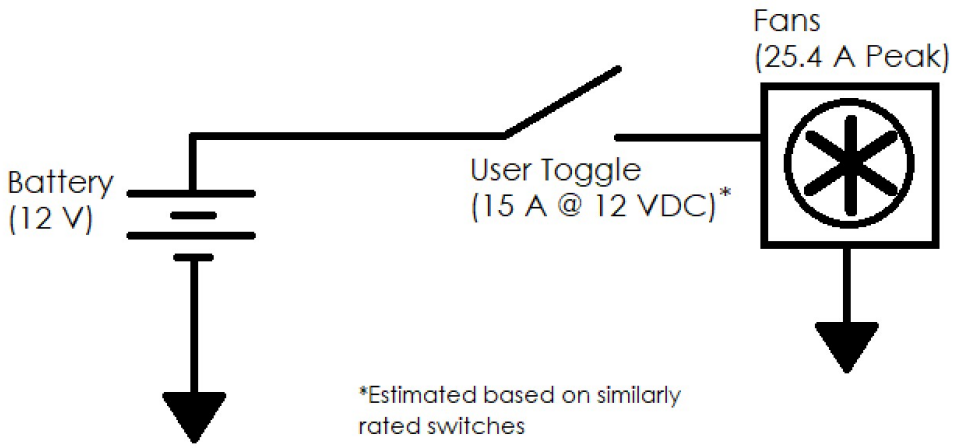

Figure 23: Circuit Diagram of Current Switching Schema

This is in line with the previous race team's account of melted switches during installation and sparking switches during racing.

To remedy the issues with the installed switches and provide additional protection, relays and fuses will be added to each switching path. The previous team had acquired, but not used, JD1912 relays. These relays are rated for 40 A at 12 VDC, meaning they can handle the current required for the most intensive systems [4]. Fuses are also to be added to each component based on the current draw expected. An example of the proposed application is shown in the circuit diagram of Figure 24 below.

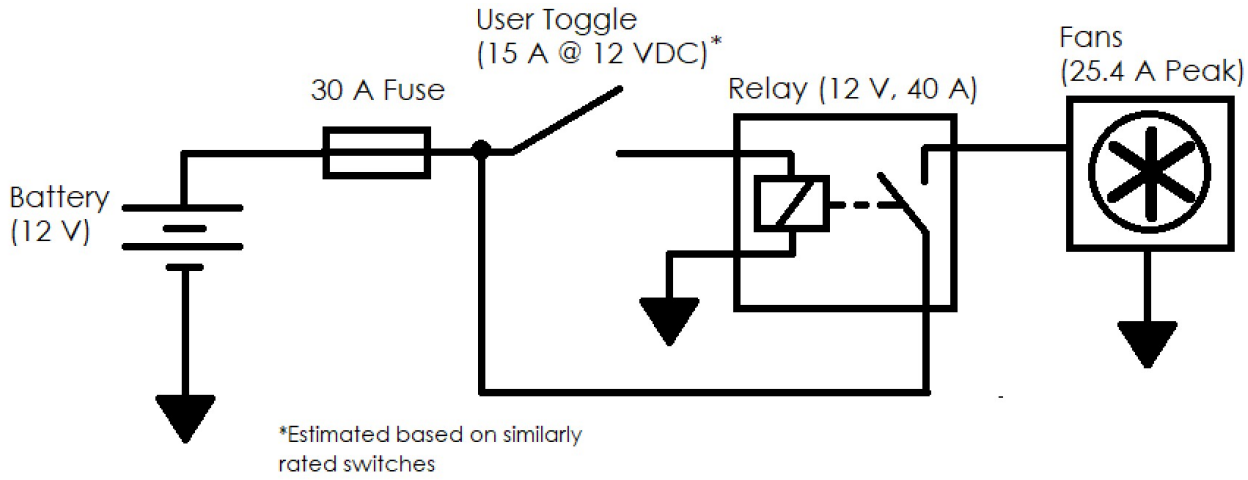

Figure 24: Circuit Diagram of Proposed Switching Schema

The proposed schema would drastically cut the current running through the user's switch, while still maintaining complete functionality. Per the JD1912 datasheet, the coil of the relay requires 1.6 W to function, meaning that it will draw 0.133 A when driven at 12VDC (calculation in Appendix B). This is well within the rating of the user switches. The comparatively low current draw of the coil means that it can share the same fuse as the fans without any interference or accidental tripping. This is true for all of the accessories, which will all see this topology but with appropriately rated fuses. This design fulfills requirement E-3, and only requires client sign-

off to fulfil requirement G-3. Because the components were acquired by the previous team and inherited for this modification for free, it also fulfills requirement G-4.

ECU Upgrade Viability/Sensor Testing

To ensure that the engine can run at a stoichiometrically balanced air-fuel ratio, benchtop testing was conducted on all the relevant sensors in the wiring harness that enable the ECU to supply a proper amount of fuel at a given load. The electrical team planned to test the following sensors: air charge temperature (ACT), engine coolant temperature (ECT), oxygen sensors (O2), and manifold absolute pressure sensor (MAP). The ACT & ECT sensors provide temperature data of the air coming into the engine and the coolant running through the engine, respectively. The ACT determined the temperature of the air entering the engine, allowing the ECU to determine if the engine timing needs retarding to prevent pre-ignition of the fuel at high temperature operation. If the ACT sensor is bad (most likely reading cold while the air is hot in a racing application), it can be detrimental to engine health as it can lead to running excessively rich and dirtying the spark plug as well as allowing engine knock to occur due to pre-ignition [5]. The ECT sensor provides temperature data for the engine block itself. This reading informs the ECU if the engine is still being warmed up or if it is overheating, which allows the ECU to dump or restrict the amount of fuel entering the engine as well as advance or retard the spark timing. If the ECT sensor is bad (most likely reading cold while the engine is hot), the ECU will be running the engine richer than it needs to be to account for the "condensing" of fuel inside the cylinders. This could again cause engine knock due to pre-ignition, and in a worst-case scenario, blowing the head gasket [6]. The MAP sensor works in conjunction with the ACT to provide a pressure value for the air coming into the engine. With the pressure value, the temperature of that air, the engines volume, and the volumetric-efficiency table within the ECU, the air mass entering the engine can be calculated for determining how much fuel is needed for stoichiometric combustion. If this sensor fails (stop reading pressure overall), the engine will enter limp-mode where it cannot run over a certain low RPM to prevent catastrophic failure [7]. The O2 sensors function as a feedback sensor, allowing the ECU to measure the amount of fuel present in the exhaust gas. These act more as fine-tuning sensors that keep the air fuel (AF) ratio oscillating around 14.7:1. If these sensors are bad (reading permanently lean at 0.1V) this can skew the AF ratio either rich or lean depending on where the sensor gets stuck [8].

In the testing plan detailed in Appendix B the MAP sensor and O2 sensors were both tested to check for proper operation.

The setup for testing the MAP, as pictured in Figure 25 below, required identifying which terminal was ground, 5V reference, and signal. Figure B2-5 in Appendix B was used to identify these terminals. A 5.1 kΩ pull-up resistor was used to bridge between the 5V pin and sensor pin so that the signal circuit received current to act upon (this allows for the generation of a square wave which outputs Hz for the ECU). As pictured in Appendix B2-1 and B2-2, the MAP sensor was able to fulfill all the requirements laid out in the testing plan and was therefore deemed a properly functioning sensor.

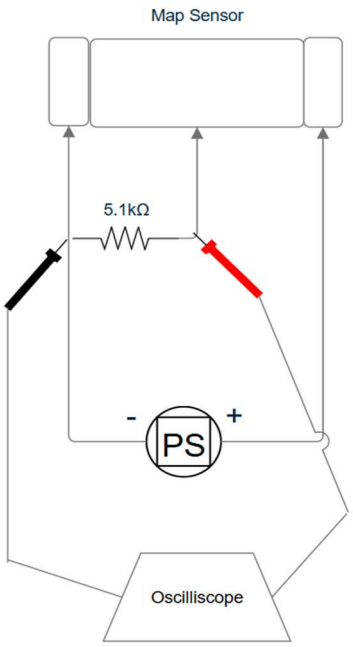

Figure 25: Map Sensor Testing Setup

The setup for the O2 sensor as pictured below in Figure 26, required that a multimeter positive probe be attached to the designated signal wire on the sensor and the negative probe be attached to the body of the sensor, which functions as the ground for the signal circuit. Heat from combustion was then applied to the end of the sensor to simulate exhaust gas passing over the sensor tip. Both sensors' outputs, as seen in Appendix B, failed to meet the requirements laid out in the testing plan, leading the team to purchase new, direct-swap parts for replacement.

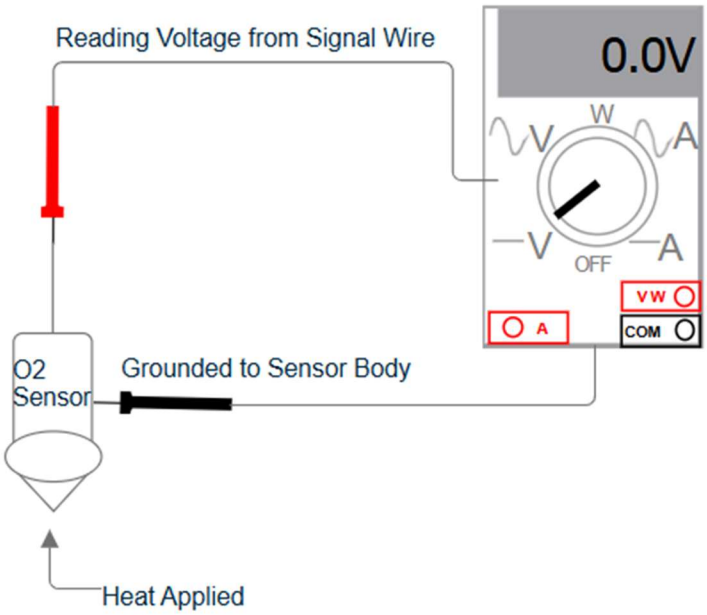

Figure 26: Oxygen Sensor Testing Setup

Due to the age of the ECT and ACT sensors, they could not be removed without incurring damage to the surrounding housing/material as well as the sensors themselves, so testing has not been performed on those specific sensors. With this lack of information, the electrical team could not confidently conclude that an ECU upgrade (A9L) was an appropriate solution to address engine inefficiency issues. If the engine does have persistent issues in operation, the ECT and ACT sensors will be deemed the first problem points that need addressed and will be replaced as if they were broken. If after replacing those sensors, the vehicle still has issues running or performing optimally, the ECU upgrade will be re-assessed and decided upon considering time frame and budget constraints.

Powertrain

Exhaust

The team's decision to use exhaust headers over the stock exhaust manifold was due to the goal of an increase of 10% in horsepower due only to changes in the intake and exhaust. The team did not have any horsepower or torque numbers from before the car was disassembled, because there was no access to a dynamometer within our budget. However, according to *Bober and Zalewska's* experimental research, in *Influence of exhaust manifold modification on engine power* [9], putting on exhaust headers increased engine horsepower by 10% and the torque by 11%, while keeping everything else on the car the same, testing on a MAHA LPS 3000 dynamometer with an accuracy of within 2%. The increase was present in rpm's from roughly 2500 rpm and above in torque, and roughly 3300rpm and above for horsepower. This test was done on a stock 6-cylinder BMW engine, so there will be some errors introduced, but the results are still well with our desired goal of a 10% horsepower increase using only the intake and exhaust. Figure 27 below is a graph of the before and after the headers are installed.

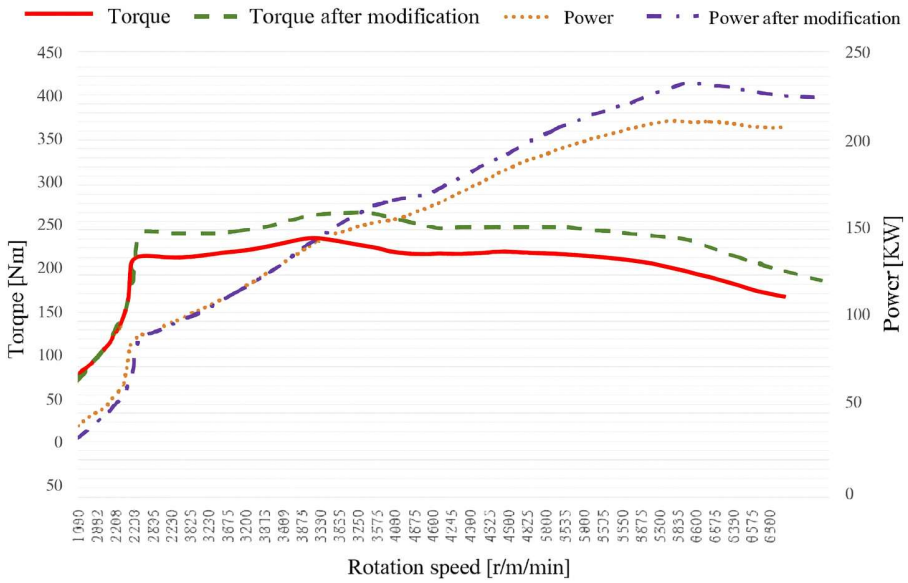

Figure 27: Before and after headers, dyno results [10]

This perfectly matches the Pulp Friction Crew's goal of increasing the engine horsepower by 10% only using the budget that we must work with. The team was able to acquire this set of headers for $104, making this a very good cost to performance ratio (Figure 28). This upgrade also will not change reliability because there are no additional parts that are being added, it is a direct swap. The welds on the headers are going to be inspected before they are installed.

Figure 28: Exhaust headers are going to be used on the car [11]

Intake

The team came to a decision to fully maximize the aerodynamic potential for the Miata, the large holes where the stock headlights should be compromising both the airflow over the car and the pressure differential needed for the intake subsystem. To meet the design requirements laid out by the team, this intake package was designed to reliably deliver airflow to the engine while withstanding the thermal, mechanical, and vibrational loads experienced during a 24-hour endurance race (Figure 29). All calculations and simulations were performed using SolidWorks Simulations. These analyses helped guide the decision-making process related to geometry, material selection, wall thickness, and mounting strategy to ensure functional performance and durability.

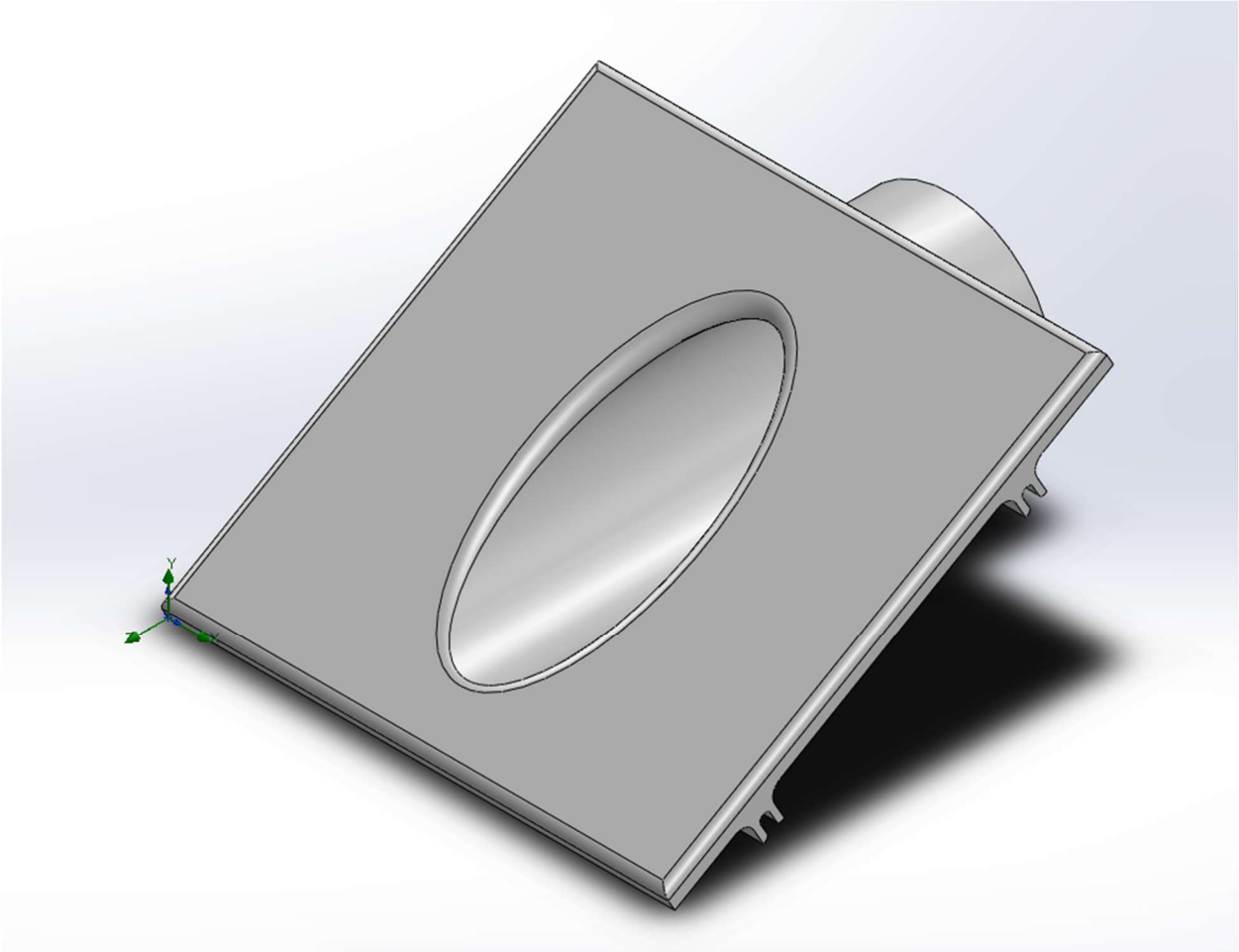

Figure 29: Designed Headlight Intake system.

For an engine to run properly, adequate airflow and pressure differentials are critical for ensuring consistent engine performance while also avoiding airflow restricting which can limit the flow. Computational Fluid Dynamics (CFD) was performed to verify that the intake geometry provides sufficient mass flow while minimizing pressure losses to the engine bay.

A steady state CFD model was conducted with SolidWorks Simulations software, where the key variables were:

- V_∞: = Freestream vehicle velocity (mph)
- $\dot{M}$ = Air mass flow rate through the intake (kg/s)
- ΔP : = Total Pressure drop across the intake (Pa)
- ρ : = Air density (std.)

For the finite element analysis, the V_∞ was modeled at 150 mph to showcase the maximum stress the component will undergo during the 24-hour race. While during the CFD simulations, V_∞ was modeled to be 60 mph, which is a high estimate for the average velocity maintained during the race.

CFD results indicate a smooth velocity distribution through the intake with minimal flow separation. The calculated pressure drop across the intake was 0.08 psi or 552 Pa while when a CFD was run on a rough Miata model there was a calculated pressure drop of 500 Pa. Figure 30 shows the pressure contour plot of the intake, and Figure 31 illustrates the pressure differential over the whole front of the Miata.

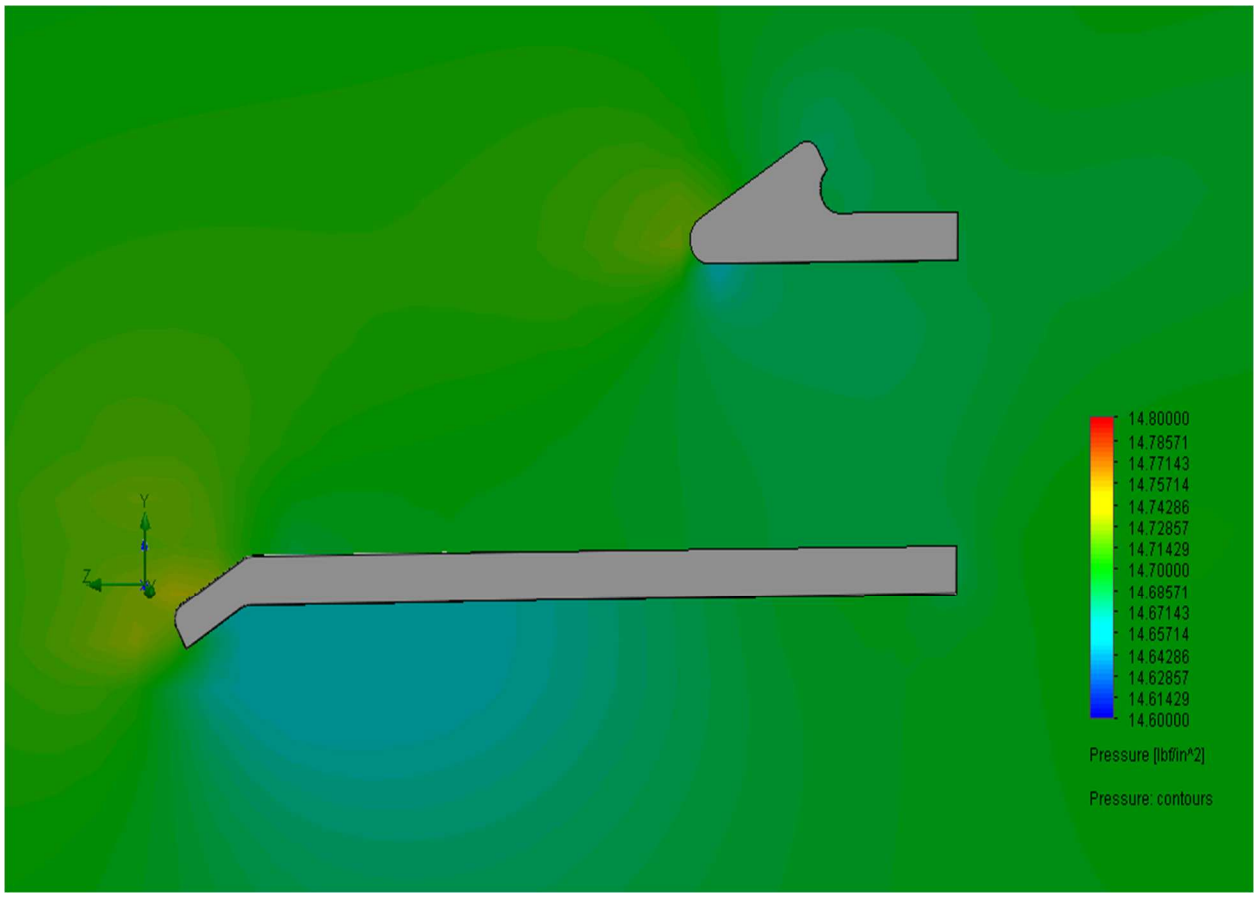

Figure 30: Pressure contour plot of intake.

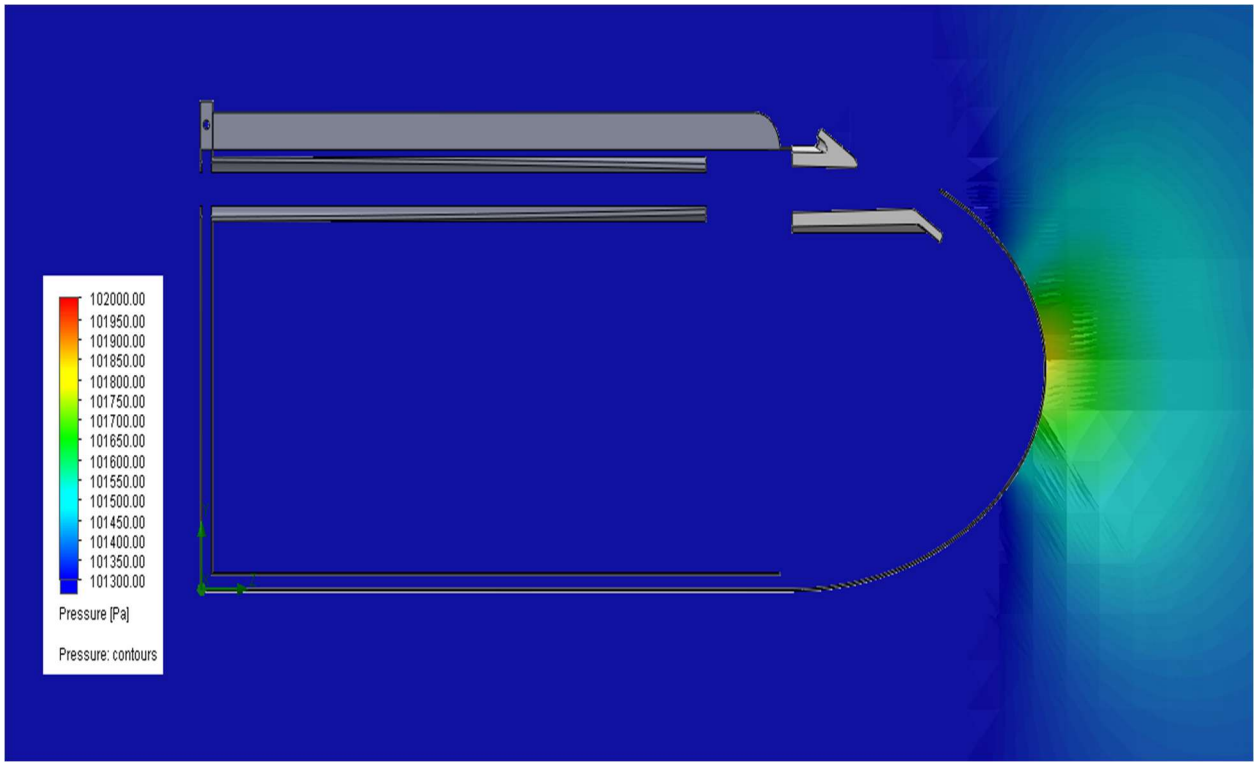

Figure 31: Pressure plot across the Miata front (60 mph).

Furthermore, the airflow results prove that the geometry of the intake allows for better airflow to the engine intake. Figures 32 and 33 demonstrate the velocity profile of the air when moving around the Miata model.

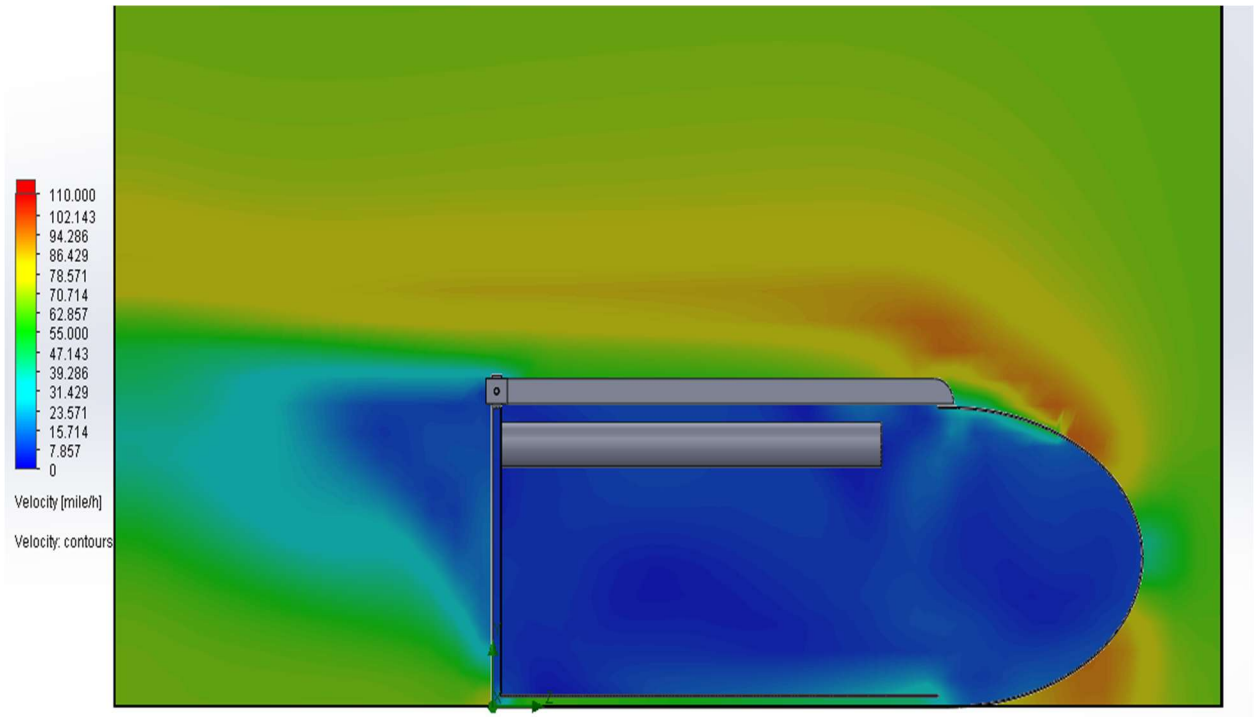

Figure 32: Velocity contour plot around Miata, no intake.

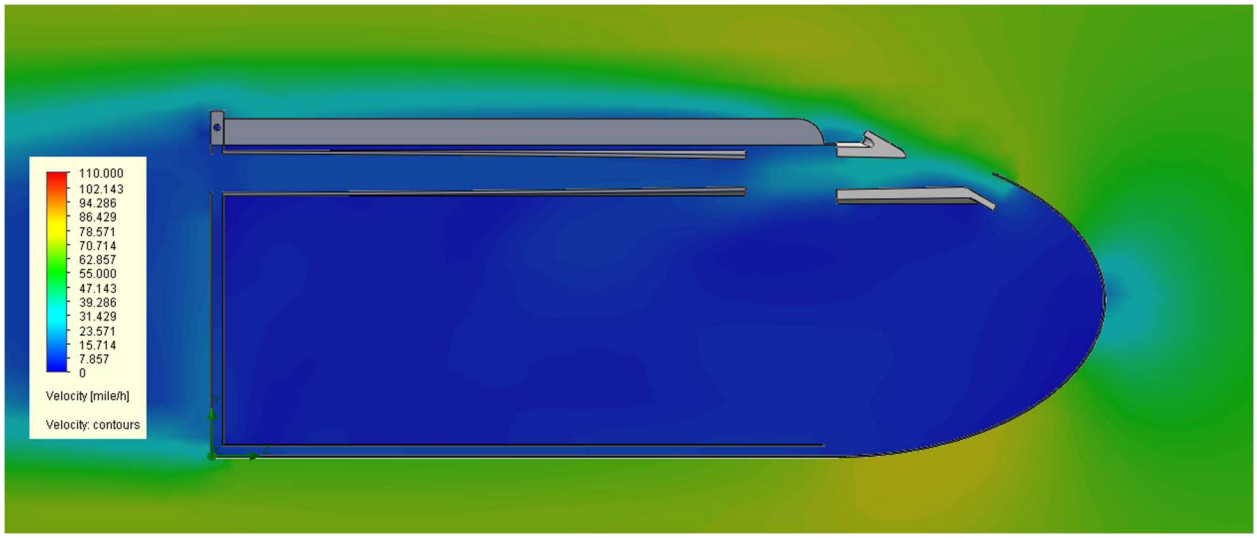

Figure 33: Velocity contour plot around Miata, with intake.

As can be seen, the flow profile into the engine is dramatically better with the use of the headlight intake with an increase of 118% more airflow.

When analyzing the structural design of the intake duct, the intake must withstand aerodynamic pressure loading, engine bay vibration, and handling loads without cracking or excessive deformation. Finite element analysis was utilized to verify that the correct material was chosen.

The material that is chosen for the initial models is ABS plastic. This material was chosen because of its high heat resistance, light weight, easy to manufacture, and ability to be redesigned. However, once a final model has been developed, the intake will be made from a nylon PA12 material due to the high temperature resistance, stiffness, and use in industry.

Material Properties [12]:

	ABS Plastic	PA12 Nylon
Elastic Modulus	1.00 - 2.65 GPa	0.04 - 100 GPa
Ultimate Tensile Strength	22.0 - 74.0 MPa	1.0 - 1750 MPa
Glass Transitions Temperature	105°C	170°C

The loading conditions are applied directly to the mounting points where fastener locations were made. Finite element analysis (FEA) shows a maximum von Mises stress of 281 psi or 1.93743 MPa, resulting in a factor of safety of 11.4 relative to the yield strength of ABS and a factor of safety of 58.8 in regard to PA12 Nylon. Maximum deformation was 0.06 mm, which does not compromise airflow or structural integrity (Figures 34 & 35).

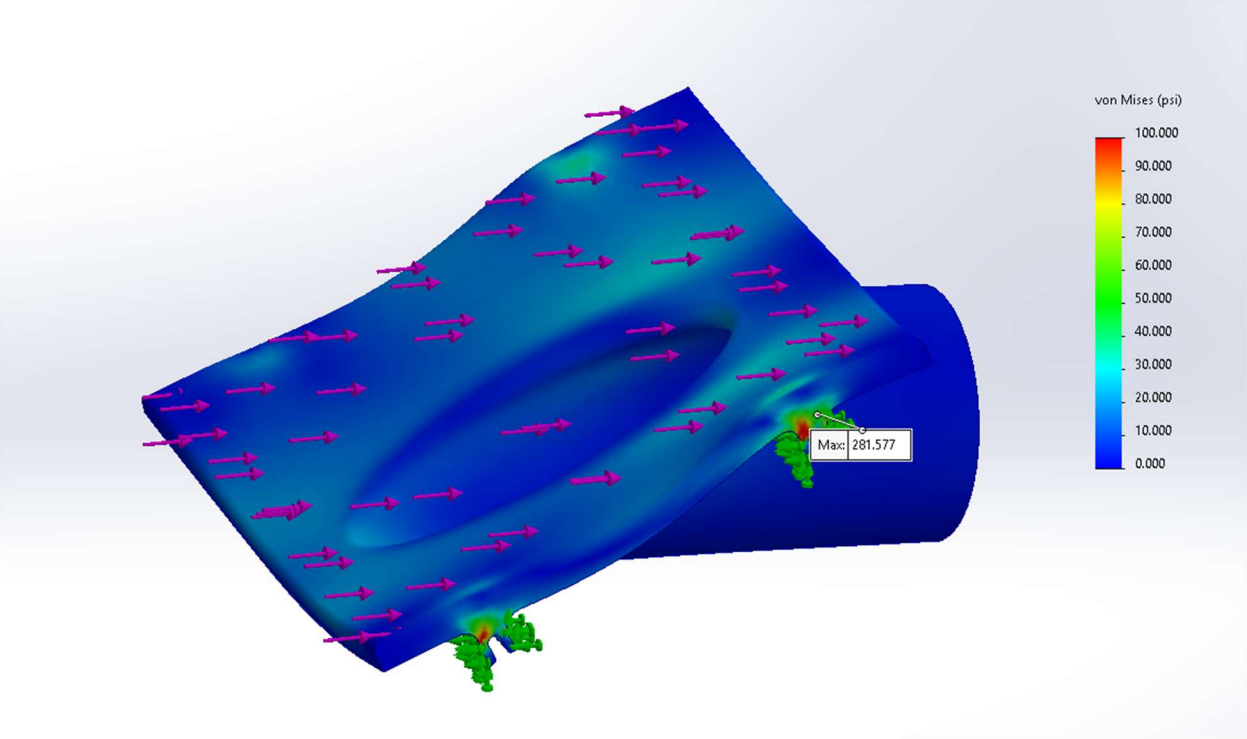

Figure 34: FEA Von Mises contour plot

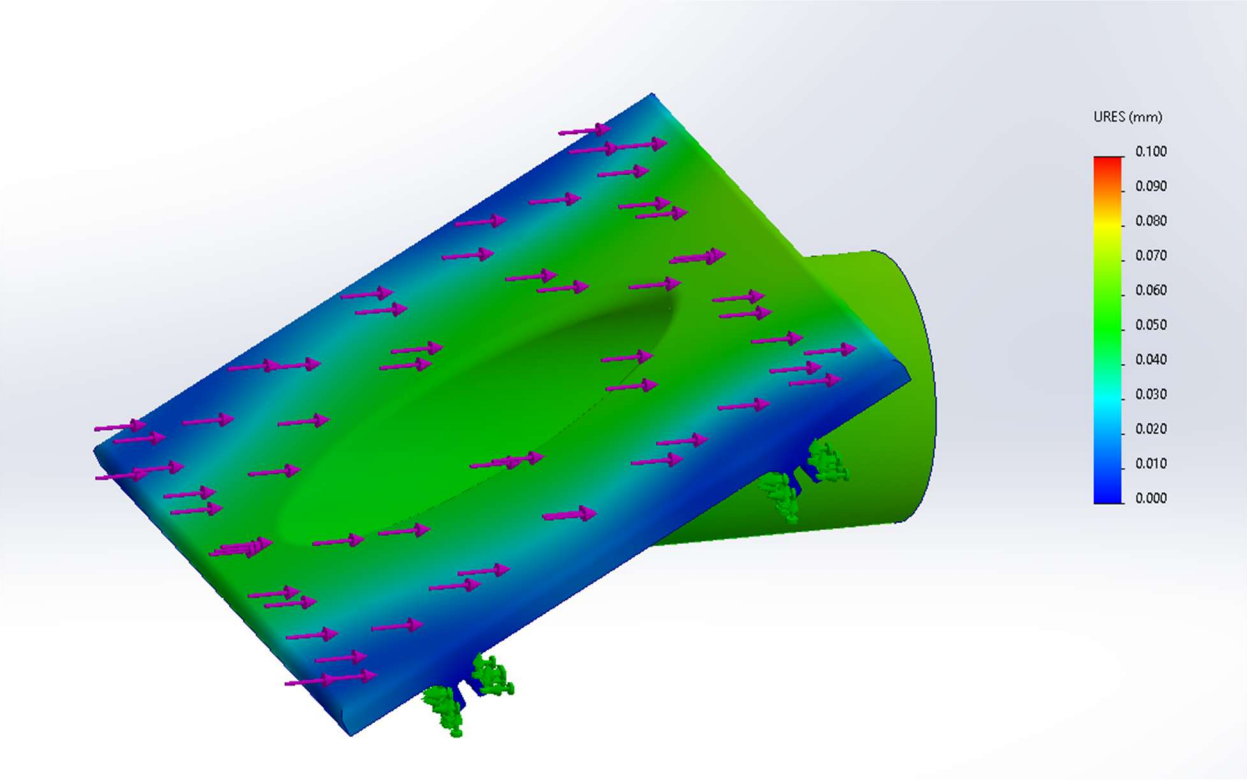

Figure 35: FEA Displacement contour plot

As for vibration and fatigue considerations, rubber washers and O-rings will be used on all mounting surfaces to absorb vibration and decrease vibration on the actual component. The

intake was designed specifically for additive manufacturing. Print orientation, layer height, and infill percentage were selected to maximize strength in primary load directions. A minimum wall thickness of 0.5 inches ensures consistent extrusion and structural robustness.

The analyses conducted demonstrate that the headlight intake will function as designed, providing necessary airflow while maintaining structural integrity and thermal stability under endurance racing conditions. CFD, FEA, and material analyses collectively inform proper design optimizations, while ensuring reliable performance over a 24-hour race duration.

Shroud

The powertrain and cooling teams have concluded that it would be beneficial to use a shroud to allow for better cooling without compromising aerodynamics, along with a water injector to allow short bursts of extra cooling when the car needs to be pushed hard. To verify the viability of the shroud, SOLIDWORKS CFD was used in combination with the MATLAB model created for the radiator.

The shroud and water injector will be made from donated sheet aluminum and a donated 12V water pump that can be wired directly to the car's current electronics for the LED lights used on the numbers. The shroud will be made from 4 separate cutouts of sheet aluminum that will be TIG welded together. The shroud will then be riveted to the radiator casing using 5 3/16" rivets.

The CFD shown below (Figures 36 & 37) shows the CFD results of the shroud with an air temperature of 75 degrees Fahrenheit with a speed of 60 mph. These numbers were chosen because this is roughly the average conditions that would be expected at High Plains Raceway based on previous experience.

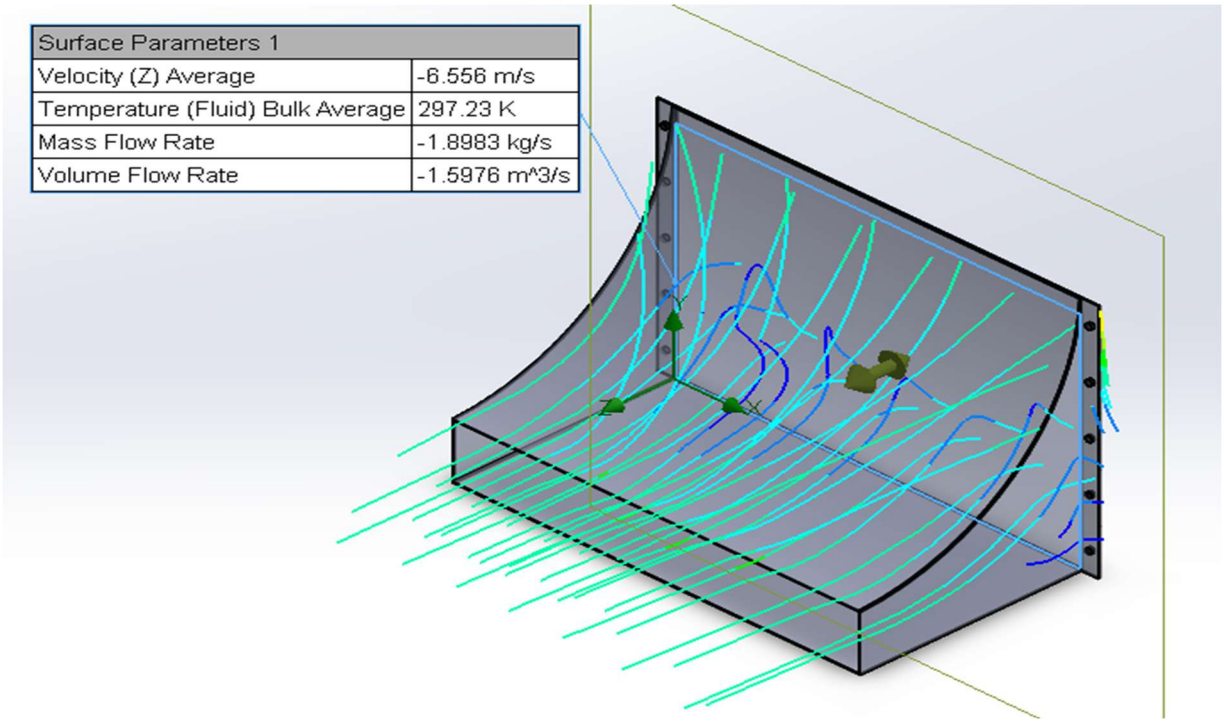

Figure 36: Shroud CFD Front

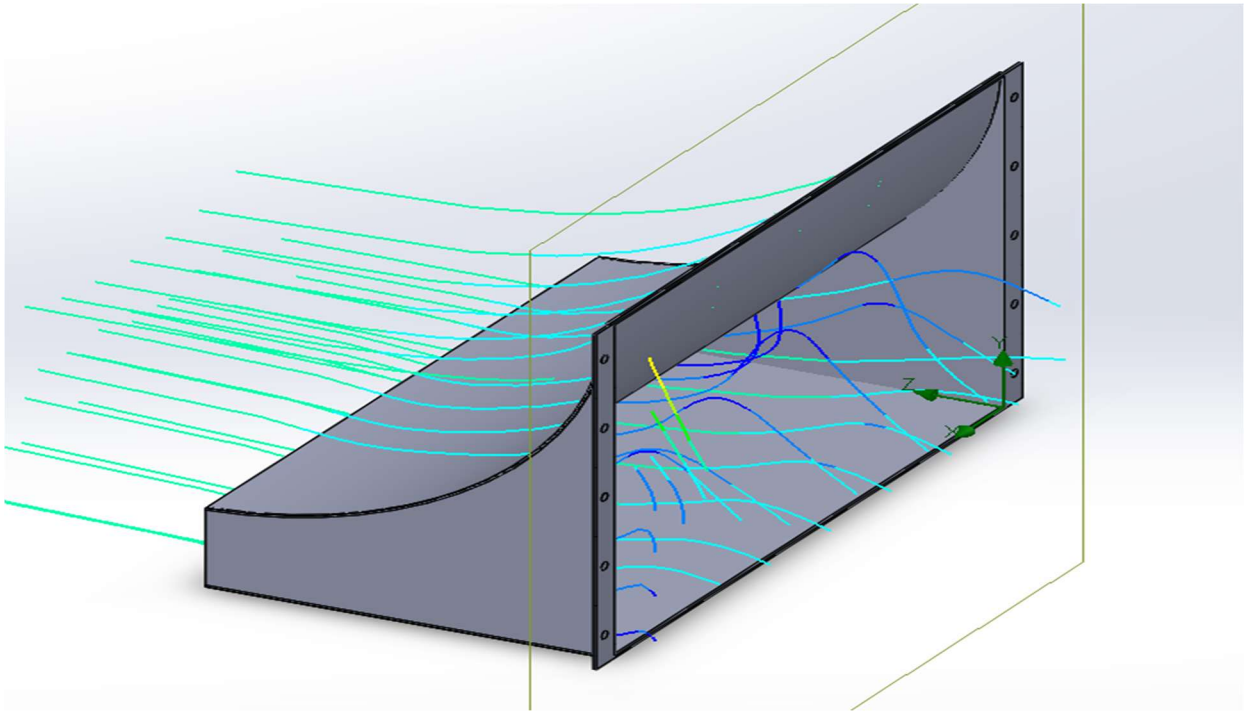

Figure 37: Shroud CFD Rear

Doing the volumetric flow calculation by hand the result is:

$$Q = \frac{60\ mph}{2.237\frac{\frac{mph}{m}}{s}} * \frac{4\ in}{39.37\frac{in}{m}} * \frac{24\ in}{39.37\frac{in}{m}} = 1.66\frac{m^3}{s}$$

The SOLIDWORKS result comes out to roughly 1.6 cubic meters per second, which shows that the turbulent air slows the volumetric flow a little, but not a huge amount. This means that it can be assumed that the shroud opening size is a sufficient estimate for the volumetric flow through the shroud, as calculated in the equation above. Taking the frontal area numbers for the shroud and plugging them into the code for estimating the radiator effectiveness yielded Figure 38. In this case, the radiator effectiveness has been increased from 0.6 to 0.95 due to the assumption that the shroud will direct air through the radiator.

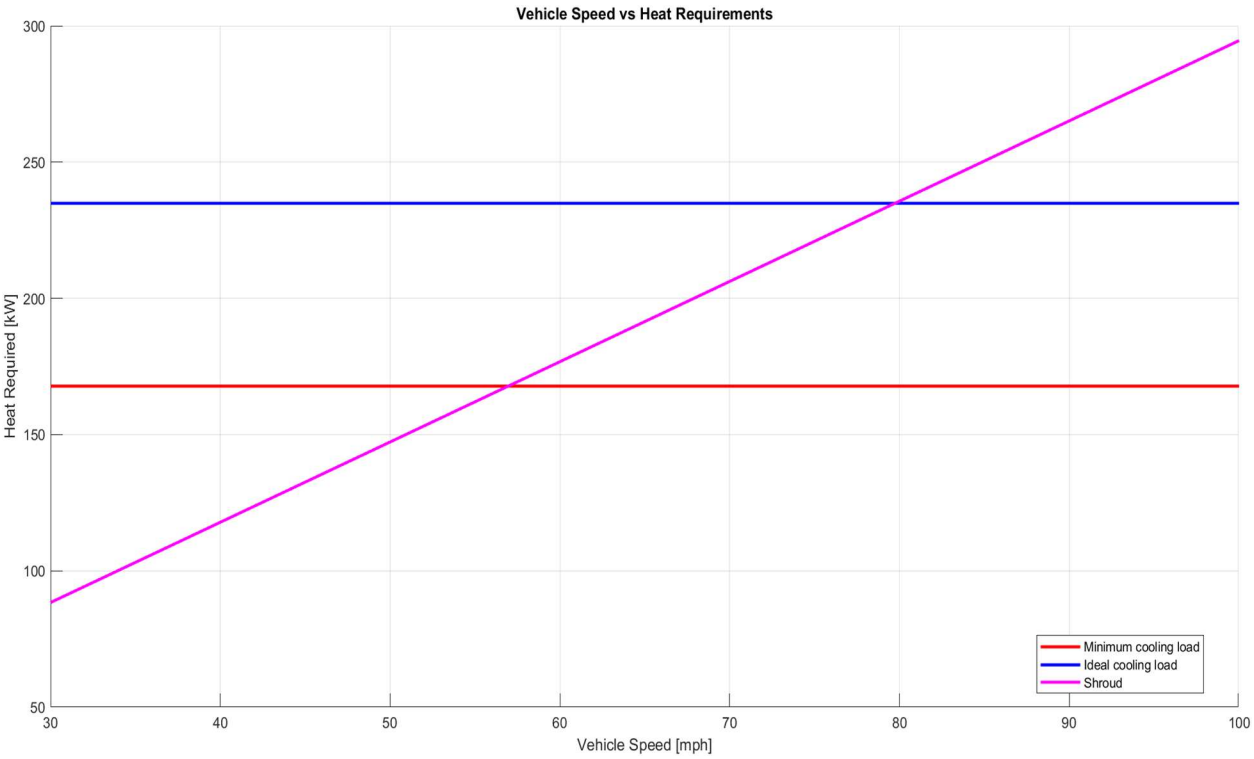

Figure 38: Shroud Graph

The cooling section below goes into much heavier detail about how the code works, but the graph above shows that at speeds above 60 mph, the shroud will provide enough cooling for the engine. This is not quite an ideal value since the minimum cooling load is not met at lower speeds. Below is the same graph, but with the shroud being expanded to 32 inches in width. This will be the width of the shroud given that the car overheats in testing with the original shroud.

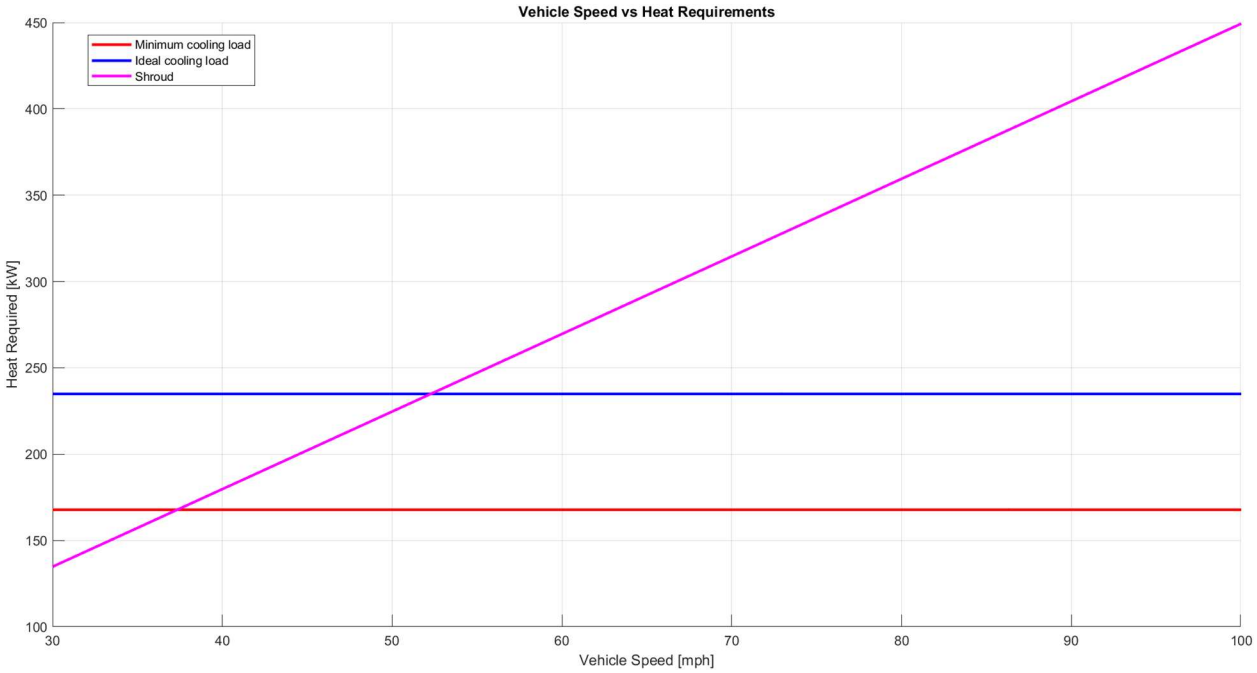

Figure X: Modified Shroud Graph

This new graph shows that the cooling needs will be met at speeds above roughly 37 mph. This should be enough cooling for racing purposes.

Further verification will have to be done by testing the car once it is assembled. In the case of the shroud not providing enough cooling, expansion of the shroud would be very easy and inexpensive to do.

Cooling

A MATLAB model was set up to simulate the performance of 3 different radiator options. 7 base variables were defined to begin the calculations. These values are shown in Table 7. Horsepower was defined using the engine specifications for a Ford 302, and engine efficiency sits between 20%-30% normally. The previous year's team saw coolant temperatures up to and above 225°F which loosely corresponds with oil temps up to 260°F. Last year's team also used 18 GPM for the water pumps, with similar values being extrapolated to oil flow rates. Vehicle velocity was calculated by taking the track length and comparing it with lap times made by team members in a similar vehicle set up. Effectiveness usually ranges from 0.4 to 0.6 but can fluctuate beyond that, so the decision was made to split the middle. Lastly, air temperature was given a base value of 75°F. The main takeaway from these base variables is that they can all be adjusted as needed, which is reflected in the model.

Table 7: Base Variable Assumptions

Variable	Value	Unit
Horsepower	225	HP
Engine Efficiency	0.25	

Coolant Temperature	225	°F
Oil Temperature	260	°F
Vehicle Velocity	50	Mph
Coolant Flow Rate	18	GPM
Oil Flow Rate	6	GPM
Effectiveness	0.5	
Air Temperature	75	°F

After defining base assumptions, it is also important to define variables associated with each of the 3 different cooling options. The frontal area for each option was calculated, and it was assumed that the entire area would receive uninterrupted clean flow. On top of this, the oil cooler would not be in front of the radiator and therefore both exchangers would receive the same air properties with the only difference being the frontal area of each component. Another assumption with option C is that the oil cooler does not add any effectiveness to the heat exchange process. The final assumption is that the only difference between option A and B, is the frontal area, the internal components and effectiveness will remain the same. These assumptions are summarized in Table 8.

Table 8: Cooling Option Variable Assumptions

Variable	**Option A: New Radiator**	**Option B: Same Radiator**	**Option C: Same Radiator and Oil Cooler**	**Unit**
Frontal Area	0.2658	0.2042	0.2427	m^2
Other Assumptions	Same Effectiveness		No overlapping airflow between oil cooler and radiator	
			No added effectiveness	
	Uninterrupted airflow equivalent to the frontal area			

To build a model the next determination was what percentage of the car's fuel energy would be output to power, exhaust, and cooling. Given that engine efficiency was already assumed to be 25%, the safe assumption is then made that 75% of the rest goes to both exhaust and cooling. From there it was assumed that around 30%-35% of the fuel energy goes to exhaust. This leaves 40%-45% to be dissipated by the radiator. Due to the uncertainty of how much the exhaust dissipates, and how efficient the engine runs, the assumption was made that a minimum of 30%

and a maximum of 50% of the fuel energy needs to be dissipated by the radiator. This is broken out in Figure 39. From here, the methodology used to solve the heat dissipated by the radiator was the effectiveness-NTU method. This method is used to "find the performance of a heat exchanger without knowing the outlet temperatures" by relating the actual heat transfer to the maximum possible heat transfer [13][14]. The first step is to solve the mass flow rates for all 3 options, along with the air mass flow rate, which is shown in Equation 1. After this, the heat capacity rate needs to be solved for each type of fluid flow. The heat capacity rate is the product of mass flow rate and specific heat capacity. To solve this, density and specific heat capacity are needed and were found using the initial temperatures for each option with the result visible in Equation 2. For all fluids, the values were specified to be at an elevation of 5280 feet. The next step was to compare the heat capacity rates with the goal being to find the minimum rate for each radiator option. The minimum rate for all options was the air heat capacity rate. From there, the max heat transfer from each option can be found using Equation 3. Then the actual heat transfer rate can be calculated with Equation 4. The only difference for option C is to solve the oil cooler separately from the radiator and then combine the heat transfer rates at the end.

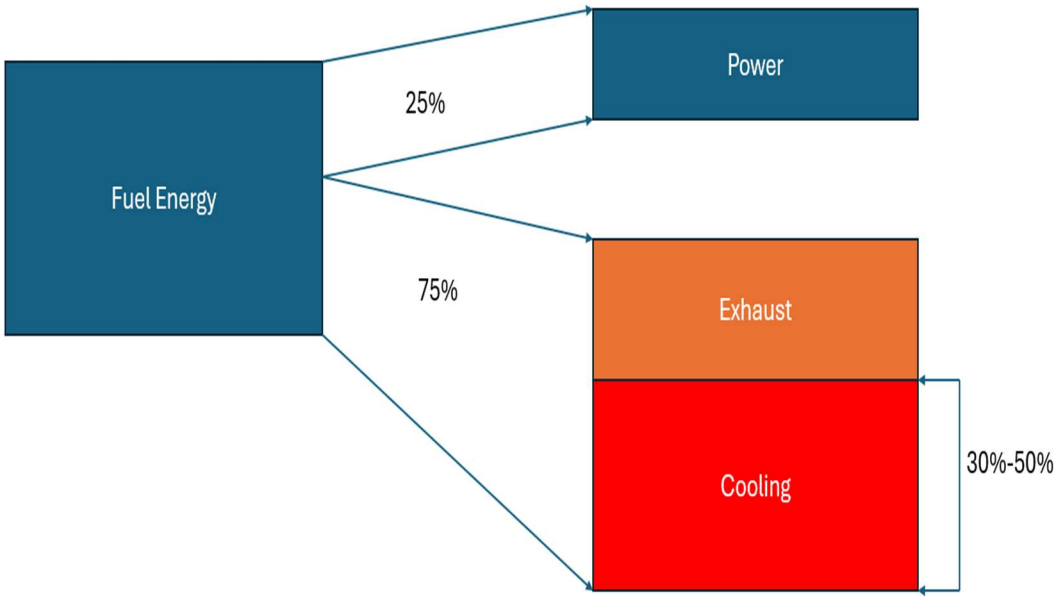

Figure 39. Fuel Energy Breakdown

$$Equation\ 1: \quad mass\ flow = Frontal\ Area * Air\ velocity \qquad Unit: \frac{m^3}{s}$$

$$Equation\ 2: \quad C = (mass\ flow * density) * specific\ heat\ capacity \quad Unit: \frac{W}{K}$$

$$Equation\ 3: \quad q_{max} = C * \frac{(T_{coolant\ in\ K} - T_{air\ in\ K})}{1000} \qquad Unit: kW$$

$$Equation\ 4:\ q_{actual} = q_{max} * effectiveness \quad Unit: kW$$

After the initial model set up, it was determined that all the base variables except for the coolant and oil flow rates needed to be variated to see how the radiators would perform under differing circumstances. 6 different tests were set up with only 1 variable change for each iteration. The only exception to this rule was the coolant temperature variation, where the oil temperature was also varied on the exact same scale as the coolant temperature. The variation set up is shown in Table 9. The horsepower and efficiency changes were straightforward and required no other changes other than to the minimum and maximum cooling loads. The temperatures were trickier as they also required changes to both density and specific heat capacity which changed the heat capacity rates and required different temperature values to be used in the heat transfer rate equations. Finally, the vehicle velocity change influenced mass flow rates and therefore the air heat capacity rates.

Table 9: Base Variable Ranges

Variable	Value	Unit
Horsepower	20-225	HP
Engine Efficiency	0.15-0.30	
Coolant Temperature	150-230	°F
Oil Temperature	180-260	°F
Vehicle Velocity	30-100	Mph
Effectiveness	0.30-0.70	
Air Temperature	50-100	°F

After performing the simulations, graphs were used to illustrate the results. These graphs are shown in Figures 40-45. The maximum cooling load is the blue line, and the minimum cooling load is the red line. The new radiator option is pink, the same radiator option is in black, and the same radiator with an oil cooler is in green. Lastly, the shaded blue area is the "target zone" or the area that the team would like the radiators to perform in. With that being said, anything above the blue line is excess heat exchanged from the system, and anything below the red line means there is not enough heat exchange occurring in the system. Looking at these results, it can be difficult to come to a firm conclusion. Some graphs show that all options will work for most scenarios while others don't show that result. The question becomes which results are the most important and which ones are trustworthy. Due to the many variables and assumptions made in this model, it is difficult to come up with a conclusion because different circumstances could change many different variables. These graphs can point the viewer in the right direction but do not allow the viewer to come to a conclusive decision.

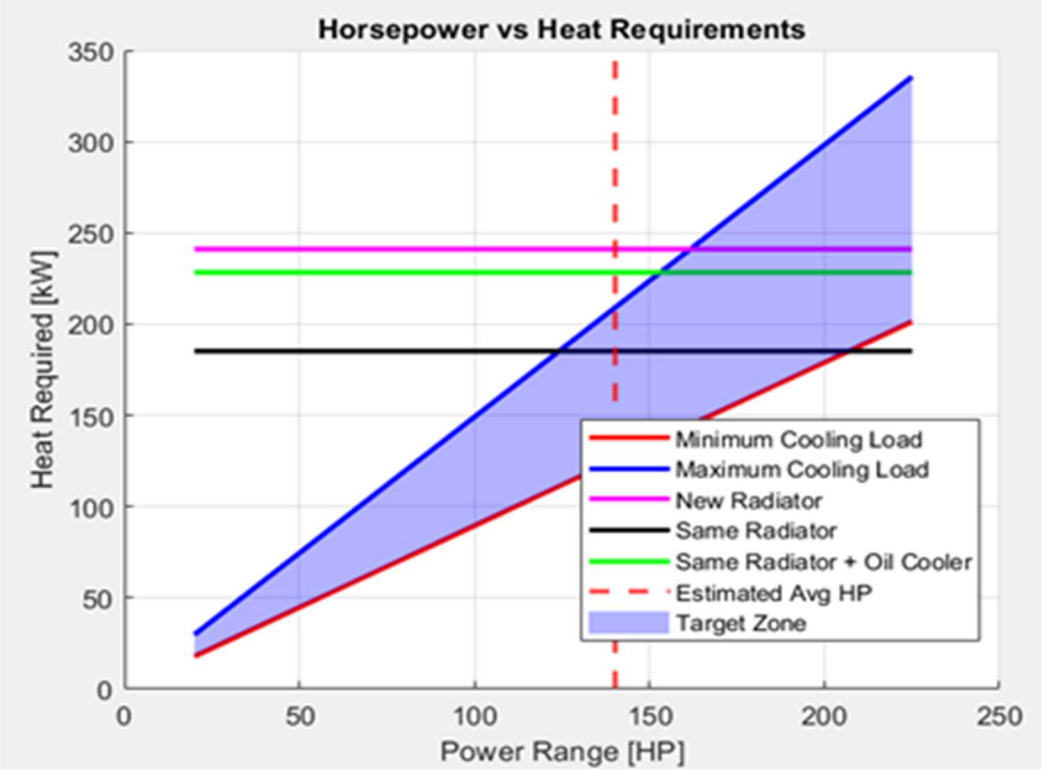

Figure 40: Engine horsepower variations compared with heat exchange results

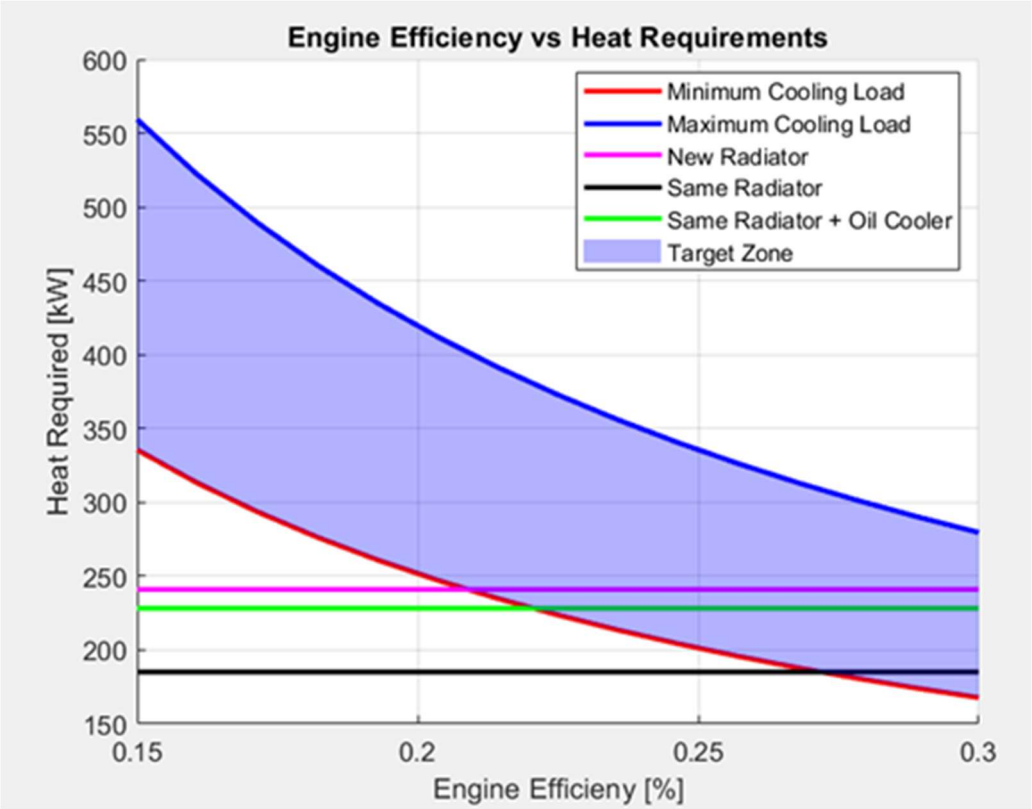

Figure 41: Engine efficiency compared with heat exchange results

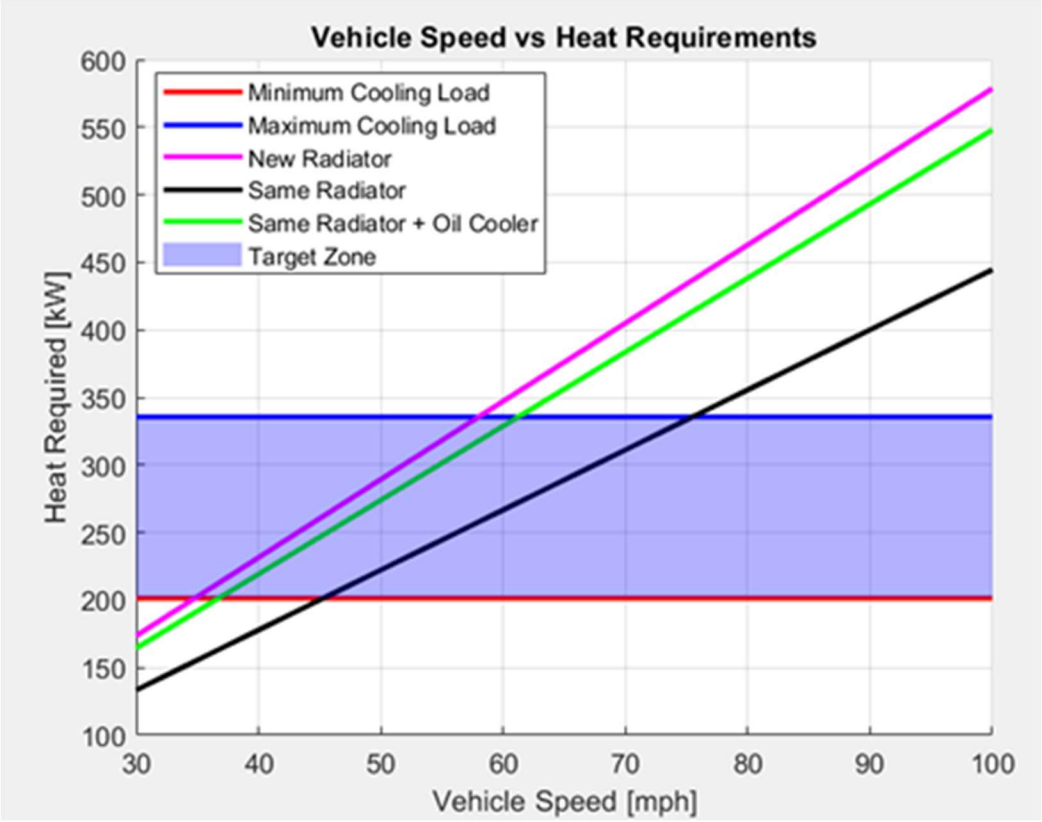

Figure 42: Vehicle speed compared with heat exchange results

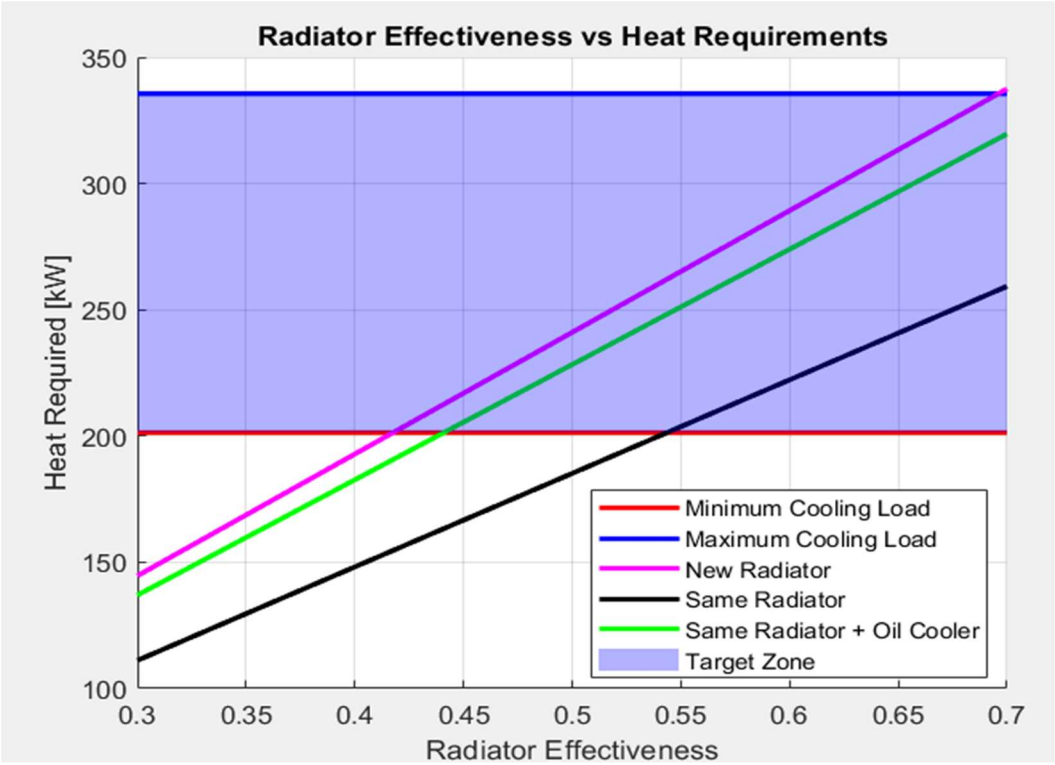

Figure 43: Radiator Effectiveness compared with heat exchange results

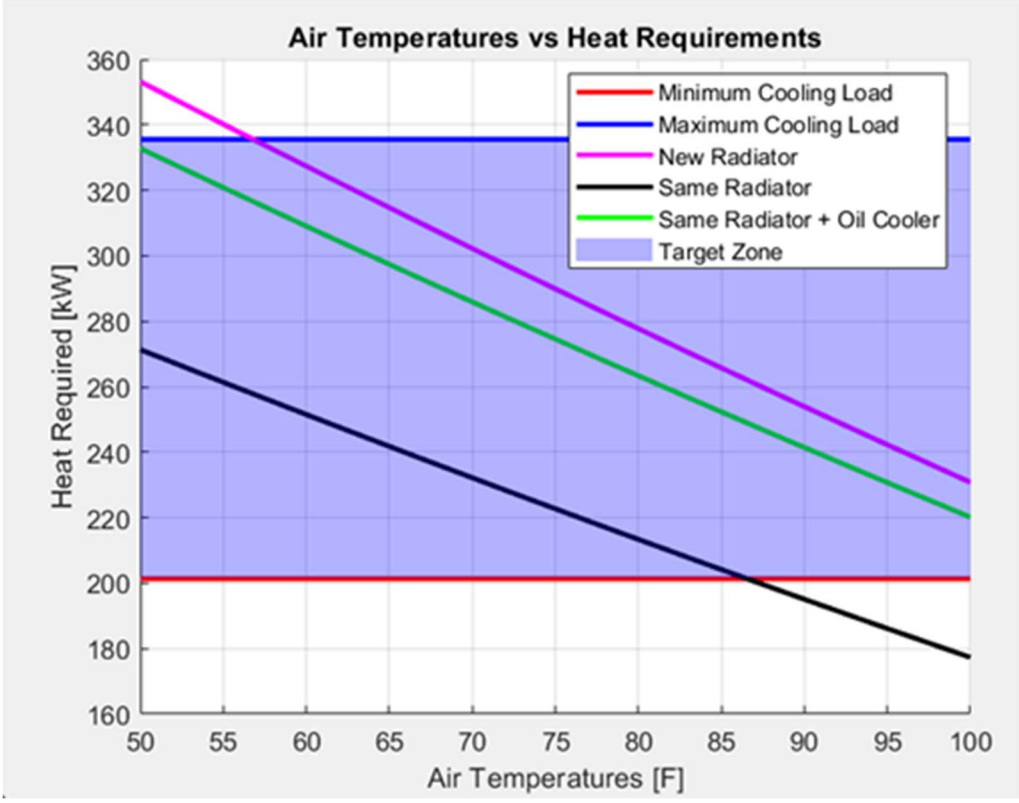

Figure 44: Air temperatures compared with heat exchange results

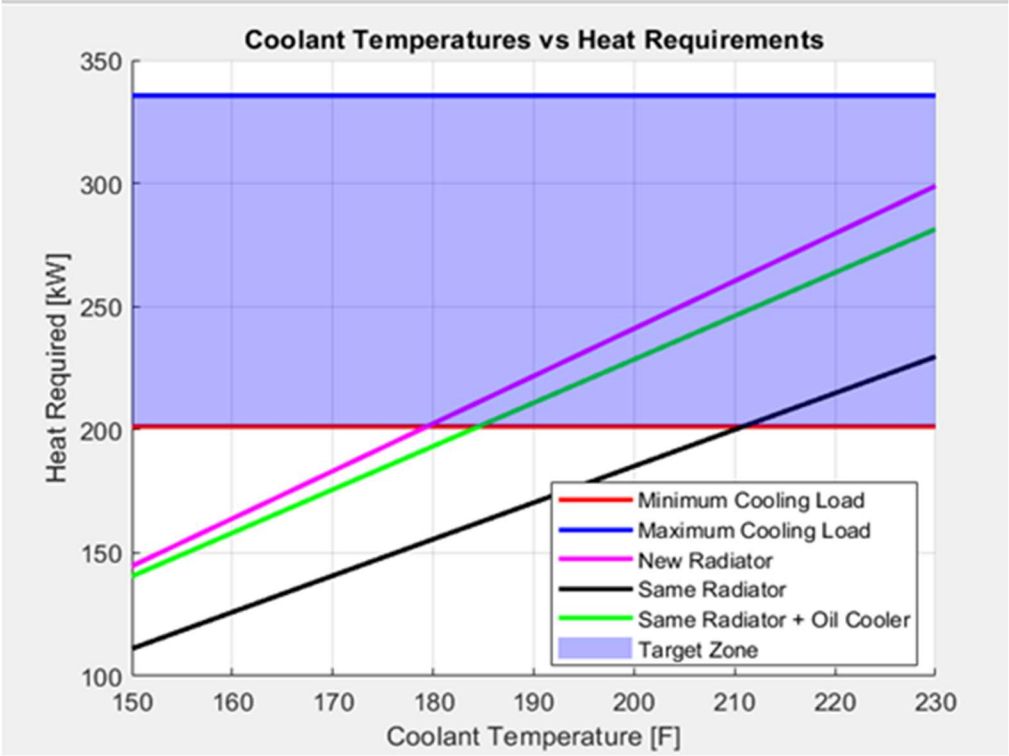

Figure 45: Oil and coolant temperatures compared with heat exchange results

Given these results, it is feasible for the client or another observer to point out that the current radiator is still a viable option for the team. With these results, the team is inclined to agree. A point of uncertainty was the previous team's inability to conduct consistent laps without a cooling issue. Upon deconstruction, the team found many different issues with the cooling system which have since been fixed and the argument could be made that these other problems were the cause of the issues, rather than the radiator. An argument for an upgrade could also be utilized because of the uncertainty of the model; it might be better to upgrade the radiator to cover the teams' bases and decrease the likelihood of a recurring issue. Given these arguments, the model results, and root cause uncertainty, the team has decided to stick with the current radiator to allow for more testing to be conducted. But the team will continue the development process with the idea of obtaining a new radiator. This will allow the team to get more definitive test results and allow for a better educated conclusion.

The next step forward for the cooling team is to deduce a plan to test the current radiator and acquire a new radiator if needed. As of now, the team has plans to install the roll cage and be testing the vehicle by the end of February. To ensure that this occurs, the cooling team will help out wherever possible to ensure that testing happens at the end of February. While this is occurring, the team will also be developing the car with the idea that there will be a newer radiator installed. This will alleviate any extra work that might need to be done if a new radiator is needed. When testing happens, the team will collect data from the radiator and determine if a change is needed. The go/no go day for a new radiator will be March 10th. It will take approximately 2 weeks to acquire the materials needed to install a radiator then 1 week to install, and 1 week to test. This timeline will push the team right up to showcase day which carries a completion risk that is detailed more below. There is also a question of budget. The cooling budget will likely need to be expanded by $200 to $300 to meet the upgrade requirements such as hoses if needed, fans if needed, and new mounting brackets. This will not be an issue as the structural team is forecasted to be $500 under budget due to discounts, and the emergency fund of $600 has not been used.

Differential

Finite Element Analysis

Analysis of the fortified differential, featuring 1/8 in structural plates welded to the differential arms to eliminate the original weak point, began with a finite element analysis (FEA). The differential is driven by a 302-engine producing an estimated 300 ft·lbf of torque. This input torque was then scaled by the drivetrain ratios: a transmission ratio of 3.1 was selected to represent 2nd–3rd gear operation (since sustained, aggressive use of 1st gear is generally unnecessary at High Plains Raceway relative to those gears), along with a 4.1 final-drive (differential) ratio. This value was scaled to 80% to reflect standard drivetrain losses [15]

The resulting ring-gear torque was converted into bearing loads using the ring-gear pitch diameter (7 in) and a 20° pressure angle, yielding tangential and radial force components that were applied to the model. Full derivations and intermediate steps are provided in Appendix A.

These bearing loads were applied to the A356-T6 housing, using an assumed yield strength of 207 MPa [16]. The resulting von Mises stress and factor of safety (FOS) distributions are shown in Figures 46 and 47.

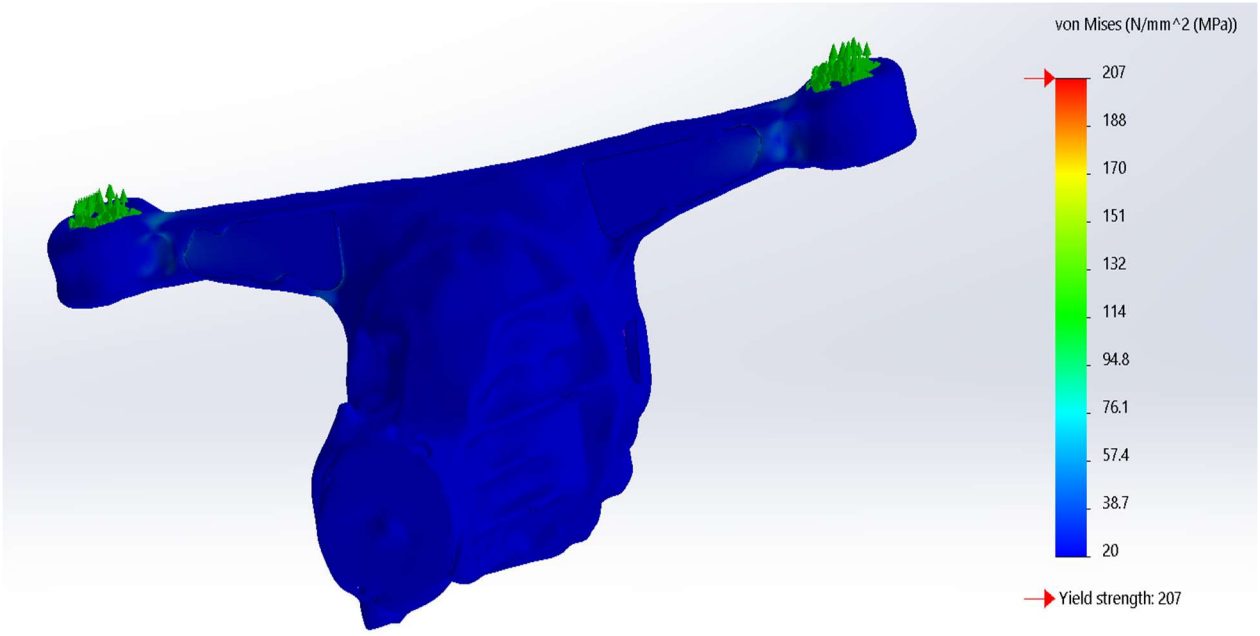

Figure 46: Standard Torque – Von Mises Plot

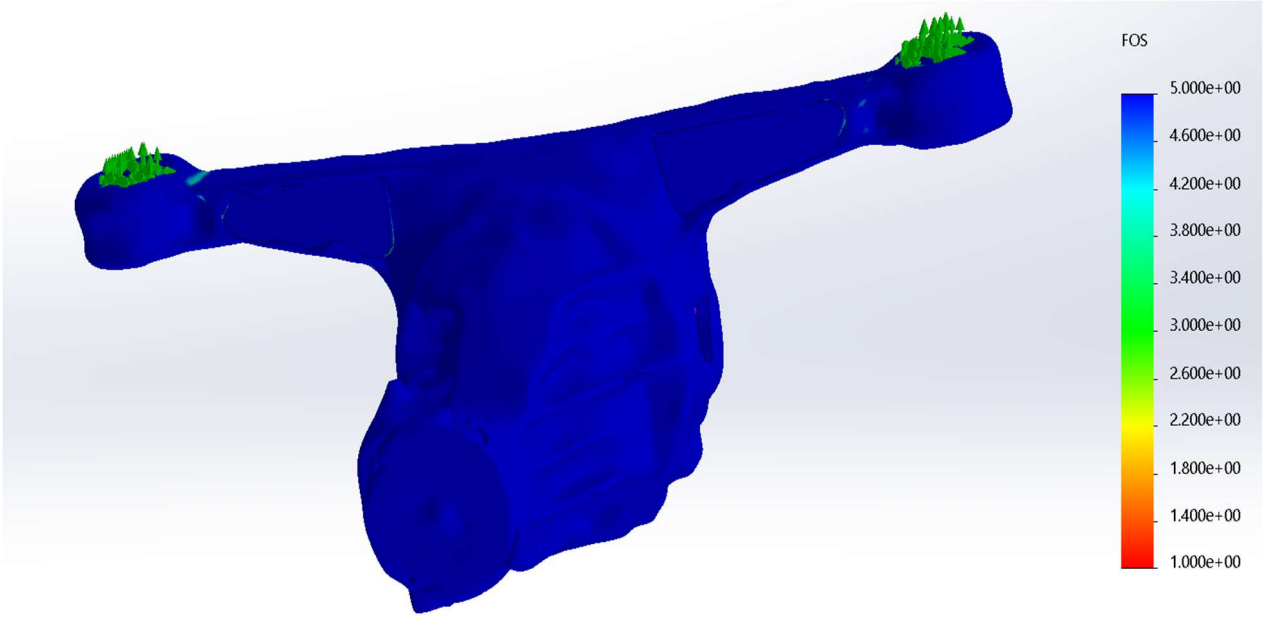

Figure 47: Standard Torque – FOS Plot

Using SolidWorks Simulation (SWS) probes, the baseline analysis produced a minimum factor of safety (FOS) of 3.89 and a maximum von Mises stress of approximately 55 MPa (meeting the criteria in requirement S-1). However, under racing conditions, aggressive clutch engagement and wheel hop can substantially increase the torque transmitted to the differential, potentially by as much as 3 times [17][18]. To capture this worst-case scenario, the calculated bearing loads were scaled by this factor, and the FEA was re-run to verify the assembly remains within safe operating limits. The resulting von Mises stress and factor of safety distributions are shown in Figures 48 and 49.

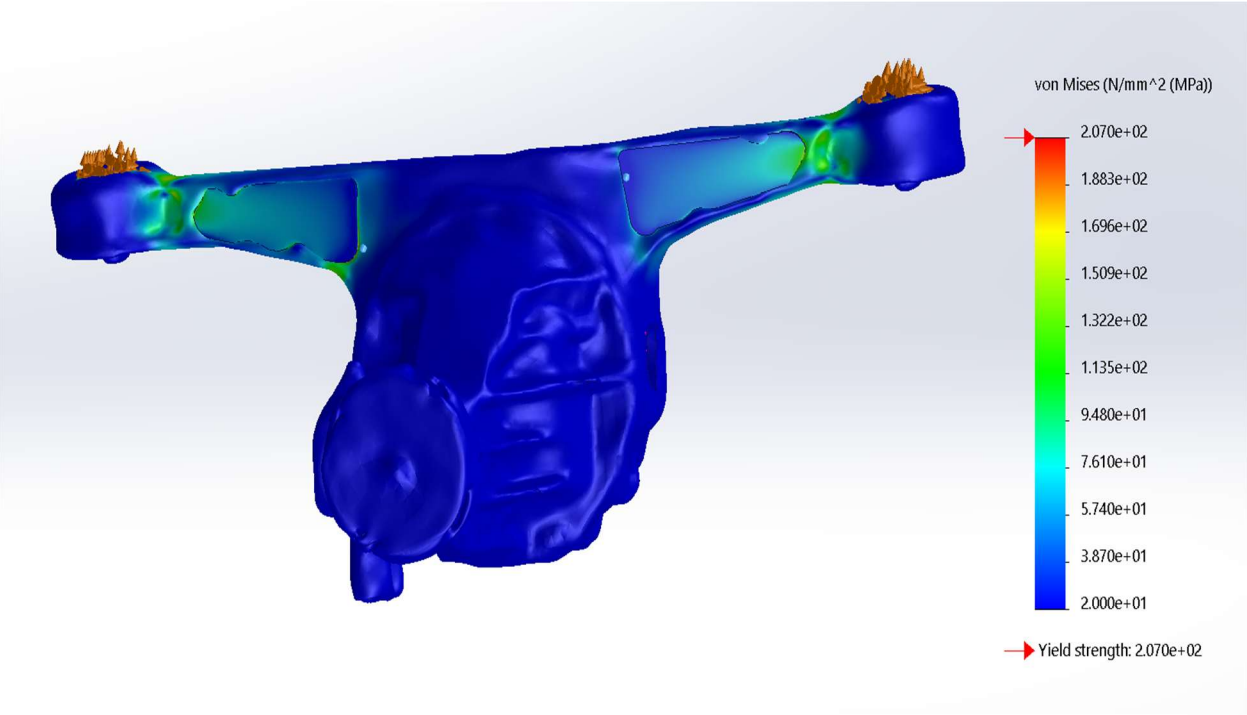

Figure 48: Amplified Torque – Von Mises Plot

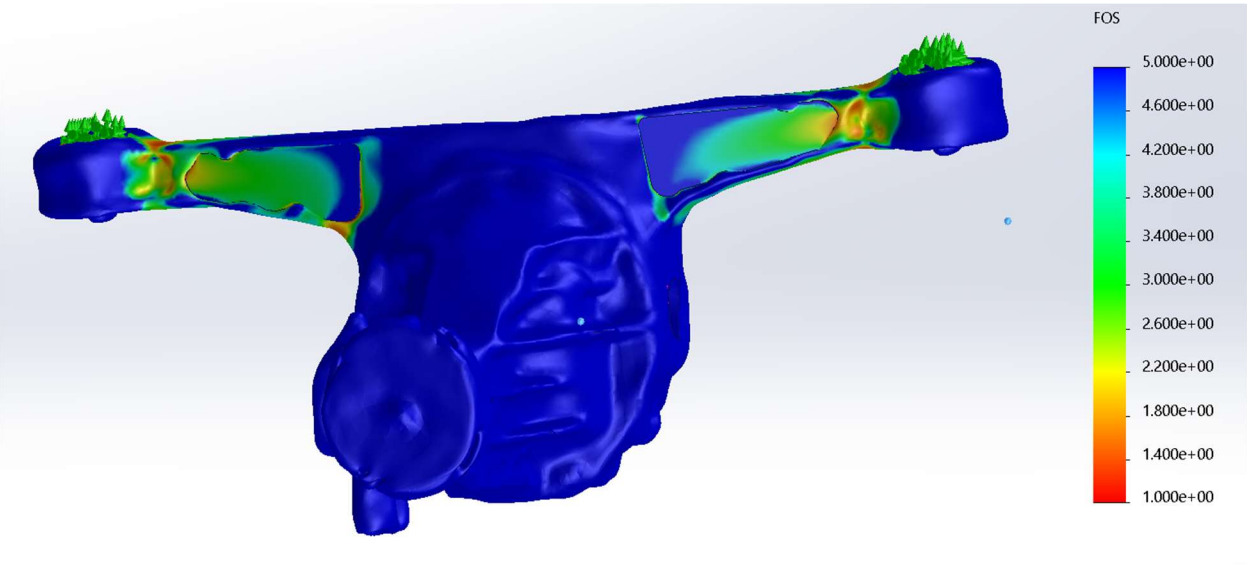

Figure 49: Amplified Torque – FOS Plot

In this worst-case scenario, the factor of safety decreases to a probed minimum of 1.5, with a corresponding maximum von Mises stress of 138 MPa. This loading case will be used as the basis for the fatigue analysis in the following sections, in lieu of a dedicated destructive testing plan. However, when considered to be only a singular shock-loading event, the differential is predicted to survive even the harshest conditions.

Fatigue Analysis

A basis for performing fatigue analysis can be found in the fractured remains of the original 7" differential. Ductile materials exhibit distinct fracture-surface characteristics depending on the failure mode (fatigue-driven crack growth versus instantaneous overload). Fatigue failures typically show smoother, "polished" regions from repeated crack-face contact and progressive propagation, while sudden overload tends to produce a rougher, more irregular texture. Figure 50 shows the differential arm at the manufactured weak point: multiple polished regions are visible (most notably around the weak point and along the arm's bottom face) while the remaining area is consistent with a final instantaneous overload once the remaining ligament could no longer carry the load.

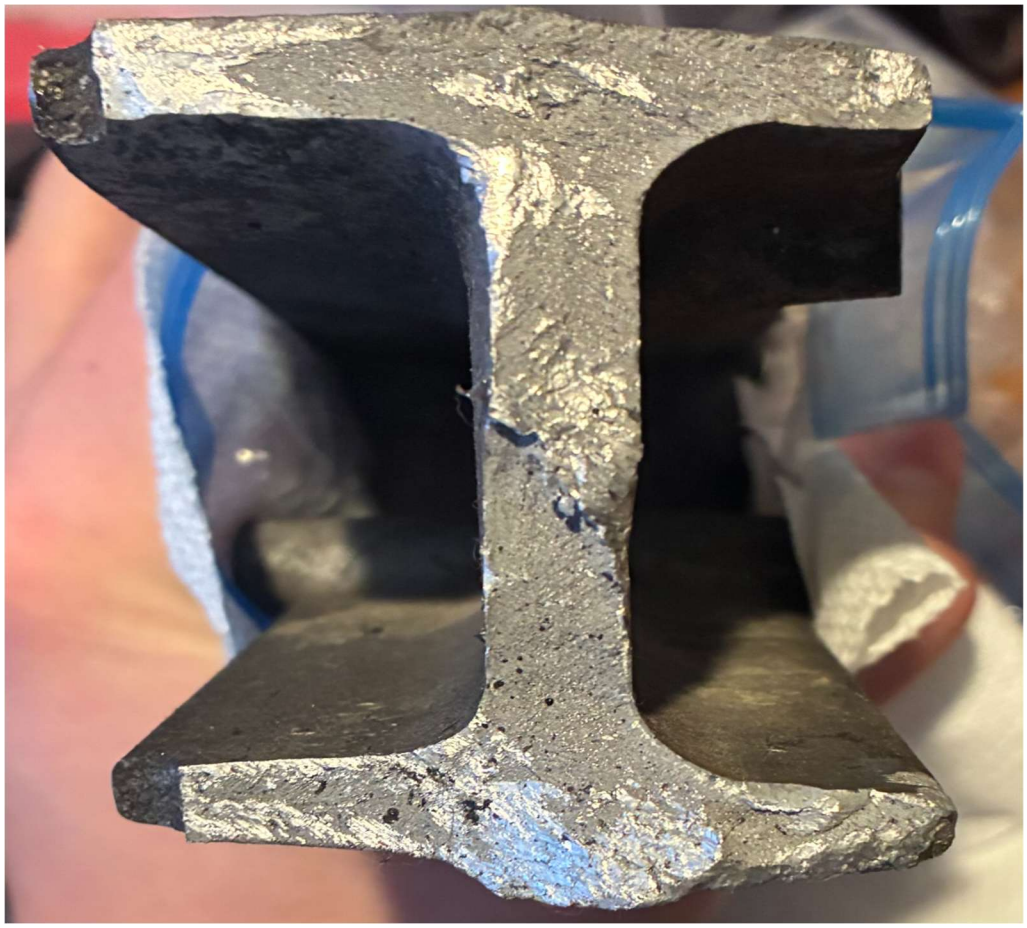

Figure 50: Weak point-side failure face

Figure 51 shows the fracture surface on the other arm, with only a small fatigue-driven region, located in an area identified as a major concern in the FEA. Together, these images help explain what occurred to the differential on track in the summer of 2025: fatigue cracks initiated at the manufactured weak points and propagated over time until the remaining cross-section could no longer support the load, leading to ultimate failure.

Figure 51: Strong-side failure face

To address this failure mode in the current differential configuration, the fatigue analysis was based on a “worst-case” load case. Applied loads were set to three times the nominal calculated values to conservatively represent wheel hop events and harsh clutch engagement.

For this, loading between the maximum (138 MPa) and minimum (-41.4 MPa, to simulate harsh braking) was considered [19][20]. Alternating stress was calculated to be 89.7 MPa and mean stresses to be approximately 48.3 MPa. Utilizing modified Goodman equations to solve for an equivalent “Se”, fatigue stress was found to be ~111.2 MPa. This stress was used for analysis in the Basquin method, using an estimation of 68.3 MPa to propagate failure at one million cycles in A356-T6 aluminum [16]. This resulted in an estimated 53,120 cycles survived under the harshest predicted use (Appendix A)

When compared to the upcoming track layout at High Plains Raceway (Figure 52), this number can be used to predict a possible number of laps.

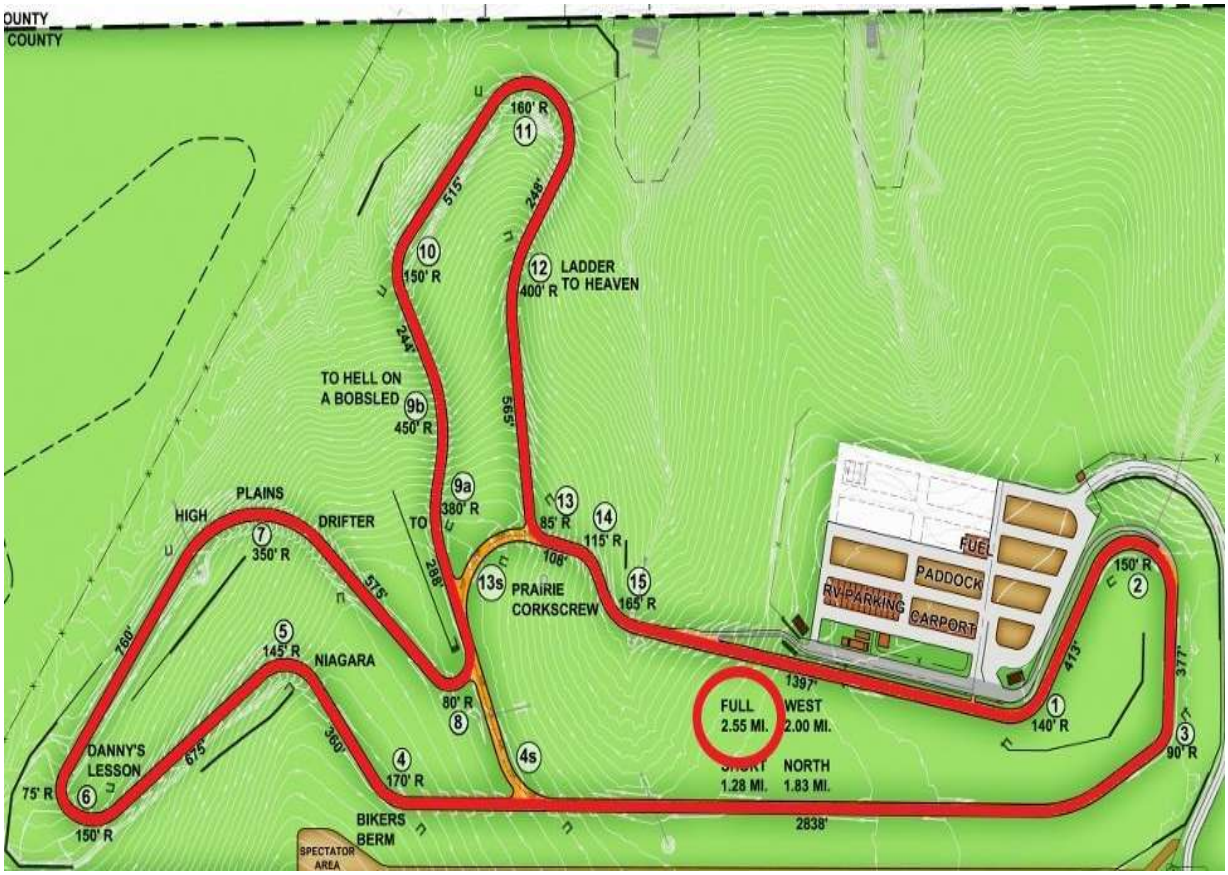

Figure 52: High plains full course

Several corners stand out as candidates for the maximum-loading case, which is driven by abrupt harsh braking, low transmission gearing, and aggressive throttle application. Turns 1, 2, 5, 6, 8, 11, and 13 all have the potential to meet these criteria; accordingly, all seven turns are included to estimate a conservative “worst-case” lap cycle count if the differential is the limiting component. Using simple division against the cycle count calculated above, 7,589 laps are possible under exclusively harsh-use conditions (gentler operation would extend this lifetime). As this is well above the expected lap count for a single event, the result verifies that the reinforced differential satisfies design requirement S-2. When considered alongside the FEA

results, this donated differential solution (provided free of charge) also satisfies all pertinent general requirements (G1, G2, G4).

Roll Cage

The roll cage is a ground-up structural redesign intended to address fitment, inspection, and load-path deficiencies observed in the previous vehicle configuration. The cage geometry was developed using a full 3D scan of the Miata tub to ensure accurate tube placement relative to the actual chassis geometry, driver envelope, and Lemons/SCCA rule constraints. This scan-driven design approach improves fitment confidence, weld accessibility, and inspection readiness prior to fabrication (Figure 53).

The structure establishes continuous load paths from the main hoop through the front down-tubes and rear stays into reinforced chassis mounting plates. Roof-level members are triangulated to distribute rollover loads across multiple load paths, reducing localized bending at individual tube junctions (Figure 54). Door bars are incorporated to improve side-impact resistance while maintaining driver ingress and egress.

All primary members are specified as 1.5 in 1020 cold rolled DOM steel tubing with a 0.120 in wall thickness. This tubing selection provides increased stiffness and strength margin while remaining compatible with the Lemons ruleset and project fabrication constraints. Chassis mounting plates are designed to distribute loads into the vehicle structure while minimizing localized deformation of the underlying sheet metal. Elastic Properties are given in Figure 55.

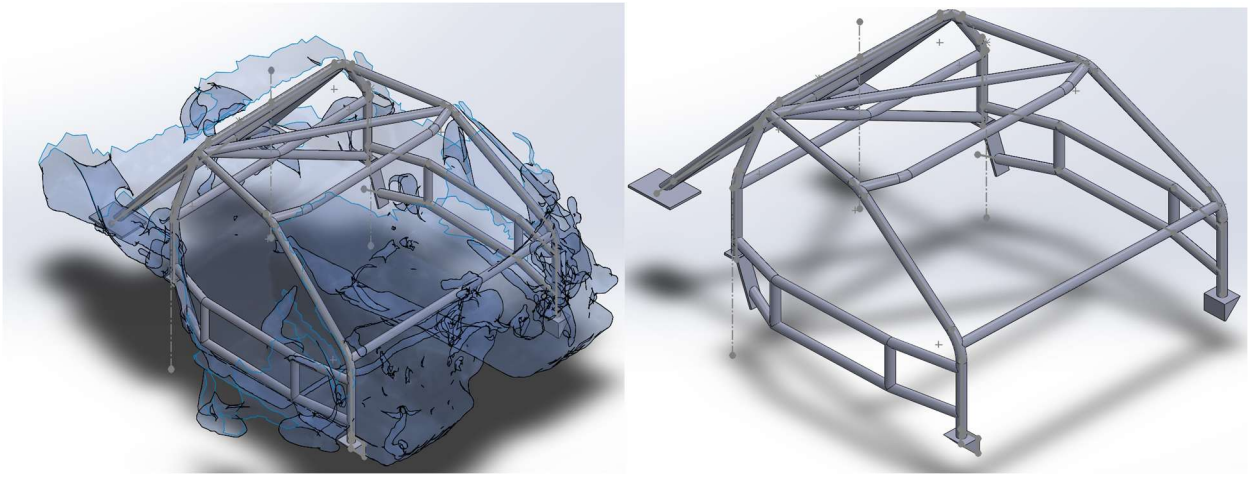

Figure 53: Scan Driven (Left) | Figure 54: Tubes Alone (Right)

Calculations and Finite Element Analysis

Structural analysis of the roll cage is intended to evaluate the response of the primary load-bearing members under conservative rollover, impact, and torsional loading conditions representative of endurance racing. The analysis methodology follows the same conservative philosophy applied to other critical structural components, emphasizing bounding load cases, realistic load paths, and evaluation of worst-case geometry.

Analysis Environment and Model Setup

The structural integrity of the roll cage was evaluated using SolidWorks Simulation utilizing a finite element analysis (FEA) approach. The assembly was modeled using second-order solid tetrahedral elements to accurately capture the volumetric stress distribution through the tube walls and at the complex intersections of the chassis. A curvature-based mesh was implemented to automatically increase mesh density around the tube joints and bends, ensuring that high-gradient stress zones were sufficiently resolved without unnecessary computational overhead. For this analysis, welded joints are idealized as perfectly rigid bonded contacts, assuming that weld penetration and throat thickness are sufficient to transfer all loads across the interface without independent failure of the filler material.

Property	Value	Units
Elastic Modulus	2.05e+11	N/m^2
Poisson's Ratio	0.29	N/A
Shear Modulus	8e+10	N/m^2
Mass Density	7870	kg/m^3
Tensile Strength	420000000	N/m^2
Compressive Strength		N/m^2
Yield Strength	350000000	N/m^2
Thermal Expansion Coefficient	1.17e-05	/K
Thermal Conductivity	51.9	W/(m·K)
Specific Heat	486	J/(kg·K)
Material Damping Ratio		N/A

Figure 55: Material Properties

Load cases are constructed to represent roof contact during a rollover event, lateral loading during a side-impact scenario, and torsional loading associated with asymmetric ground contact. Rollover loading is applied through distributed forces at the roof structure, primarily at the main

hoop and front down-tube intersections, to represent load transfer during roof-to-ground contact (Figure 56). Side-impact loading is applied laterally at the upper side structure to evaluate door bar and side-member load paths. Torsional loading is applied through opposing vertical loads at diagonally opposite corners to assess global cage stiffness.

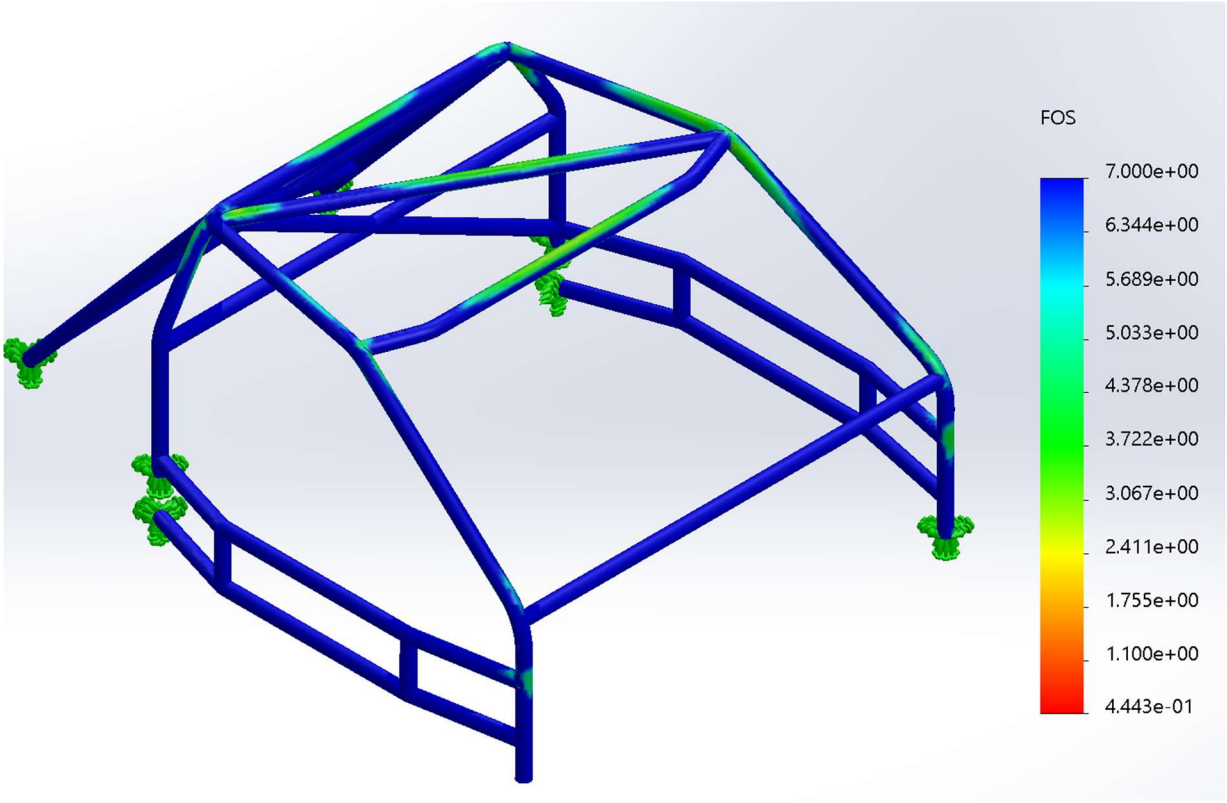

Figure 56: Top Load

To validate the cage against catastrophic failure, two primary static load cases were analyzed based on expected vehicle mass and safety margins. A rollover case was simulated by applying a 4,000 lb static load as a distributed force across the top plane of the cage (main hoop and roof halo). Additionally, a side-impact case was modeled with a 3,000 lb static load distributed across the door bar assembly. These magnitudes represent a Dynamic Amplification Factor (DAF) of approximately 1.6x the anticipated race-ready vehicle weight, providing a conservative margin for impact energy. The model is constrained via fixed geometry at the base of the spreader plates, simulating the rigid integration of the cage into the Miata's floor pans and frame rails. ANSI 1020 Cold Rolled Steel properties were used to baseline the DOM tubing, ensuring the peak Von Mises stresses remain below the material yield strength.

Top load: 4klbs (2x weight of car)

Side load: 3klbs (1.5x weight of car)

Boundary conditions are applied at the chassis mounting plates to represent welded attachment to the vehicle structure. These constraints are selected to conservatively approximate load transfer into the chassis while avoiding artificial stiffening of the cage structure (Figure 57).

Evaluation of analysis results focuses on stress distribution, deformation behavior, and relative load sharing between primary members. Critical locations are identified based on geometric transitions and load path convergence, including the main hoop to roof-member intersections, front down-tube junctions, door bar connections, and mounting plate interfaces (Figure 57).

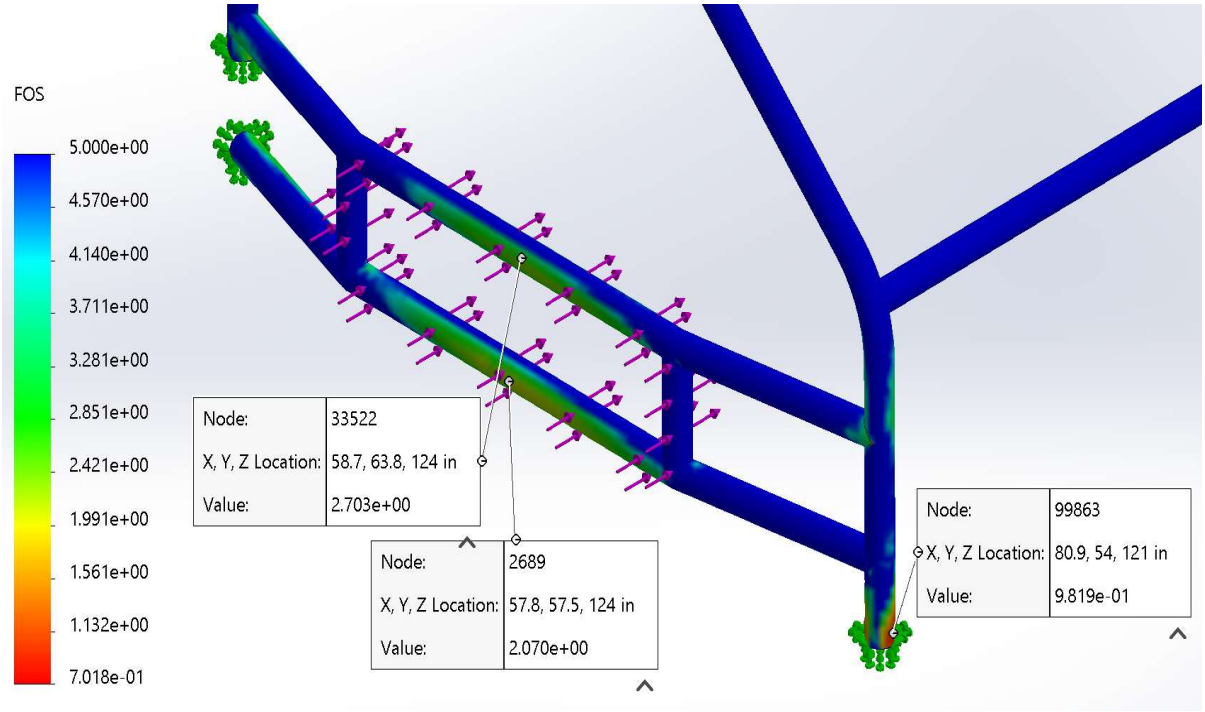

Figure 57: Side Load

To evaluate the structural performance, specific probe locations were selected at critical junctions, including the main hoop-to-spreader plate interface and the door bar intersections. The evaluation method focused on identifying peak Von Mises stresses and comparing them against the yield strength of the 1020 DOM steel. While a "hot spot" was identified near the base of the vertical main hoop post, this is attributed to Saint-Venant's Principle; the proximity to the fixed boundary condition at the spreader plate creates a stress concentration that does not accurately reflect the physical behavior of the steel. Final analysis plots, deformation contours, and quantitative summaries will be included in Appendix F and referenced here once analysis is complete.

Risk Mitigation & Test Plans

Purpose and verification approach

Risks are prioritized using the FMEA tool (included in a separate document). The plan below links the highest-priority failure modes to mitigation actions and defines the tests/inspections and pass-fail criteria used to confirm readiness for sustained track operation.

System-level verification sequence

Bench/static: continuity, sensor checks, relay/switch checks, leak/pressure checks, and dimensional/material verification.

Shakedown: short runs to establish stable baselines (temps, oil pressure, fault codes) and catch integration defects early.

Track validation: progressively higher load and duration sessions to prove sustained operation and to drive upgrade decisions (cooling).

All results are logged; any failed acceptance item triggers stop-and-fix before continued high-load testing.

Subsystem risk-to-test matrix

Subsystem	Top risks (from FMEA)	Mitigation + verification tests (with acceptance criteria)
Electrical	Intermittent opens/shorts from vibration-loosened joints Heat/abrasion degrading insulation and sensor signal integrity	**Mitigate:** crimp + seal joints; add strain relief/abrasion protection; replace damaged terminals; route away from heat. **Verify:** bench sensor check with harness manipulation (O2/MAP/ECT/ACT); pull/cycle durability check; relay/switch bench test; 10-min steady runtime installed. **Accept:** continuity stable after cycling; stable sensor readings; no wiring-driven fault codes; switching stable with no abnormal heating.
Differential	Crack initiation/propagation at arms and bushing interface Leak development during service life	**Mitigate:** analysis-backed reinforcement; fracture lab/technical advisor review of assumptions and load cases. **Verify:** install inspection (mounts, bushings, leaks) + pit-stop inspections every session focused on critical regions.

		Accept: no visible crack initiation/progression and no leaks during early track testing; any crack triggers removal from race conditions.
Roll cage	Rule non-compliance (tube spec or dimensions) Weld defects or fabrication errors requiring rework	**Mitigate:** scan-derived geometry + CAD checks; tubing meets/exceeds minimums; staged checks; mock inspection at tack stage. **Verify:** pre-weld (OD/wall/material + fit), post-weld (weld quality + key dimensions), operational (post-session checks for crack indicators). **Accept:** meets rule specs/dimensions; no weld defects requiring rework; no early anomaly indicators during shakedown.
Powertrain	Leaks or fault codes from integration errors Overheating or oil pressure loss under sustained load	**Mitigate:** inspection gates pre-start and post-session for the revitalized engine/transmission; driver monitors oil pressure and temps with conservative shutdown thresholds. **Verify:** post-install (alignment, mounts, grounds, leaks), first startup (fault codes, baselines), progressive track sessions (easy to full pace) with logging + post-session checks. **Accept:** no persistent leaks; temps/pressures within requirement limits; no sustained fault codes; no degradation trend across sessions.
Cooling	Cannot maintain temperature requirement under race load Schedule/packaging risk if upgrade decision is late	**Mitigate:** go/no-go upgrade decision by March 10 using track data; parallel-plan procurement/packaging; use fit/positioning options as needed. **Verify:** pressure test; stationary repeatability test (10-min run, 10-min cooldown, repeat); track sessions with increasing intensity recording max/avg temps. **Accept:** no leaks; coolant temp stays below requirement limit during track validation;

		decision gate met by March 10 with sufficient data to commit.
Aerodynamics	Component loosening/failure under vibration/loads Performance uncertainty without specialized instrumentation	**Mitigate:** controlled-failure (sacrificial) features; fastener retention + inspection-driven operation; repairs via replaceable sacrificial elements. **Verify:** pre/post session inspections; tuft testing (flow direction/attachment); repeatable ride-height photo captured at consistent track point; driver feedback. **Accept:** no progressive structural degradation; fasteners secure; trends repeatable/consistent; damage repairable without major redesign.

Safety

All fabrication, integration, and testing activities will be conducted in accordance with Colorado School of Mines EHS requirements and the project's Design Hazards/Safety Plan. The team will use task-appropriate PPE at all times (eye protection minimum; face shield/hearing protection for cutting and grinding; welding PPE and ventilation controls for hot work), maintain clean work areas to reduce trip and fire hazards, and keep fire extinguishers available during hot work and first startup operations. Vehicle work will follow standard lifting practices (rated jack stands, never a jack alone), and torque-critical fasteners will be verified prior to operation.

During shakedown and track testing, safety will be managed through conservative stop criteria. The driver will continuously monitor coolant temperature and oil pressure and will terminate a session immediately if readings exceed defined limits or if abnormal vibration/noise is observed. After each run, the team will inspect for leaks, loosened connections, and structural concerns; any critical anomaly triggers a stop-and-fix action before continued testing.

Preliminary Drawings

Wing

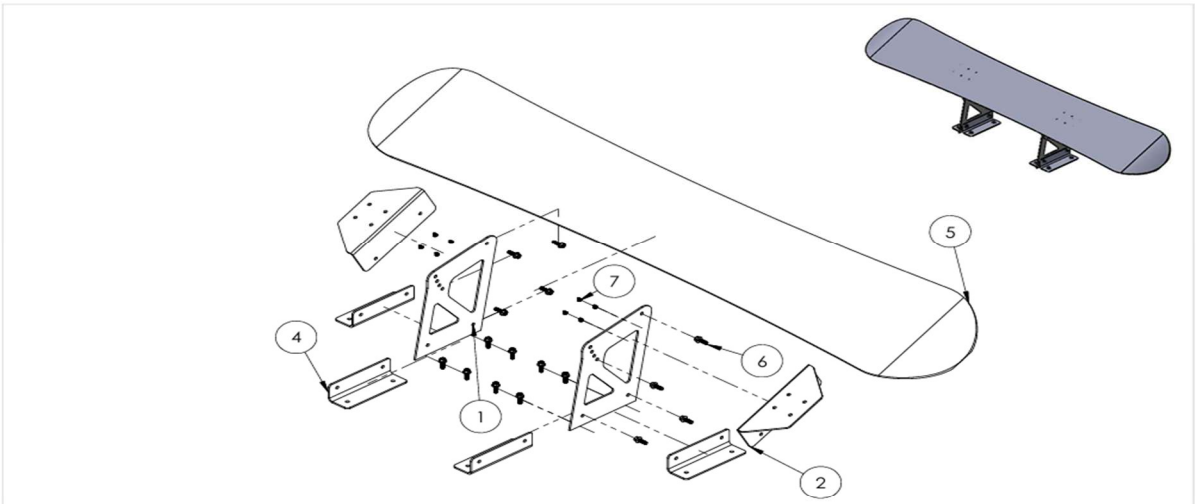

ITEM NO.	PART NUMBER	DESCRIPTION	QTY.
1	2564-V	Steel	2
2	2564-B	Steel	1
3	2564-BM	Steel	1
4	2564-T	Steel	4
5	N/A	Composite	1
6	90409A121	1/4"-28	16
7	91772A190	M6 14mm	8

DIMENSIONS ARE IN INCHES
TOLERANCES:
FRACTIONAL ± 1/16
ANGULAR: ± 1°
X.X ± 0.030
X.XX ± 0.010
X.XXX ± 0.005
UNLESS OTHERWISE SPECIFIED

MATERIAL: PART DEPENDENT
FINISH: PART DEPENDENT
QUANTITY: 1

	NAME	DATE
ENGINEER	JACKSON MCCOOL	01/23/2026
CHECKED		
ENG APPR.		
MFG APPR.		
Q.A.		
COMMENTS:		

MECHANICAL ENGINEERING
COLORADO SCHOOL OF MINES

PART NAME: WING ASSEMBLY
DESC: FULL WING ASSEMBLY & EXPLODED VIEW

SIZE A | PART NO. 2564 | REV.
SCALE: 1:4 | FILE: MOUNTINGASSEMBLYDRAWING | SHEET 1 OF 5

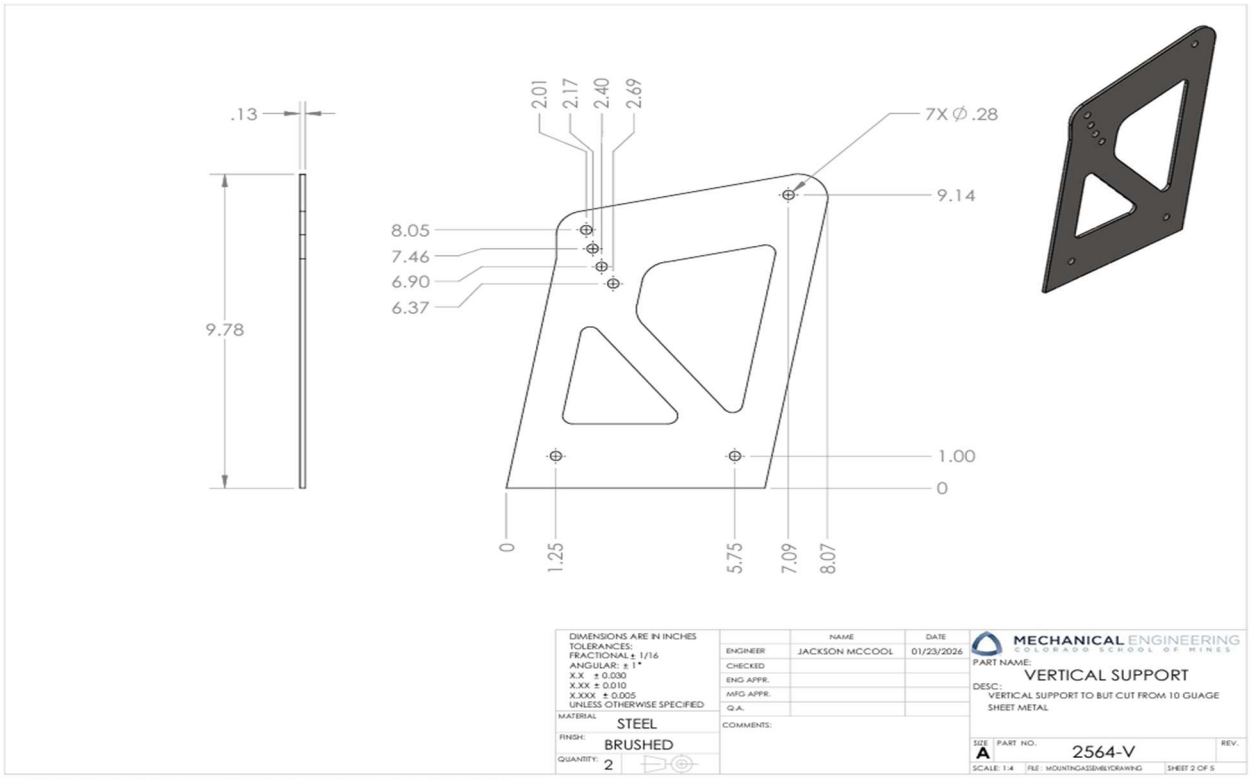

DIMENSIONS ARE IN INCHES TOLERANCES: FRACTIONAL ± 1/16 ANGULAR: ± 1° X.X ± 0.030 X.XX ± 0.010 X.XXX ± 0.005 UNLESS OTHERWISE SPECIFIED		NAME	DATE
MATERIAL: STEEL	ENGINEER	JACKSON MCCOOL	01/23/2026
FINISH: BRUSHED	CHECKED		
QUANTITY: 2	ENG APPR.		
	MFG APPR.		
	Q.A.		
	COMMENTS:		

MECHANICAL ENGINEERING
COLORADO SCHOOL OF MINES

PART NAME: VERTICAL SUPPORT

DESC: VERTICAL SUPPORT TO BUT CUT FROM 10 GUAGE SHEET METAL

SIZE	PART NO.	REV.
A	2564-V	

SCALE: 1:4 | FILE: MOUNTINGASSEMBLYDRAWING | SHEET 2 OF 5

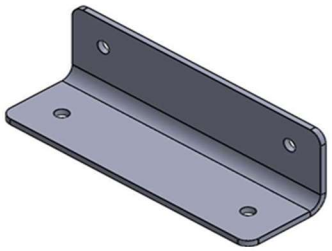

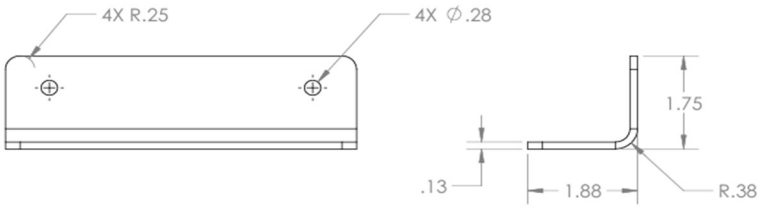

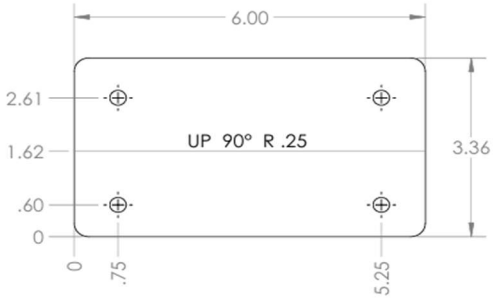

DIMENSIONS ARE IN INCHES TOLERANCES: FRACTIONAL ± 1/16 ANGULAR: ± 1° X.X ± 0.030 X.XX ± 0.010 X.XXX ± 0.005 UNLESS OTHERWISE SPECIFIED		NAME	DATE
MATERIAL: STEEL	ENGINEER	JACKSON MCCOOL	01/23/2026
FINISH: BRUSHED	CHECKED		
QUANTITY: 2	ENG APPR.		
	MFG APPR.		
	Q.A.		
	COMMENTS:		

MECHANICAL ENGINEERING
COLORADO SCHOOL OF MINES

PART NAME: TRUNK BRACKET

DESC: 10 GUAGE STEEL SHEET METAL BRACKET TO BOLT TO TRUNK & VERTICAL BRACKET

SIZE	PART NO.	REV.
A	2564-T	

SCALE: 1:2 | FILE: MOUNTINGASSEMBLYDRAWING | SHEET 3 OF 5

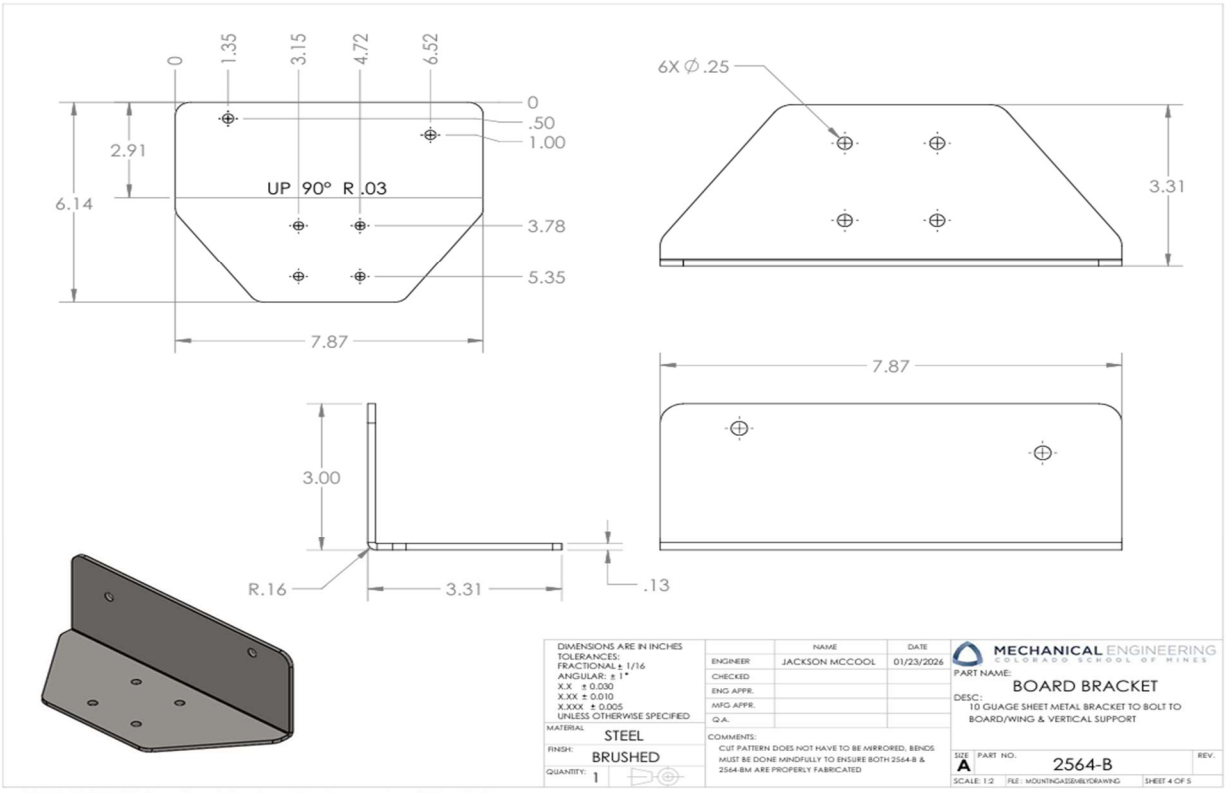

SOLIDWORKS Educational Product. For Instructional Use Only.

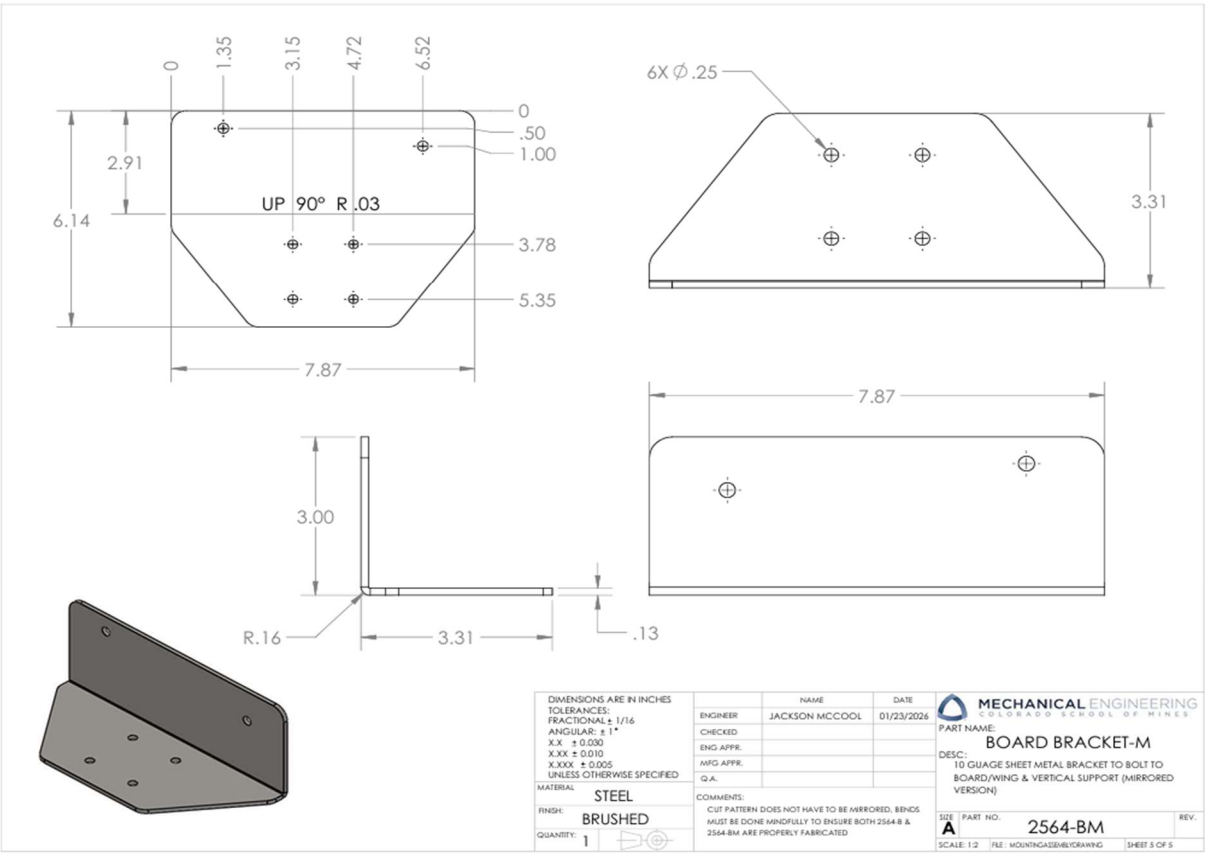

SOLIDWORKS Educational Product. For Instructional Use Only.

Splitter

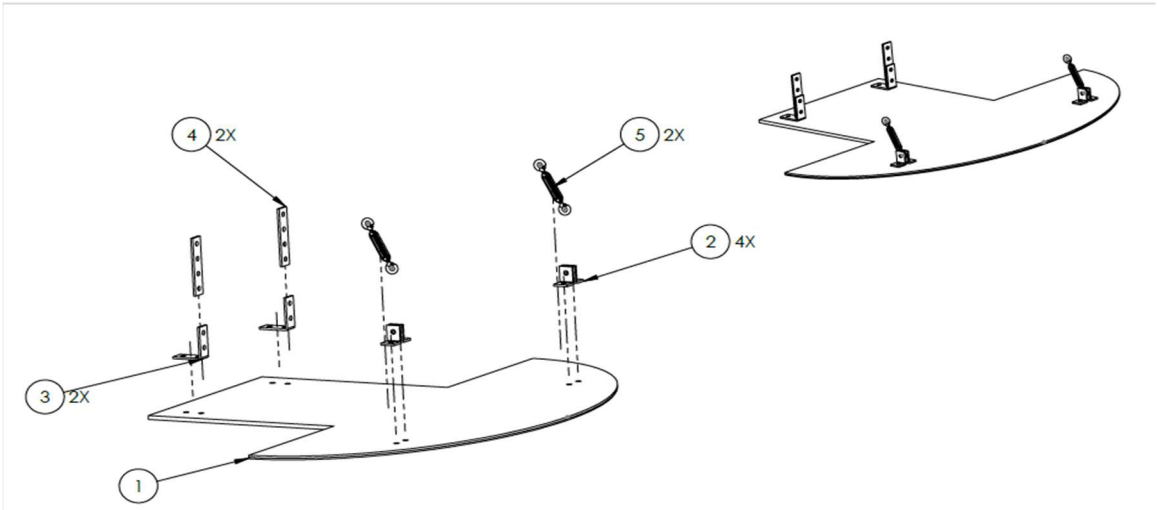

ITEM NO.	PART NUMBER	DESCRIPTION	QTY.
1	11726	Plywood Splitter	1
2	33125T32	Strut Channel Bracket	4
3	33125T34	Strut Channel Bracket	2
4	33125T163	Strut Channel Bracket	2
5	3003T19	Cast Aluminum Turnbuckle-Not for Lifting	2

DIMENSIONS ARE IN INCHES
TOLERANCES:
FRACTIONAL ± 1/16
ANGULAR: ± 1°
X.X ± 0.030
X.XX ± 0.010
X.XXX ± 0.005
UNLESS OTHERWISE SPECIFIED
MATERIAL
FINISH:
QUANTITY: 1

	NAME	DATE
ENGINEER	STERLING SCHRADER	1/27/2026
CHECKED		
ENG APPR.		
MFG APPR.		
Q.A.		

COMMENTS: COMMENTS

MECHANICAL ENGINEERING
COLORADO SCHOOL OF MINES
PART NAME:
DESC: MIATA SPLITTER AND MOUNTING ASSEMBLY
SIZE A | PART NO. | REV. 2
SCALE: 1:12 | SHEET 1 OF 1

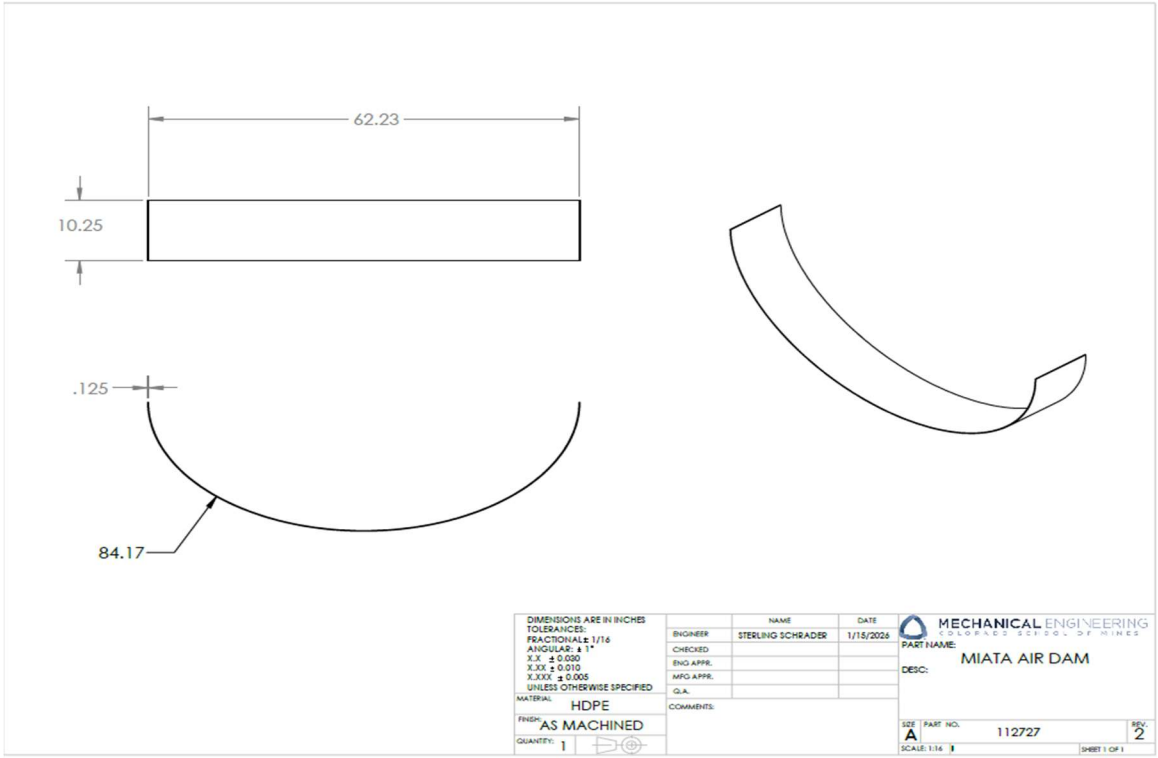

DIMENSIONS ARE IN INCHES
TOLERANCES:
FRACTIONAL ± 1/16
ANGULAR: ± 1°
X.X ± 0.030
X.XX ± 0.010
X.XXX ± 0.005
UNLESS OTHERWISE SPECIFIED
MATERIAL: HDPE
FINISH: AS MACHINED
QUANTITY: 1

	NAME	DATE
ENGINEER	STERLING SCHRADER	1/15/2026
CHECKED		
ENG APPR.		
MFG APPR.		
Q.A.		

COMMENTS:

MECHANICAL ENGINEERING
COLORADO SCHOOL OF MINES
PART NAME:
DESC: MIATA AIR DAM
SIZE A | PART NO. 112727 | REV. 2
SCALE: 1:16 | SHEET 1 OF 1

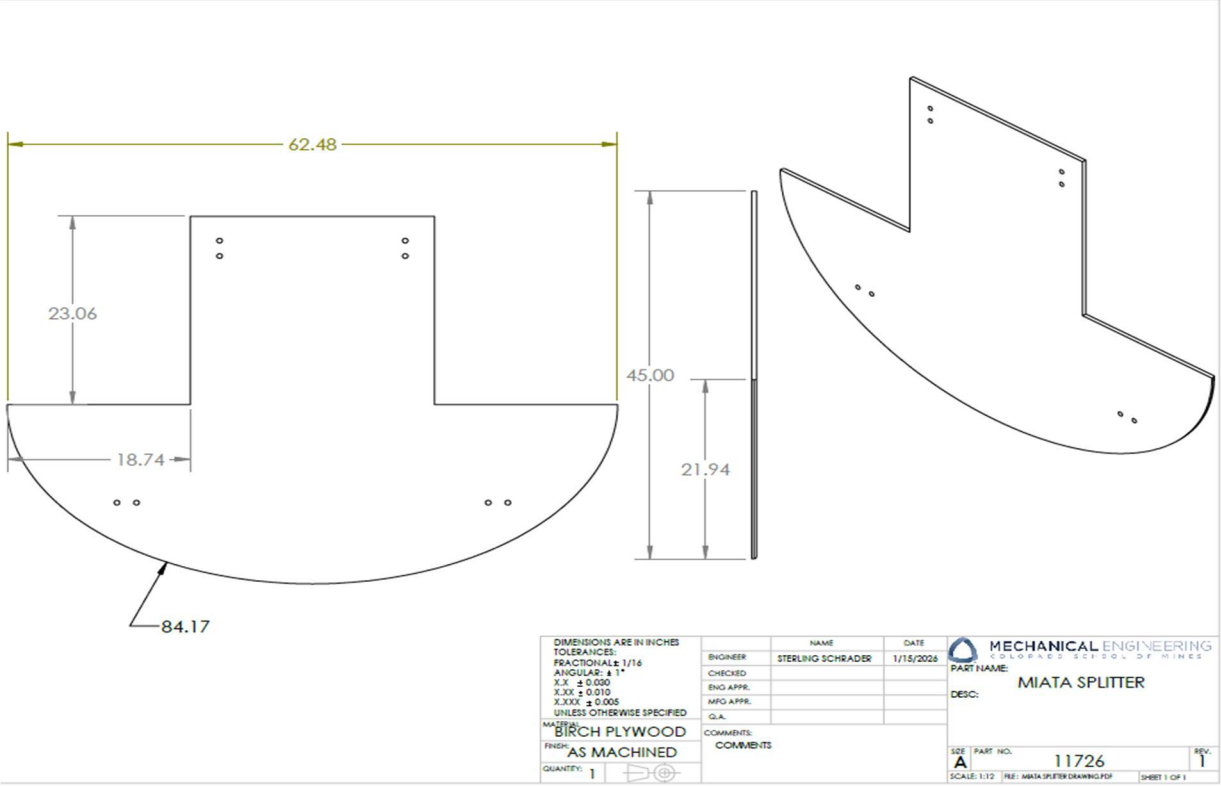

Headlight Intake

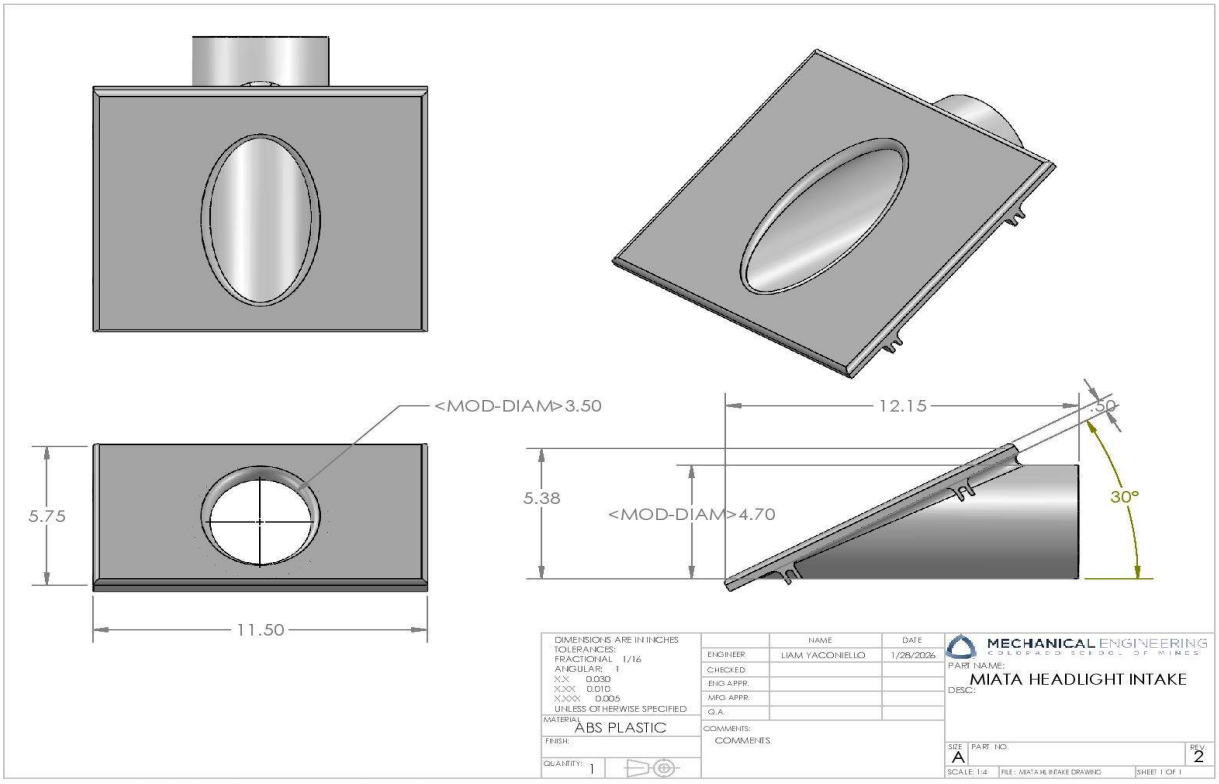

Differential Plates

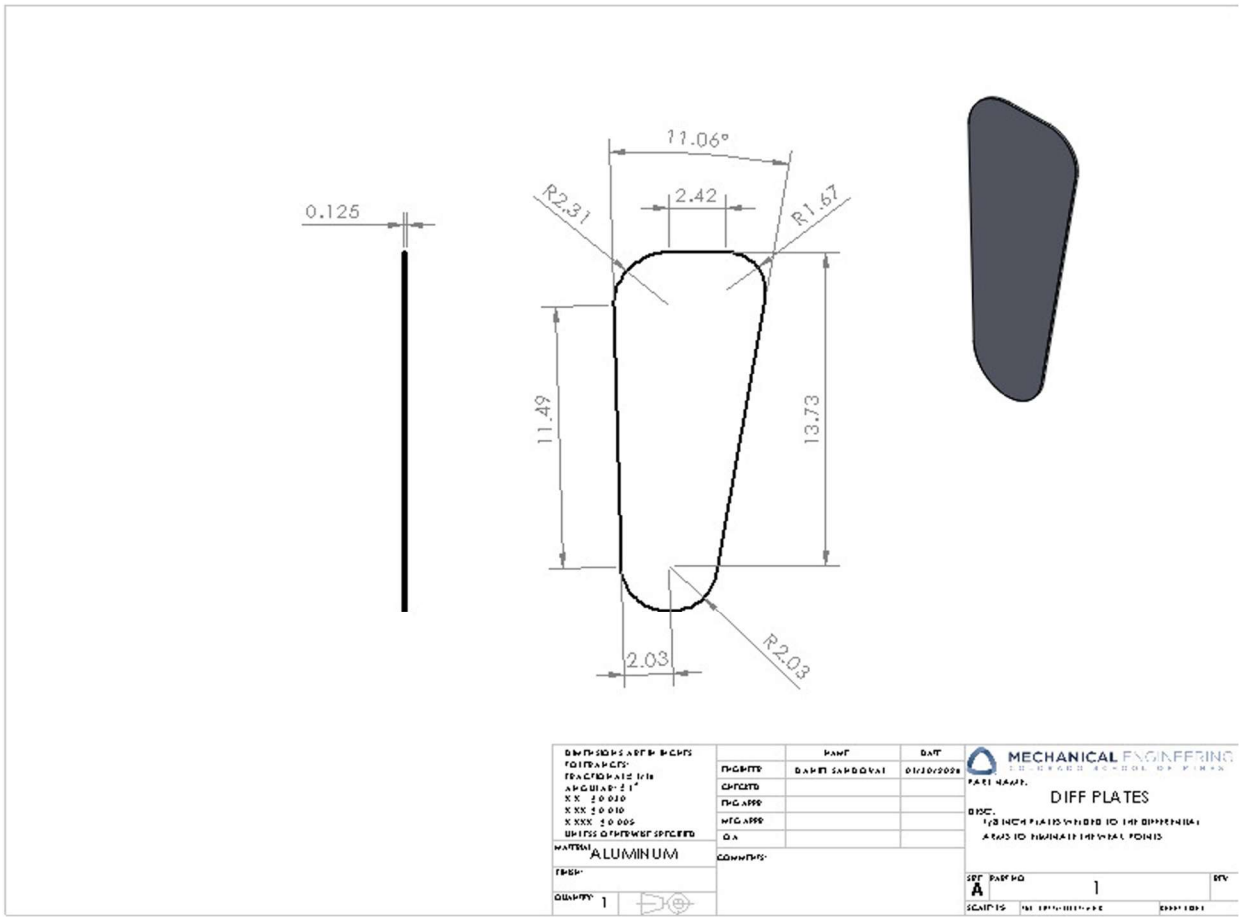

Conclusion

This Critical Design Report (CDR) documents the Pulp Friction Crew's build-ready design direction for a rule-compliant Mazda Miata endurance race car targeting Summer 2026 competition at High Plains Raceway. Since the PDR, the team has converged on final subsystem architectures across Powertrain, Structures, Electronics, and Aerodynamics, with design selections driven by the specific reliability failures observed in the prior campaign (differential housing cracking, chronic overheating, wiring/harness degradation, and roll-cage deficiencies). The resulting design package is intended to be sufficiently complete for client/advisor review, fabrication planning, and verification execution, with requirements traceability maintained through the system and subsystem requirement tables (Tables 1–5).

Across subsystems, the design approach emphasizes durability and inspect ability first, then performance improvements that do not compromise reliability or manufacturability. Key outcomes include: (1) a revitalized powertrain system focused on dependable endurance operation refreshing high-wear components, improving service access, and ensuring driveline compatibility with the selected gearing and operating regime, (2) a reinforced differential strategy that preserves geometry while improving fatigue robustness, (3) a cooling and ducting direction intended to maintain safe operating temperatures under sustained race loading, (4) an electronics reliability plan centered on harness remediation, relay/fusing protection, and staged integration of instrumentation, and (5) aerodynamic components (splitter/diffuser/wing and ducting interfaces) validated via analysis with checks against structural feasibility and packaging constraints. Collectively, these decisions support the project's top-level requirements: survival of race loadings (G-1), Lemon's compliance (G-2), client approval prior to fabrication (G-3), and budget adherence (G-4).

The updated project schedule (critical path and dependencies) and the current budget status are provided in the appendices. The schedule is organized to complete fabrication and subsystem integration early enough to enable meaningful shakedown and track validation prior to race execution, reducing risk of late discovery failures. Budget tracking is maintained with the same intent: ensure required safety/reliability items are funded first, protect long-lead purchases, and document sponsorship/assumption dependencies. As of 1/31, the team's cost position is $1664.00 against a planned total of $3962.40. Additional information is available in the budget tracker (attached separately).

Appendices

APPENDIX A - Differential Calculations

$T_{flywheel} := 300 \cdot ft \cdot lbf \quad i_t := 3.1 \quad i_d := 4.1 \quad \eta := .8 \quad \theta := 20 \cdot deg$

$RGT := i_t \cdot i_d \cdot T_{flywheel} \cdot .8 = (4.136 \cdot 10^3)\ N \cdot m \quad Ring\_Gear\_D := 7\ in$

$r := \frac{Ring\_Gear\_D}{2} = 0.089\ m \quad F_t := \frac{RGT}{r} = (4.652 \cdot 10^4)\ N \quad F_r := F_t \cdot \tan(\theta) = (1.693 \cdot 10^4)\ N$

Normal Predicted Torque:

$F\_PINION_{res} := \left(\sqrt[2]{F_t^{\,2} + F_r^{\,2}}\right) = (4.951 \cdot 10^4)\ N$

$F_{res\_bearing} := \frac{F\_PINION_{res}}{2} = (2.475 \cdot 10^4)\ N$

3x torque modification due to wheel hop, harsh driving

$MOD := 3 \quad F\_PINION_{res} := \left(\sqrt[2]{F_t^{\,2} + F_r^{\,2}}\right) \cdot MOD = (1.485 \cdot 10^5)\ N$

$F_{res\_bearing} := \frac{F\_PINION_{res}}{2} = (7.426 \cdot 10^4)\ N$

Fatigue Calculations (k = 0.3 to simulate harsh braking)

$\sigma_{max} := 138 \cdot MPa \quad k := 0.3 \quad \sigma_{min} := -k \cdot \sigma_{max} = -41.4\ MPa$

$\sigma_a := \frac{\sigma_{max} - \sigma_{min}}{2} = 89.7\ MPa \quad \sigma_m := \frac{\sigma_{max} + \sigma_{min}}{2} = 48.3\ MPa$

Modified Goodman (est. Sut @ 250 MPa):

$S_e := \frac{\sigma_a}{1 - \left(\frac{\sigma_m}{250 \cdot MPa}\right)} = 111.18\ MPa$

Basquin Model (b = ~ -0.166) (~68.3 MPa @ 10^6):

$\sigma'_f := 68.3 \cdot MPa \cdot \left(10^6\right)^{0.166} = 676.738\ MPa \quad N := \left(\frac{\sigma'_f}{S_e}\right)^{\frac{1}{.166}} = 5.312 \cdot 10^4$

With ~7 shocks possible per lap (conservative estimate):

$\frac{N}{7} = 7.589 \cdot 10^3$ laps possible

APPENDIX B – Electrical

Appendix B1 – Testing Plans/Procedures

Electrical Test Plan

The procedures for benchtop testing these components are as follows:

- ACT & ECT Sensors [21]
  - As both sensors are thermistors, their respective positive & negative leads will be attached to a multimeter and resistance across each will be read
  - The sensors will be subjected to room temperature (~74 degrees Fahrenheit) with an expected resistance of 35k – 40k Ohms
  - The sensors will be subjected to cold air/ice water (~32 degrees Fahrenheit or below) with an expected resistance of 58k – 60k Ohms or more depending on the final temperature of the air/water
    - If the sensor does not increase resistance, it will be deemed dead
    - This should be sufficient to see if the sensors work as intended, but for a full spectrum test, hot conditions will be used as well
  - The sensors will be subjected to hot air/heated water (~100 degrees Fahrenheit) with an expected resistance of 20k – 22k Ohms or less depending on the final temperature of the air/water
    - If the sensor does not decrease resistance, it will be deemed dead
- MAP Sensor [21]
  - The sensor must be powered, so it will be set up to a 5V power source to its V-ref terminal and ground terminal. An oscilloscope will be connected to the ground terminal and signal terminal of the MAP sensor. A 5.1kΩ pullup resistor must bridge between the V-ref and signal wire to power the device as well.
  - The ambient pressure in Denver will produce a signal from the sensor around 146Hz. (Sea Level = 29.92 inHg = 159Hz, Denver=~24.3 inHg = 146Hz)
    - If the reading does not move from 0Hz, the sensor will be deemed dead
  - A vacuum will be pulled on the sensor to approximately 7 inHg from Denver's reference pressure with the expected signal of ~125Hz
    - If the reading stays at 146Hz, the sensor will be deemed dead.
- O2 Sensors [21]
  - The sensor will be clamped in a vice grip to ensure a secure mounting spot for testing
    - The vice should not clamp onto the threads or body, only the hex nut of the sensor to reduce damage
  - The signal wire and sensor body (signal circuit ground) will be attached to the multimeter probe wires respectively, ignoring the two remaining heating wires
  - A butane torch will be used to heat up the tip of the sensor so that it may begin producing a signal.
  - The tip of sensor will be heated for ~30 seconds to extract a voltage reading
    - If after heating there is no change in voltage reading or the voltage reading never surpassed 0.5V, the sensor will be deemed dead

- The heat will then be removed from the sensor, and the following voltage drop will be recorded
    - If the sensor takes over 1 second to begin dropping its signal, drops sluggishly or never drops from above its peak voltage reading, the sensor will be deemed dead

- Relay Module
    - Each module of the switching relay system will be assembled according to the diagram of figure B2-5
    - A 12 V power supply will be used as the voltage source for testing, and a multimeter in continuity testing mode will be attached to the switching ends of the relay
    - When the user interface switch is flipped, the multimeter will be read
        - If the multimeter displays a connection, the relay module will be deemed working
        - If the multimeter displays an open loop, the relay module will be deemed unworking
    - The switching process will be repeated at least 15 times to ensure reliable functionality
- Integration/Track Day Testing
    - The fully repaired wiring harness, switching relay modules, working sensors, and OneGauge system shall be integrated with the assembled car
    - The car will be tested to ensure it turns on, and that the switching relay modules and OneGauge system work as intended
    - The car will be taken to a racetrack and driven for at least an hour, emulating the racing conditions expected
        - After at least one hour of successful running, the wiring harness will be visually evaluated for any breaks, worn insulation, or torn connectors
            - If no issues are visible, the changes to the wiring harness will be considered successful
    - Any failures will be documented and addressed appropriately

Appendix B2 – Test Results

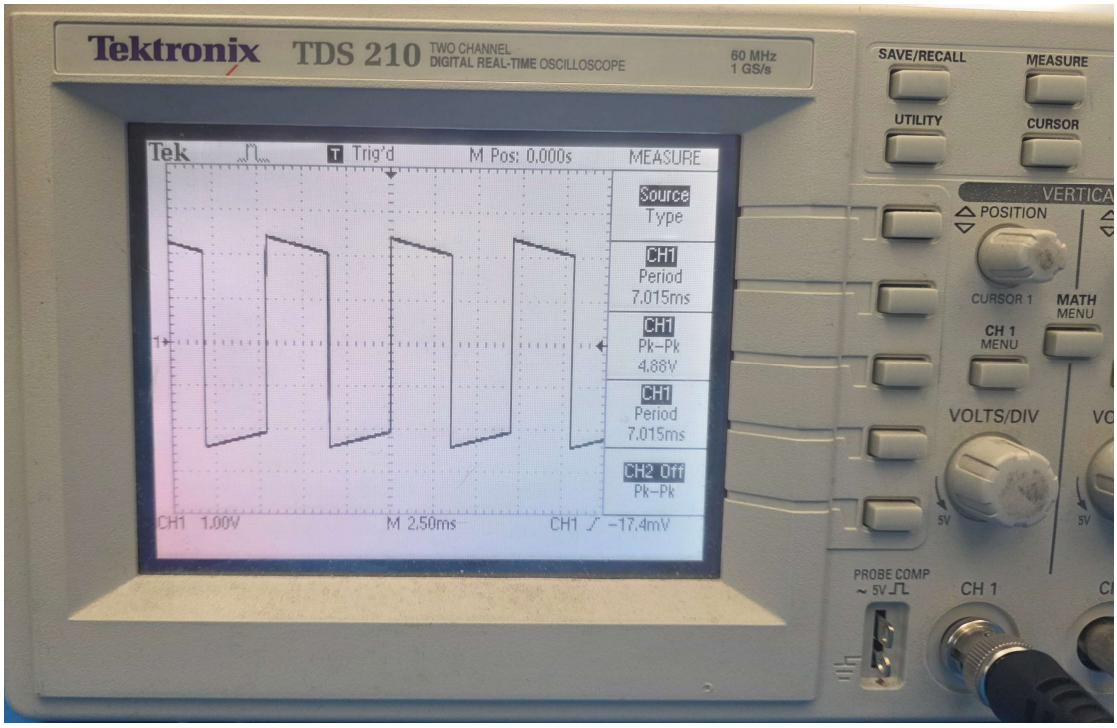

Figure B2-1: MAP Sensor Frequency at Denver Altitude

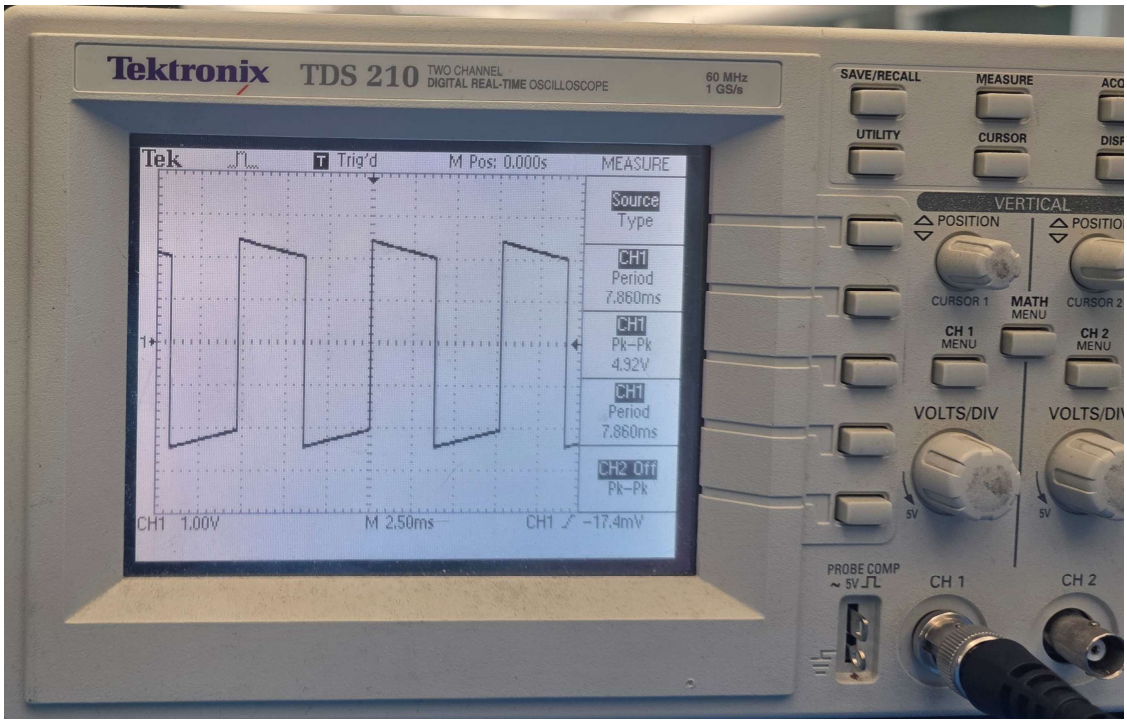

Figure B2-2: MAP Sensor Frequency at 7inHg Vacuum from Denver Altitude

Figure B2-3: Physically Damaged O2 Sensor

Figure B2-4: O2 Sensor Placement in Exhaust Manifold

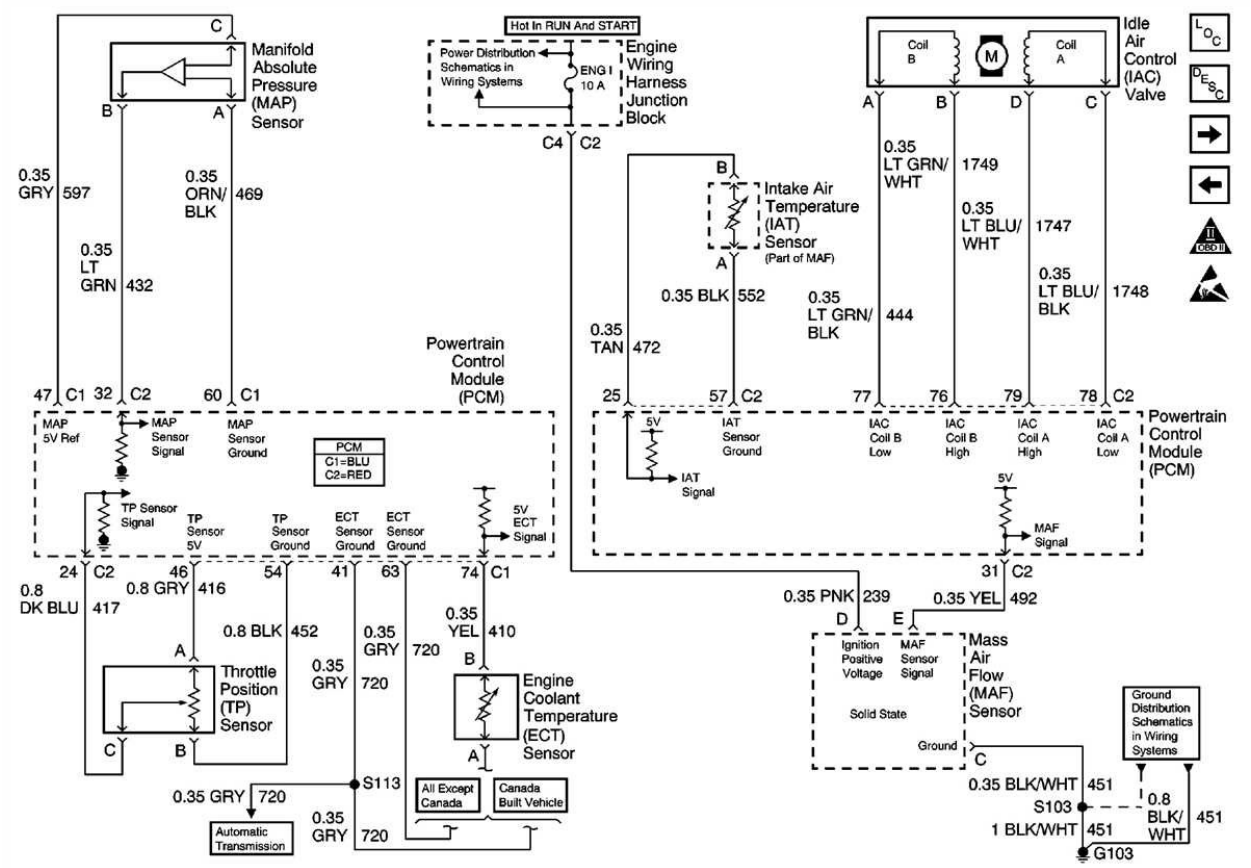

Figure B2-5: Wiring Diagram of ECT, ACT and MAP Sensors

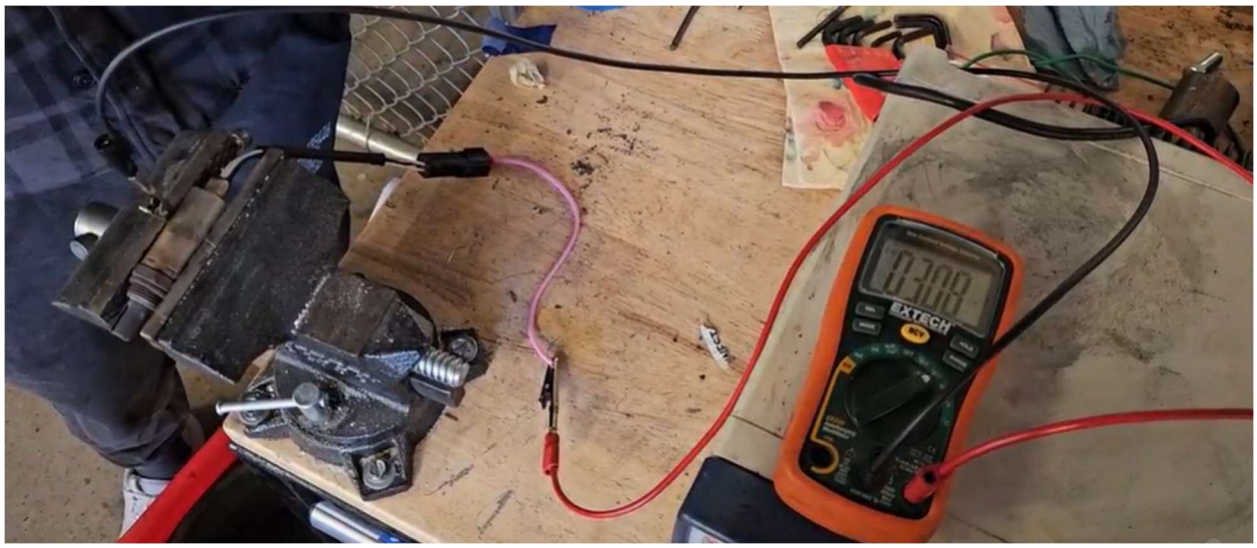

Figure B2-6: Voltage Reading After 5 Seconds of Removed Heat

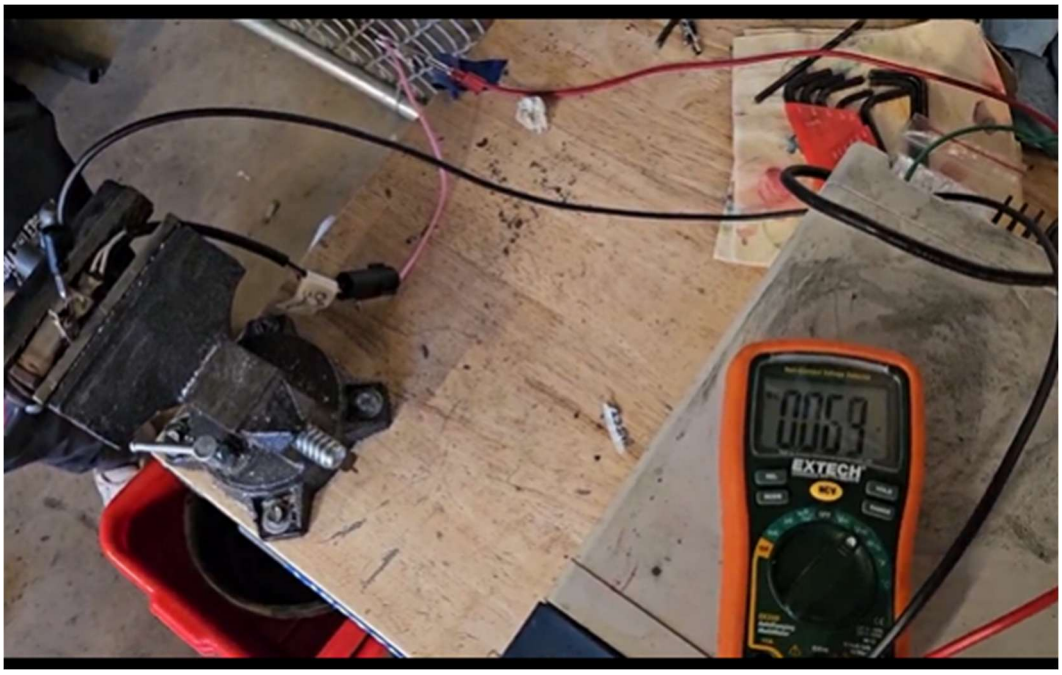

Figure B2-7: Voltage Reading After 5 Seconds of Heating

Appendix B3 – Calculations

Relay coil current draw:

$$I = \frac{P}{V} = \frac{1.6W}{12\ VDC} = 0.133A$$

APPENDIX C - Cooling Calculations

MATLAB Model:

%Heat Transfer - Radiator Model

%Initial Thoughts

%Using Rule of 1/3rds base assumption

%1/3 fuel energy goes to exhuast, brake power, and the radiator

%From here, Need radiator to dissipate between 30-75%

%Engine

HP = 225;

HP_sweep = linspace(20, 225, 41);

HP_avg = 140;

%assume 25% efficiency

```
eng_eff = 0.25;
eng_eff_sweep = linspace(0.15,0.3, 15);

engine_power_kw = 225 *.7457; %convert HP to kW
%Min_cooling_load = engine_power_kw; %car would run hot due to 25% FE to power and 25% to radiator

Fuel_energy = engine_power_kw/eng_eff;
Fuel_energy_eff_sweep = Min_cooling_load * eng_eff_sweep;

%Ideal_cooling_load = Fuel_energy * 0.35; %radiator to dissipate 30-50% of fuel energy
%Ideal_cooling_load_sweep_eff = Fuel_energy_eff_sweep *0.35;
% Ideal cooling load is 234.8955 kW SS

% Operating / environmental
T_coolant_in_F = 225;        % degF
T_oil_in_F     = 260;        % degF
T_air_in_F     = 75;         % ambient air degF
V_air_mph      = 50;         % vehicle speed (mph)
Coolant_flow_GPM = 18;       % coolant volumetric flow (GPM)
Oil_flow_GPM     = 6;        % oil volumetric flow (GPM)
%effectiveness constant at 50%

% Air properties (approx at ambient) (mile high at 75 F)
Prop_air.rho = 0.968; %kg/m^3
Prop_air.cp = 1006; %J/kgK

% Typical fluid properties (approx) - can refine these based on temps
% Water-based coolant at ~380 K
Prop_c.rho = 953.5; %kg/m^3
```

```
Prop_c.cp = 4217; %J/kgK



% Oil at ~400 K
Prop_o.rho = 825; %kg/m^3
Prop_o.cp = 2250; %J/kgK

%Air speed conversion
U_air = V_air_mph * .44704; % m/s

%Convert GPM to m^3/s
Coolant_flow_m3s = Coolant_flow_GPM * 0.000063090196;
Oil_flow_m3s = Oil_flow_GPM * 0.000063090196;

%Solve for heat capacity rates C=mdot*cp; mdot has to be in kg/s
C_coolant = (Coolant_flow_m3s * Prop_c.rho) * Prop_c.cp;
C_oil = (Oil_flow_m3s * Prop_o.rho) * Prop_o.cp;

%Frontal Areas for radiator options
%Options:
%     A: larger radiator
%     B: smaller radiator (DPI 1140 like geometry)
%     C: smaller radiator + separate oil cooler
% Core Definitions: [L_in, H_in, tube_thickness_in, n_rows, 'Fluid', 'Name']
CoreDefinitions = {
    24.45, 16.85, 2.05, 3, 'Coolant', 'Option A (Large Radiator)';
    25.12, 12.60, 2.05, 3, 'Coolant', 'Option B (Small Radiator DPI1140)';
    % Option C: small radiator + oil cooler
    25.2, 12.60, 2.05, 3, 'Coolant', 'Option C (Small Radiator DPI1140)';
    11.00, 5.43,  1.97, 19,'Oil',     'Option C (Oil Cooler)';
```

```
};

optionA_area = 24.45 * 16.85; %in^2
optionB_area = 25.12 * 12.60; %in^2
optionC_area_oil = 11.00 * 5.43; %in^2

%convert frontal areas to m^2
optionA_area_m2 = optionA_area * 0.00064516;
optionB_area_m2 = optionB_area * 0.00064516;
optionC_area_oil_m2 = optionC_area_oil * 0.00064516;



%mass flow rates for air
mass_flow_air_A = optionA_area_m2 * U_air;
mass_flow_air_B = optionB_area_m2 * U_air;
mass_flow_air_C = (optionB_area_m2) * U_air; %assumes oil cooler and radiator dont have
overlapping flow
mass_flow_air_D = optionC_area_oil_m2 *U_air;

%Air Heat Capacity Rates
C_airA = (mass_flow_air_A * Prop_air.rho) * Prop_air.cp;
C_airB = (mass_flow_air_B * Prop_air.rho) * Prop_air.cp;
C_airC = (mass_flow_air_C * Prop_air.rho) * Prop_air.cp;
C_airD = (mass_flow_air_D * Prop_air.rho) * Prop_air.cp;



%Using Effectivenss - NTU method
%Can we reasonably assume the radiator options will be about 70% effective?
T_coolant_in_K = (T_coolant_in_F + 459.67)*(5/9);
T_oil_in_K = (T_oil_in_F+459.67)*(5/9);
```

```
T_air_in_K = (T_air_in_F + 459.67)*(5/9);


%compare C values
C_airA;
C_airB;
C_airC;
C_oil;
C_coolant;

%Airs are the lower C values

%qmax = Cmin*(Thi-Tci)
q_max_A = C_airA * (T_coolant_in_K-T_air_in_K) / 1000; %divide by 1000 to get kW

effectiveness = 0.5; %radiator effectiveness is around 40-60% we will assume mid end for now
%vary effectiveness

q_A = effectiveness*q_max_A;

q_max_B = C_airB * (T_coolant_in_K-T_air_in_K) / 1000;

q_B = effectiveness * q_max_B;

q_max_a = C_airC * (T_coolant_in_K-T_air_in_K) / 1000;

q_a = effectiveness * q_max_a; %air for option 3 = B

q_max_o = C_airD * (T_oil_in_K-T_air_in_K) / 1000; % oil for option 3
```

```
q_o = effectiveness*q_max_o;

q_max_C = (q_max_o+q_max_a)*effectiveness;

q_C = q_o+q_a;

%Varying HP
Min_cooling_load_HP=zeros(size(HP_sweep));
Fuel_energy_HP = zeros(size(HP_sweep));
Ideal_cooling_load_HP = zeros(size(HP_sweep));

for i = 1:length(HP_sweep)
   engine_power_HP(i) = HP_sweep(i) * .7457;

   Fuel_energy_HP(i) = engine_power_HP(i) / eng_eff;

   Min_cooling_load_HP(i) = Fuel_energy_HP(i) * 0.30;

   Max_cooling_load_HP(i) = Fuel_energy_HP(i) * 0.5;

   q_A_HP(i) = q_A;

   q_B_HP(i) = q_B;

   q_C_HP(i) = q_C;
end

figure(1);
hold on;
```

```
plot(HP_sweep, Min_cooling_load_HP, 'Color', 'red', 'LineWidth', 2, "DisplayName", 'Minimum Cooling Load');

plot(HP_sweep, Max_cooling_load_HP, 'Color', 'blue', 'LineWidth', 2, "DisplayName", 'Maximum Cooling Load');

plot(HP_sweep, q_A_HP, 'Color','magenta','LineWidth', 2, "DisplayName", 'New Radiator');

plot(HP_sweep, q_B_HP, 'Color','black','LineWidth', 2, "DisplayName", 'Same Radiator');

plot(HP_sweep, q_C_HP, 'Color','green', 'LineWidth', 2, "DisplayName", 'Same Radiator + Oil Cooler');

xline(HP_avg, '--r','LineWidth', 2, "DisplayName", 'Estimated Avg HP' );

patch([HP_sweep fliplr(HP_sweep)], [Max_cooling_load_HP fliplr(Min_cooling_load_HP)], '--b', 'FaceAlpha', 0.3, 'EdgeColor', 'none', 'DisplayName', 'Target Zone');

xlabel('Power Range [HP]');

ylabel('Heat Required [kW]');

title('Horsepower vs Heat Requirements');

grid on;

legend('show', 'Location', 'best');

hold off;



%Varying Engine Efficiency everything else at OG constant

Min_cooling_load_eff=zeros(size(eng_eff_sweep));

Fuel_energy_eff = zeros(size(eng_eff_sweep));

Max_cooling_load_eff = zeros(size(eng_eff_sweep));

%HP_eff = linspace(20, 225, 15);


for i = 1:length(eng_eff_sweep)

    engine_power_eff(i) = HP * .7457;


    Fuel_energy_eff(i) = engine_power_eff(i) / eng_eff_sweep(i);


    Min_cooling_load_eff(i) = Fuel_energy_eff(i) * 0.30;
```

```
    Max_cooling_load_eff(i) = Fuel_energy_eff(i) * 0.5;

    q_A_eff(i) = q_A;

    q_B_eff(i) = q_B;

    q_C_eff(i) = q_C;
end
figure(2);
hold on;
plot(eng_eff_sweep, Min_cooling_load_eff, 'Color', 'red', 'LineWidth', 2, "DisplayName", 'Minimum Cooling Load');
plot(eng_eff_sweep, Max_cooling_load_eff, 'Color', 'blue', 'LineWidth', 2, "DisplayName", 'Maximum Cooling Load');
plot(eng_eff_sweep, q_A_eff, 'Color','magenta', 'LineWidth', 2, "DisplayName", 'New Radiator');
plot(eng_eff_sweep, q_B_eff, 'Color','black', 'LineWidth', 2, "DisplayName", 'Same Radiator');
plot(eng_eff_sweep, q_C_eff, 'Color','green', 'LineWidth', 2, "DisplayName", 'Same Radiator + Oil Cooler');
patch([eng_eff_sweep fliplr(eng_eff_sweep)], [Max_cooling_load_eff fliplr(Min_cooling_load_eff)], '--b', 'FaceAlpha', 0.3, 'EdgeColor', 'none', 'DisplayName', 'Target Zone');
xlabel('Engine Efficieny [%]');
ylabel('Heat Required [kW]');
title('Engine Efficiency vs Heat Requirements');
grid on;
legend('show', 'Location', 'best');
hold off;

%Varying Vehicle Speed
V_air_mph_sweep = linspace(30,100, 14);
U_air_vary = V_air_mph_sweep * .44704;
```

```
for i = 1:length(V_air_mph_sweep)
    engine_power_speed(i) = HP * .7457;

    Fuel_energy_speed(i) = engine_power_speed(i) / eng_eff;

    Min_cooling_load_speed(i) = Fuel_energy_speed(i) * 0.30;
    Max_cooling_load_speed(i) = Fuel_energy_speed(i) * 0.5;

    mass_flow_air_A_air(i) = optionA_area_m2 * U_air_vary(i);
    mass_flow_air_B_air(i) = optionB_area_m2 * U_air_vary(i);
    mass_flow_air_C_air(i) = (optionB_area_m2) * U_air_vary(i); %assumes oil cooler and
radiator don't have overlapping flow (likely will)
    mass_flow_air_D_air(i) = optionC_area_oil_m2 * U_air_vary(i);

    %Air Heat Capacity Rates
    C_airA_speed(i) = (mass_flow_air_A_air(i) * Prop_air.rho) * Prop_air.cp;
    C_airB_speed(i) = (mass_flow_air_B_air(i) * Prop_air.rho) * Prop_air.cp;
    C_airC_speed(i) = (mass_flow_air_C_air(i) * Prop_air.rho) * Prop_air.cp;
    C_airD_speed(i) = (mass_flow_air_D_air(i) * Prop_air.rho) * Prop_air.cp;

    %qmax = Cmin*(Thi-Tci)
    q_max_A_speed(i) = C_airA_speed(i) * (T_coolant_in_K-T_air_in_K) / 1000; %divide by
1000 to get kW

    effectiveness = 0.6; %radiator effectiveness is around 40-60% we will assume high end for
now
    %vary effectiveness
```

```
    q_A_speed(i) = effectiveness*q_max_A_speed(i);

    q_max_B_speed(i) = C_airB_speed(i) * (T_coolant_in_K-T_air_in_K) / 1000;

    q_B_speed(i) = effectiveness * q_max_B_speed(i);

    q_max_a_speed(i) = C_airC_speed(i) * (T_coolant_in_K-T_air_in_K) / 1000;

    q_a_speed(i) = effectiveness * q_max_a_speed(i);

    q_max_o_speed(i) = C_airD_speed(i) * (T_oil_in_K-T_air_in_K) / 1000;

    q_o_speed(i) = effectiveness*q_max_o_speed(i);

    q_C_speed(i) = q_o_speed(i)+q_a_speed(i);



end
figure(3);
hold on;
plot(V_air_mph_sweep, Min_cooling_load_speed, 'Color', 'red', 'LineWidth', 2, "DisplayName", 'Minimum Cooling Load');
plot(V_air_mph_sweep, Max_cooling_load_speed, 'Color', 'blue', 'LineWidth', 2, "DisplayName", 'Maximum Cooling Load');
plot(V_air_mph_sweep, q_A_speed, 'Color','magenta', 'LineWidth', 2, "DisplayName", 'New Radiator');
plot(V_air_mph_sweep, q_B_speed, 'Color','black', 'LineWidth', 2, "DisplayName", 'Same Radiator');
plot(V_air_mph_sweep, q_C_speed, 'Color','green', 'LineWidth', 2, "DisplayName", 'Same Radiator + Oil Cooler');
```

```
patch([V_air_mph_sweep fliplr(V_air_mph_sweep)], [Max_cooling_load_speed
fliplr(Min_cooling_load_speed)], '--b', 'FaceAlpha', 0.3, 'EdgeColor', 'none', 'DisplayName',
'Target Zone');
xlabel('Vehicle Speed [mph]');
ylabel('Heat Required [kW]');
title('Vehicle Speed vs Heat Requirements');
grid on;
legend('show', 'Location', 'best');
hold off;



%Varying Radiator Effectiveness
effectiveness_sweep = linspace(0.3,0.7, 30);

for i = 1:length(effectiveness_sweep)
    engine_power_effec(i) = HP * .7457;

    Fuel_energy_effec(i) = engine_power_effec(i) / eng_eff;

    Min_cooling_load_effec(i) = Fuel_energy_effec(i) * 0.30;
    Max_cooling_load_effec(i) = Fuel_energy_effec(i) * 0.5;

    q_A_effec(i) = effectiveness_sweep(i) * q_max_A;

    q_B_effec(i) = effectiveness_sweep(i) * q_max_B;

    q_a_effec(i) = effectiveness_sweep(i) * q_max_a;

    q_o_effec(i) = effectiveness_sweep(i) * q_max_o;
```

```
    q_C_effec(i) = q_o_effec(i)+q_a_effec(i);

end



figure(4);
hold on;
plot(effectiveness_sweep, Min_cooling_load_effec, 'Color', 'red', 'LineWidth', 2, "DisplayName", 'Minimum Cooling Load');
plot(effectiveness_sweep, Max_cooling_load_effec, 'Color', 'blue', 'LineWidth', 2, "DisplayName", 'Maximum Cooling Load');
plot(effectiveness_sweep, q_A_effec, 'Color','magenta', 'LineWidth', 2, "DisplayName", 'New Radiator');
plot(effectiveness_sweep, q_B_effec, 'Color','black', 'LineWidth', 2, "DisplayName", 'Same Radiator');
plot(effectiveness_sweep, q_C_effec, 'Color','green', 'LineWidth', 2, "DisplayName", 'Same Radiator + Oil Cooler');
patch([effectiveness_sweep fliplr(effectiveness_sweep)], [Max_cooling_load_effec fliplr(Min_cooling_load_effec)], '--b', 'FaceAlpha', 0.3, 'EdgeColor', 'none', 'DisplayName', 'Target Zone');
xlabel('Radiator Effectiveness');
ylabel('Heat Required [kW]');
title('Radiator Effectiveness vs Heat Requirements');
grid on;
legend('show', 'Location', 'best');
hold off;



%Vary Outdoor Temperatures
T_air_F_sweep = linspace(50, 100, 10);
rho_air_sweep = linspace(1.014, 0.923, 10);
```

```
cp_air_sweep = linspace(1005, 1010, 10);
C_airA_air = zeros(size(T_air_F_sweep));
C_airB_air = zeros(size(T_air_F_sweep));
C_airC_air = zeros(size(T_air_F_sweep));
for i = 1:length(T_air_F_sweep)
    T_air_in_K_air(i) = (T_air_F_sweep(i) + 459.67)*(5/9);

    engine_power_air(i) = HP * .7457;

    Fuel_energy_air(i) = engine_power_air(i) / eng_eff;

    Min_cooling_load_air(i) = Fuel_energy_air(i) * 0.30;
    Max_cooling_load_air(i) = Fuel_energy_air(i) * 0.5;



    C_airA_air(i) = (mass_flow_air_A * rho_air_sweep(i)) * cp_air_sweep(i);
    C_airB_air(i) = (mass_flow_air_B * rho_air_sweep(i)) * cp_air_sweep(i);
    C_airC_air(i) = (mass_flow_air_C * rho_air_sweep(i)) * cp_air_sweep(i);
    C_airD_air(i) = (mass_flow_air_D * rho_air_sweep(i)) * cp_air_sweep(i);

    %qmax = Cmin*(Thi-Tci)
    q_max_A_air(i) = C_airA_air(i) * (T_coolant_in_K-T_air_in_K_air(i)) / 1000; %divide by
1000 to get kW

    effectiveness = 0.6; %radiator effectiveness is around 40-60% we will assume high end for
now
    %vary effectiveness

    q_A_air(i) = effectiveness*q_max_A_air(i);
```

```
    q_max_B_air(i) = C_airB_air(i) * (T_coolant_in_K-T_air_in_K_air(i)) / 1000;

    q_B_air(i) = effectiveness * q_max_B_air(i);

    q_max_a_air(i) = C_airC_air(i) * (T_coolant_in_K-T_air_in_K_air(i)) / 1000;

    q_a_air(i) = effectiveness * q_max_a_air(i);

    q_max_o_air(i) = C_airD_air(i) * (T_oil_in_K-T_air_in_K_air(i)) / 1000;

    q_o_air(i) = effectiveness * q_max_o_air(i);

    q_C_air(i) = q_o_air(i)+q_a_air(i);
end


figure(5);
hold on;
plot(T_air_F_sweep, Min_cooling_load_air, 'Color', 'red', 'LineWidth', 2, "DisplayName", 'Minimum Cooling Load');
plot(T_air_F_sweep, Max_cooling_load_air, 'Color', 'blue', 'LineWidth', 2, "DisplayName", 'Maximum Cooling Load');
plot(T_air_F_sweep, q_A_air, 'Color','magenta', 'LineWidth', 2, "DisplayName", 'New Radiator');
plot(T_air_F_sweep, q_B_air, 'Color','black', 'LineWidth', 2, "DisplayName", 'Same Radiator');
plot(T_air_F_sweep, q_C_air, 'Color','green', 'LineWidth', 2, "DisplayName", 'Same Radiator + Oil Cooler');
patch([T_air_F_sweep fliplr(T_air_F_sweep)], [Max_cooling_load_air fliplr(Min_cooling_load_air)], '--b', 'FaceAlpha', 0.3, 'EdgeColor', 'none', 'DisplayName', 'Target Zone');
xlabel('Air Temperatures [F]');
ylabel('Heat Required [kW]');
```

```
title('Air Temperatures vs Heat Requirements');
grid on;
legend('show', 'Location', 'best');
hold off;

%Vary Coolant Temps (and oil)
T_coolant_F_sweep = linspace(150,230, 16);
T_oil_F_sweep = linspace(180, 260, 16);

for i = 1:length(T_coolant_F_sweep)
    T_oil_in_K_cool(i) = (T_oil_F_sweep(i) +459.67)*(5/9);
    T_coolant_in_K_cool(i) = (T_coolant_F_sweep(i) + 459.67)*(5/9);

    engine_power_cool(i) = HP * .7457;

    Fuel_energy_cool(i) = engine_power_cool(i) / eng_eff;

    Min_cooling_load_cool(i) = Fuel_energy_cool(i) * 0.30;

    Max_cooling_load_cool(i) = Fuel_energy_cool(i) * 0.5;

    q_max_A_cool(i) = C_airA * (T_coolant_in_K_cool(i)-T_air_in_K) / 1000; %divide by 1000
to get kW

    q_A_cool(i) = effectiveness*q_max_A_cool(i);

    q_max_B_cool(i) = C_airB * (T_coolant_in_K_cool(i)-T_air_in_K) / 1000;

    q_B_cool(i) = effectiveness * q_max_B_cool(i);
```

```
    q_max_a_cool(i) = C_airC * (T_coolant_in_K_cool(i)-T_air_in_K) / 1000;

    q_a_cool(i) = effectiveness * q_max_a_cool(i);

    q_max_o_cool(i) = C_airD *(T_oil_in_K_cool(i) - T_air_in_K) / 1000;

    q_o_cool(i) = effectiveness * q_max_o_cool(i);

    q_C_cool(i) = q_o_cool(i) + q_a_cool(i);
end
figure(6);
hold on;
plot(T_coolant_F_sweep, Min_cooling_load_cool, 'Color', 'red', 'LineWidth', 2, "DisplayName", 'Minimum Cooling Load');
plot(T_coolant_F_sweep, Max_cooling_load_cool, 'Color', 'blue', 'LineWidth', 2, "DisplayName", 'Maximum Cooling Load');
plot(T_coolant_F_sweep, q_A_cool, 'Color','magenta', 'LineWidth', 2, "DisplayName", 'New Radiator');
plot(T_coolant_F_sweep, q_B_cool, 'Color','black', 'LineWidth', 2, "DisplayName", 'Same Radiator');
plot(T_coolant_F_sweep, q_C_cool, 'Color','green', 'LineWidth', 2, "DisplayName", 'Same Radiator + Oil Cooler');
patch([T_coolant_F_sweep fliplr(T_coolant_F_sweep)], [Max_cooling_load_cool fliplr(Min_cooling_load_cool)], '--b', 'FaceAlpha', 0.3, 'EdgeColor', 'none', 'DisplayName', 'Target Zone');
xlabel('Coolant Temperature [F]');
ylabel('Heat Required [kW]');
title('Coolant Temperatures vs Heat Requirements');
grid on;
legend('show', 'Location', 'best');
hold off;
```

APPENDIX D – Aerodynamics Calculations

Appendix D1 – Lift & Energy Calculations

Force to balance engine

Engine Mass [2] [3]

$F_{miata} := 290\ lbf$

$F_{V8} := 379\ lbf$

Lever Arm Approximation

$L_{motor} := 2350\ mm$

$L_{aero} := 2820\ mm$

$L_{COM} := 1132.5\ mm$

Force per axel (stock) [4]

$F_{curb} := 2348\ lbf$

$F_{fz} := \frac{F_{curb}}{2} = 1174\ lbf$

$F_{rz} := \frac{F_{curb}}{2} = 1174\ lbf$

Rear bumper force required (V8)

$F_{V8dif} := F_{V8} - F_{miata}$

$F_{aero} := \frac{F_{V8dif} \cdot L_{motor}}{L_{aero}} = 329.91\ N$

Dimensions [1]

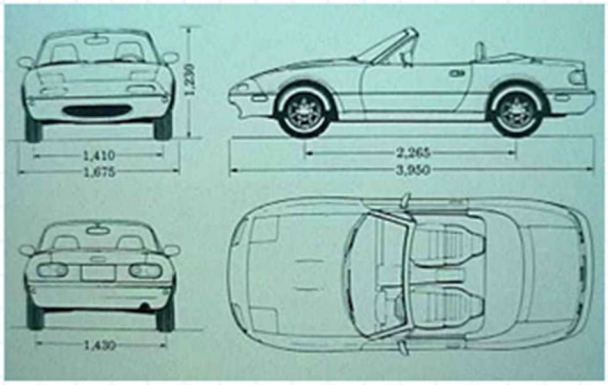

Figure D1-1: Miata balance calculations [22] [23] [24] [25]

Flat Plate Airfoil

$ORIGIN := 1$

$i := 1 .. 12$

Angle of attack [1] [2]

$\alpha := 10\ deg$

Velocity $V := \begin{bmatrix} 4.47 \\ 8.941 \\ 13.411 \\ 17.882 \\ 22.352 \\ 26.822 \\ 31.293 \\ 35.763 \\ 40.234 \\ 44.704 \\ 49.174 \\ 53.645 \end{bmatrix} \frac{m}{s} = \begin{bmatrix} 10 \\ 20 \\ 30 \\ 40 \\ 50 \\ 60 \\ 70 \\ 80 \\ 90 \\ 100 \\ 110 \\ 120 \end{bmatrix} mph$

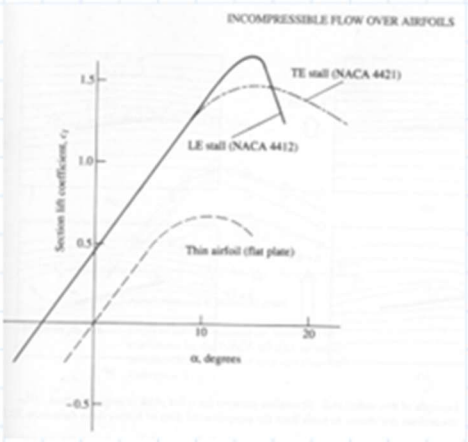

$j := 6.28319 \frac{1}{rad}$ $A := 144\ cm \cdot 25\ cm$ $\rho := 1.225 \frac{kg}{m^3}$

$C_L := j \cdot \alpha$

$F_{L_i} := \frac{1}{2} \cdot C_L \cdot \rho \cdot A \cdot V_i^2 = \begin{bmatrix} 4.83 \\ 19.33 \\ 43.49 \\ 77.32 \\ 120.81 \\ 173.96 \\ 236.79 \\ 309.27 \\ 391.43 \\ 483.24 \\ 584.71 \\ 695.86 \end{bmatrix} N$

Figure D1-2: Wing downforce calculations [26] [27]

Aero vs. Bricks Energy Analysis

Force/mass required

$F_{req} := 337.528\ N$

$m_{req} := \frac{F_{req}}{g} = 75.879\ lb$

Road Load Terms

$t := 7.9\ s \quad v_i := 0\ mph \quad v_f := 60\ mph \quad m_{curb} := 2348\ lb$

$m_{eqi} := 1.05 \cdot m_{curb} \qquad m_{eqf} := 1.05 \cdot (m_{curb} + m_{req})$

$a := \frac{v_f - v_i}{t} = 3.395\ \frac{m}{s^2} \qquad d := v_i \cdot t + \frac{1}{2} \cdot a \cdot t^2 = 105.948\ m$ Constant acc assumed

Forces

$F_{inertia\_i} := m_{eqi} \cdot a = 3.797\ kN \qquad F_{inertia\_f} := m_{eqf} \cdot a = 3.92\ kN$

$F_{aero60} := 387\ N \qquad F_{noaero60} := 336\ N$ From CFD, C_d = 0.52 & 0.44

Energy

$E_{inertia\_i} := F_{inertia\_i} \cdot d = 402270.705\ J \qquad E_{aero} := F_{aero60} \cdot d = 41002.062\ J$

$E_{inertia\_f} := F_{inertia\_f} \cdot d = 415270.715\ J \qquad E_{noaero} := F_{noaero60} \cdot d = 35598.689\ J$

Energy Differences

$E_{aero} - E_{noaero} = 3985.323\ ft \cdot lbf$

$E_{inertia\_f} - E_{inertia\_i} = 9588.316\ ft \cdot lbf$

Figure D1-3 - Downforce vs mass energy analysis

Appendix D2 – CFD Data

No Aero

Velocity [mph]	Drag [N]	C_D	Downforce [N]
10	9.4416	0.444757	-36.12
20	37.7328	0.444361	-35.96
30	84.3948	0.441723	-50.43
40	151.788	0.446884	-68.98
50	239.484	0.451246	-96.98
60	336.168	0.439877	-150.7
70	454.524	0.436956	-165.8
80	594.636	0.437671	-259.1
90	768.6	0.446984	-314.2
100	929.04	0.437634	-316.8
110	1110.48	0.432317	-364.2
120	1337.28	0.437458	-496.9
C_D Average	0.441489		

Full Aero

Velocity [mph]	Drag [N]	C_D	Downforce [N]
10	11.0964	0.522707844	-26.97
20	46.998	0.553472822	9.084
30	106.26	0.556165719	50.57
40	176.988	0.521075619	88.58
50	272.664	0.513765227	157.8
60	386.988	0.506374598	335.9
70	545.328	0.524250232	374.9
80	729.456	0.53690326	618.6
90	874.44	0.508536244	685.9
100	1114.68	0.525081991	880.3
110	1281.84	0.499028516	982.7
120	1517.88	0.49653728	1112
C_D Average	0.521991613		

Wing Only

Velocity [mph]	Drag [N]	C_D	Downforce [N]
10	11.1216	0.523895	-32.93
20	45.4608	0.53537	-21.5
30	99.12	0.518795	0.3309
40	179.004	0.527011	25.39

50	273.672	0.515665	27.12
60	405.384	0.530446	64.61
70	546.924	0.525785	64.4
80	705.852	0.51953	97.69
90	910.56	0.529542	225.9
100	1101.24	0.518751	241.3
110	1339.8	0.521593	209.3
120	1580.88	0.517146	344.9
C_D Average	0.523627		

Split Diff Only

Velocity [mph]	Drag [N]	C_D	Downforce [N]
10	9.42396	0.443926	-32.28
20	37.63536	0.443214	-28.002
30	83.85132	0.438879	-9.61
40	148.5708	0.437412	20.624
50	227.0125	0.427747	25.66
60	323.5873	0.423415	41.631
70	440.6564	0.423624	42.293
80	568.8715	0.418708	103.517
90	712.315	0.414251	134.495
100	883.05	0.41597	148.109
110	1063.196	0.413909	156.7
120	1254.347	0.410329	212.337
C_D Average	0.425949		

Full Aero w/ Roof

Velocity [mph]	Drag [N]	C_D	Downforce [N]
10	10.77636	0.507632	-27.36
20	41.3154	0.486552	4.731
30	91.0812	0.47672	41.91
40	166.6812	0.490731	108.89
50	260.6352	0.4911	234.39
60	367.3824	0.480721	280.8
70	494.3652	0.475257	441.7
80	641.214	0.471954	514.36
90	808.3824	0.47012	637.04
100	1014.888	0.478074	771.35
110	1177.73	0.458498	987.86
120	1382.27	0.452176	1021.82
C_D Average	0.478295		

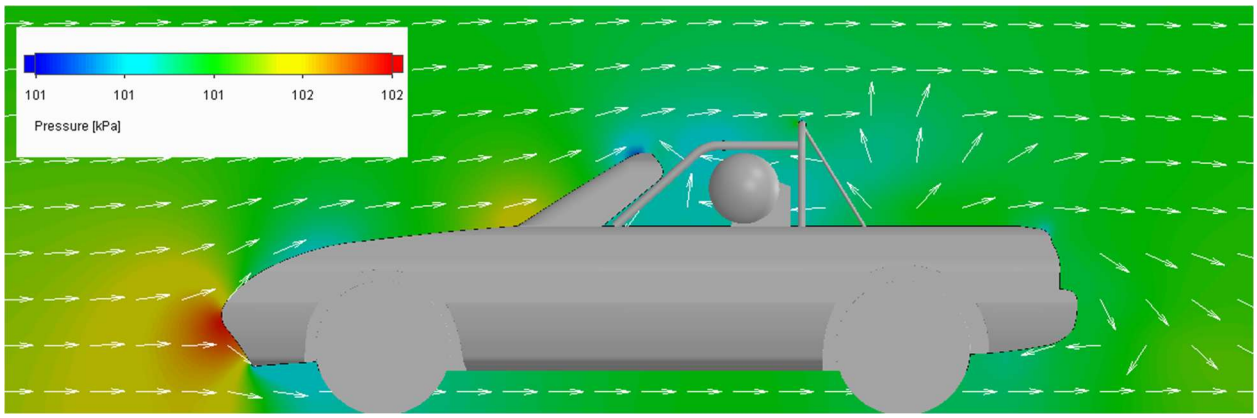

Figure D2-1: Pressure cut plot-stock-60 mph

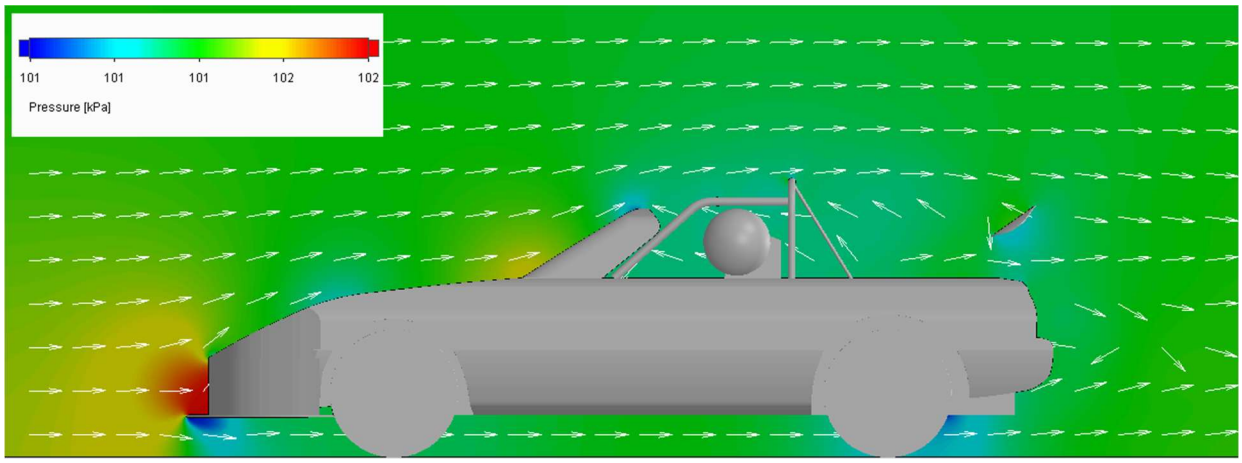

Figure D2-2: Pressure cut plot-full aero-60 mph

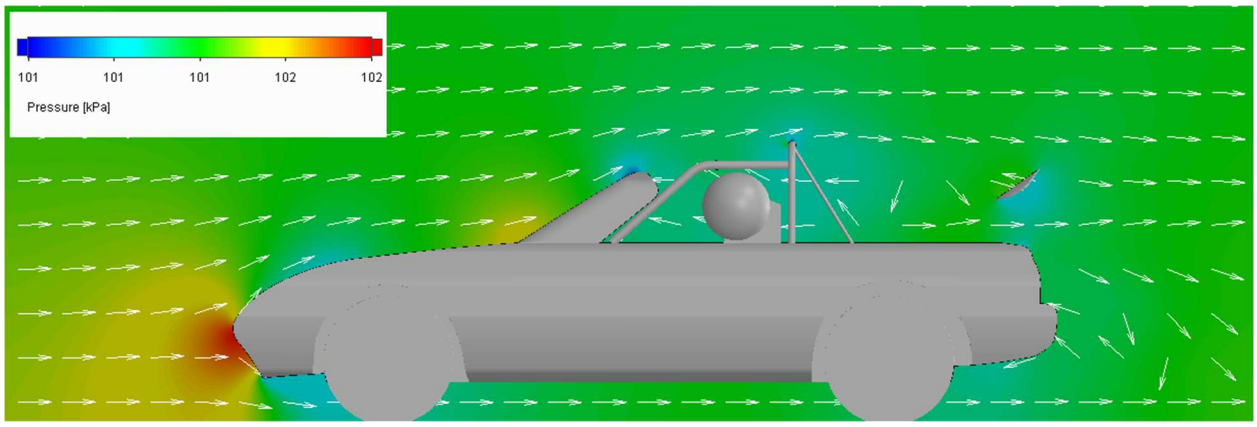

Figure D2-3: Pressure cut plot-wing only-60 mph

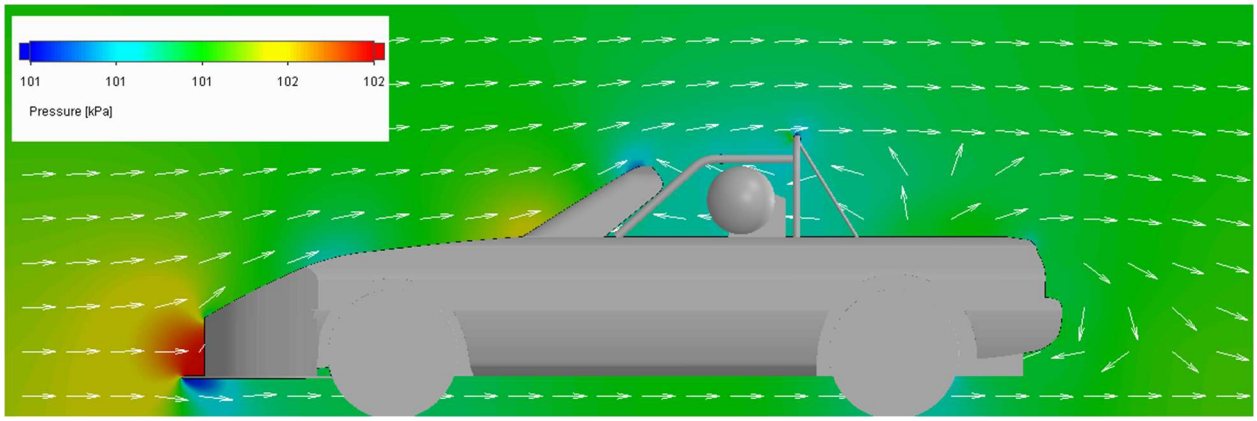

Figure D2-4: Pressure cut plot-split diff only-60 mph

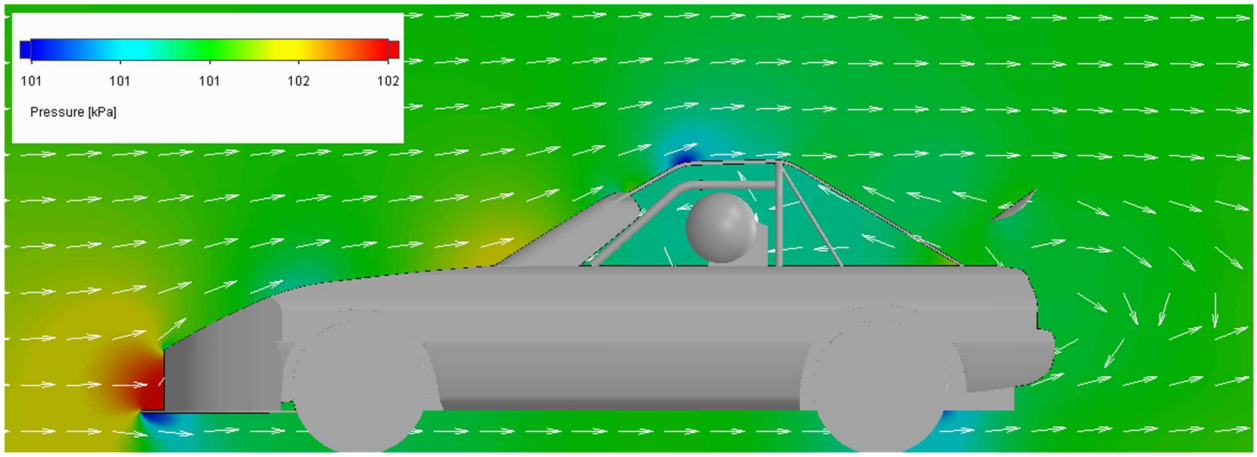

Figure D2-5 Pressure cut plot-full aero w/ roof-60 mph

Appendix D3 – Wing FEA results & verification

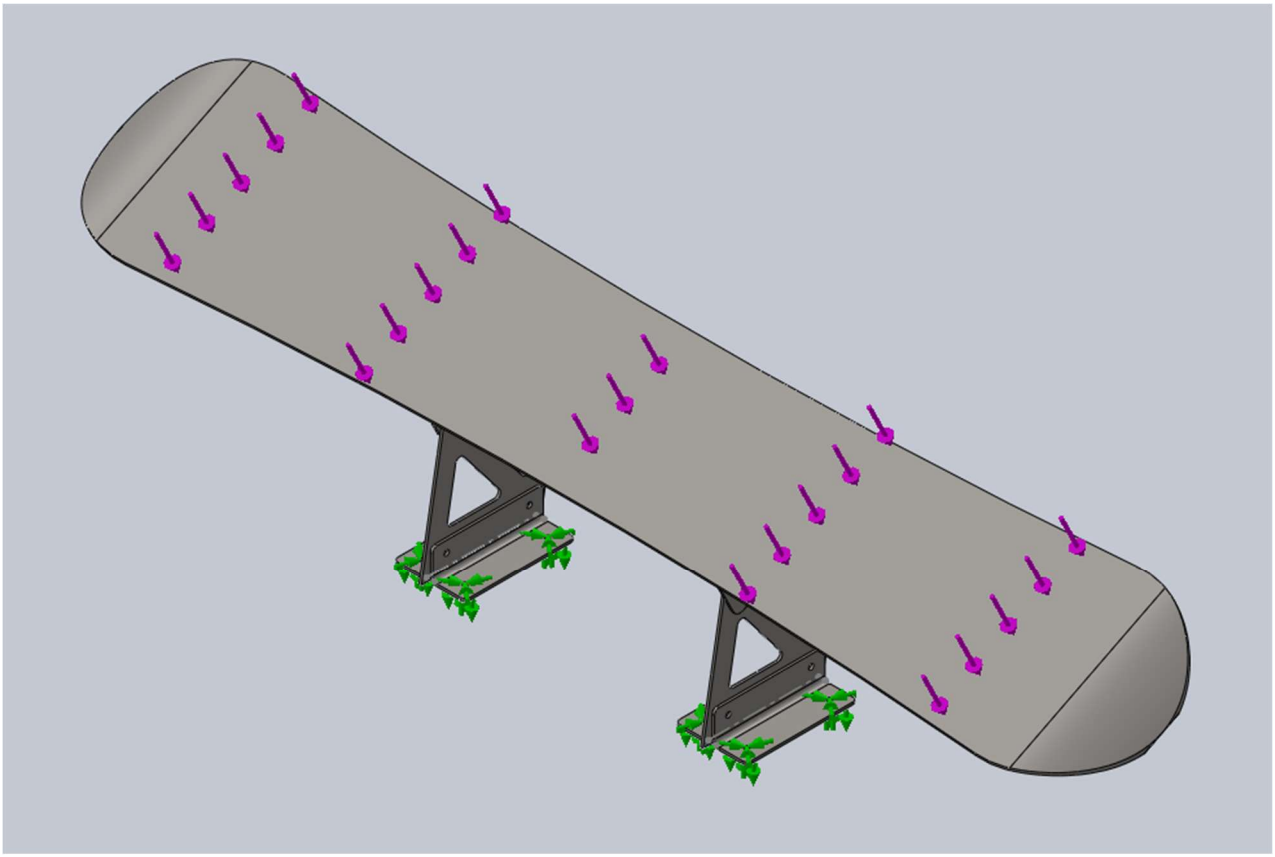

Figure D3-1: Full wing FEA configuration

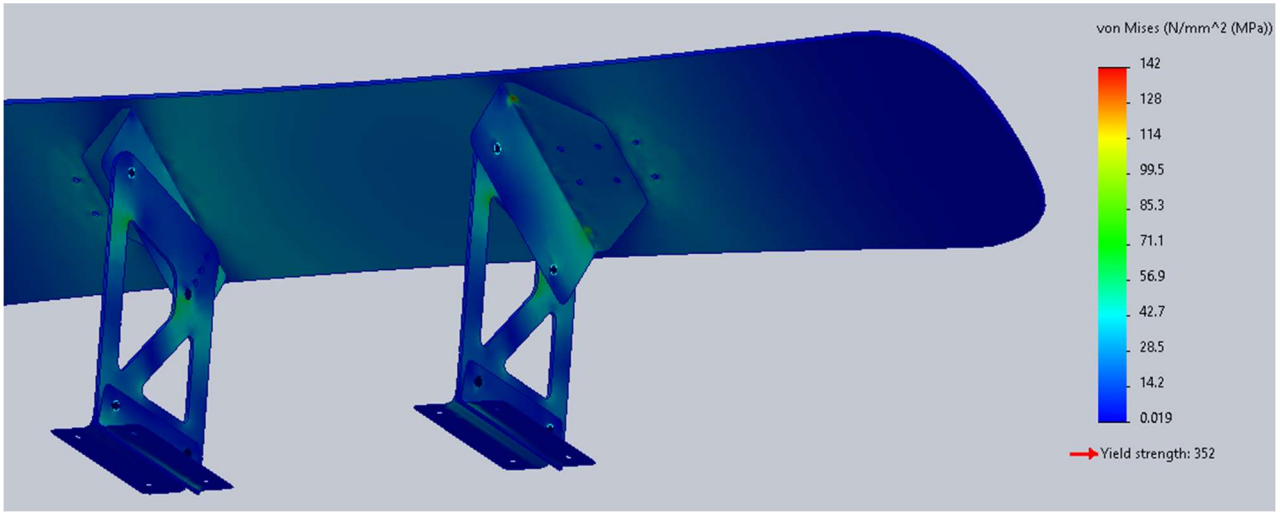

Figure D3-2: Full wing configuration von Mises plot

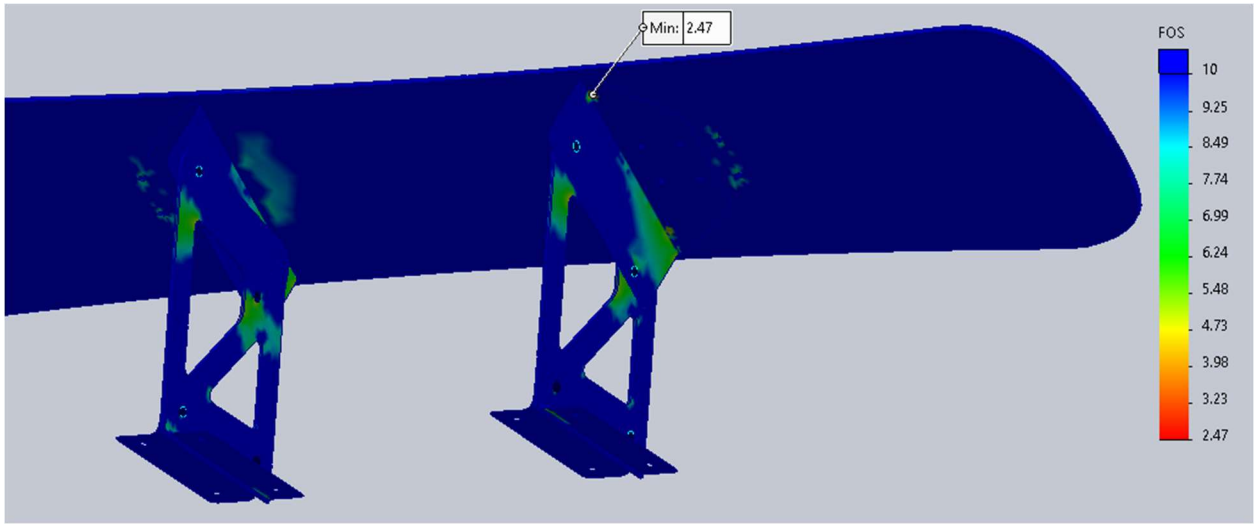

Figure D3-3: Full wing configuration factor of safety plot

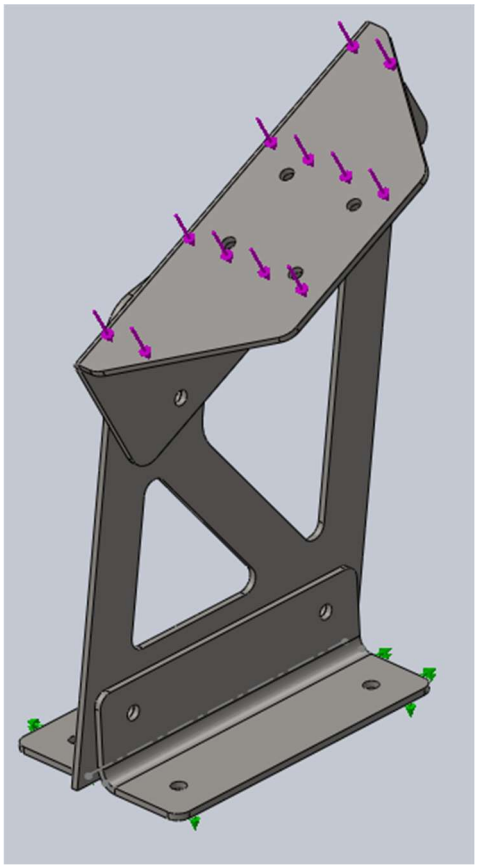

Figure D3-4: Wing support assembly FEA configuration

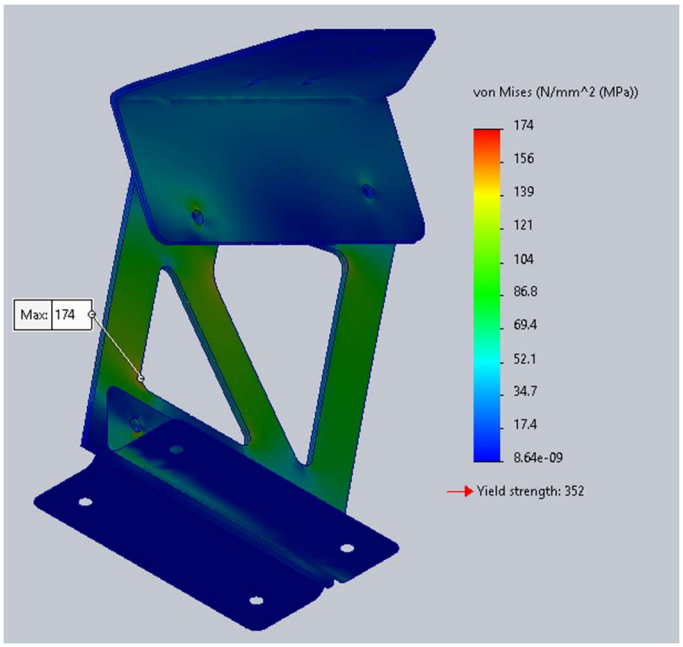

Figure D3-5: Wing support assembly von Mises plot

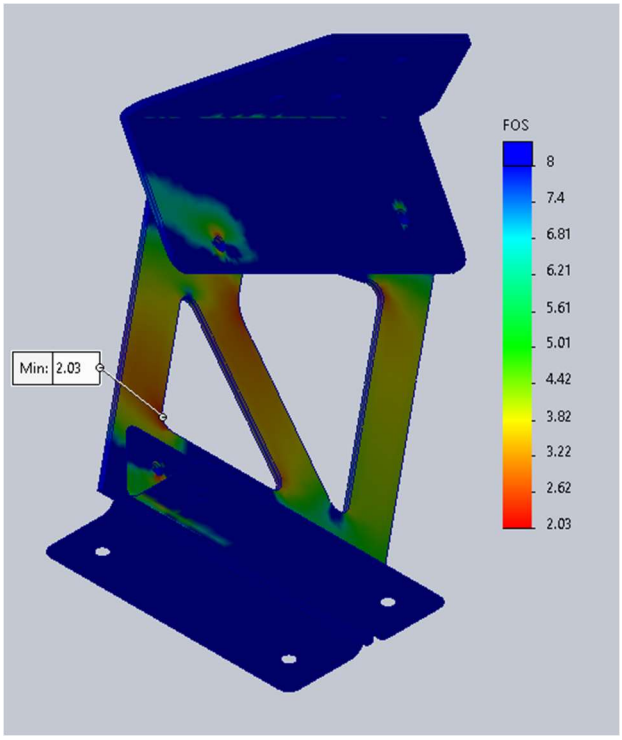

Figure D3-6: Wing support assembly factor of safety plot

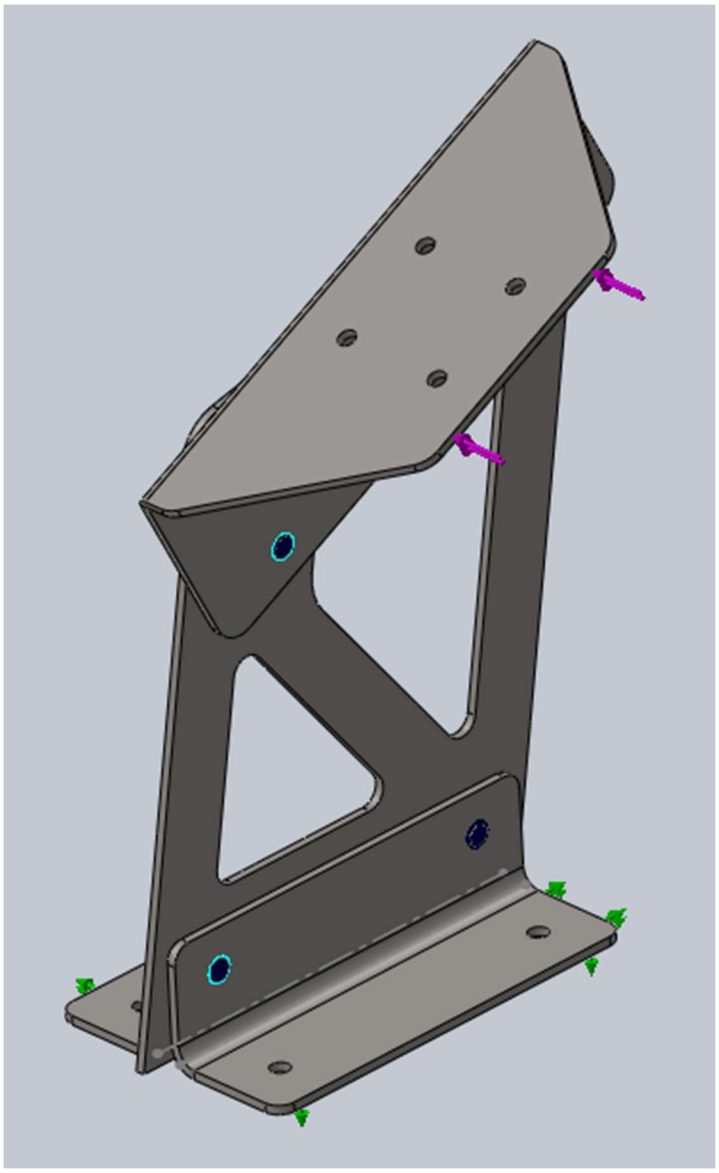

Figure D3-7: Wing support crosswind FEA configuration

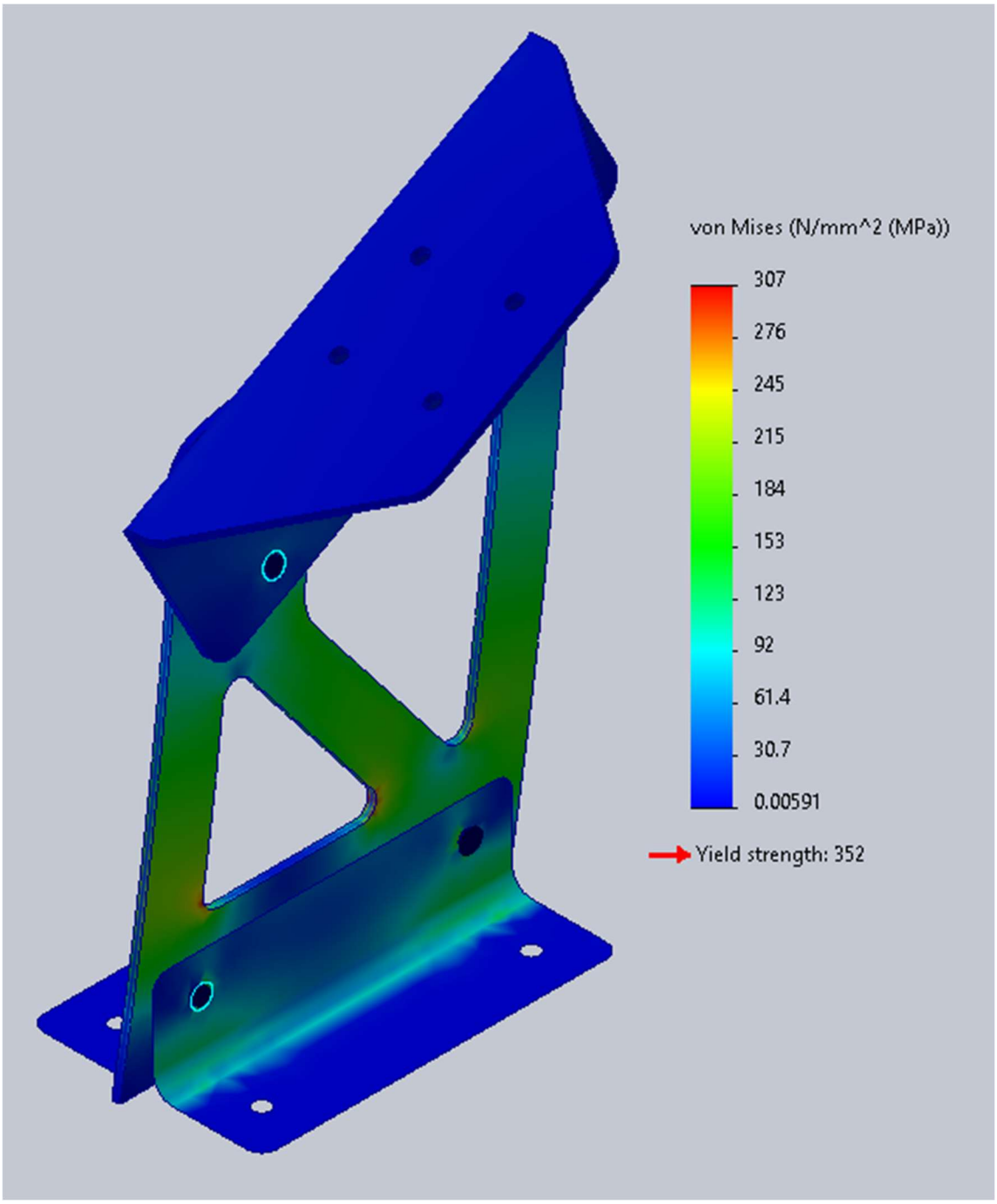

Figure D3-8: Wing support crosswind von Mises plot

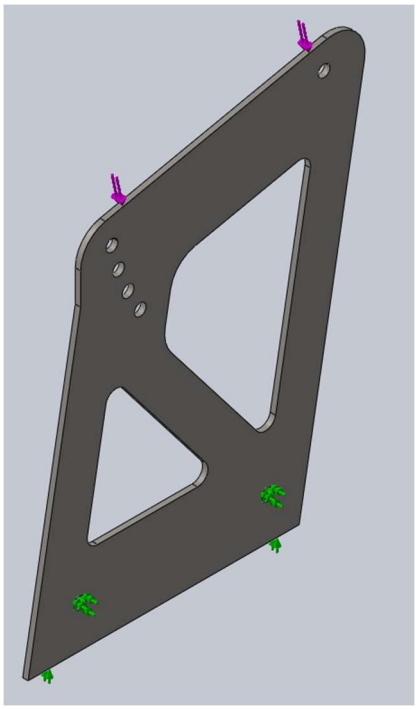

Figure D3-9: Wing vertical support 2000 Newton FEA configuration

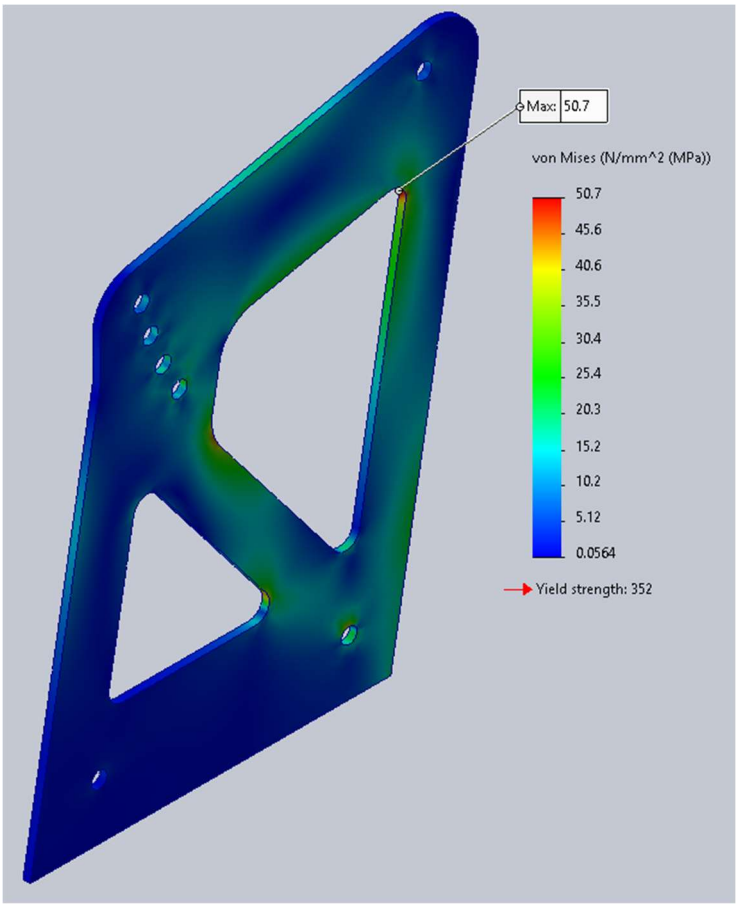

Figure D3-10: Wing vertical support 2000 Newton von Mises plot

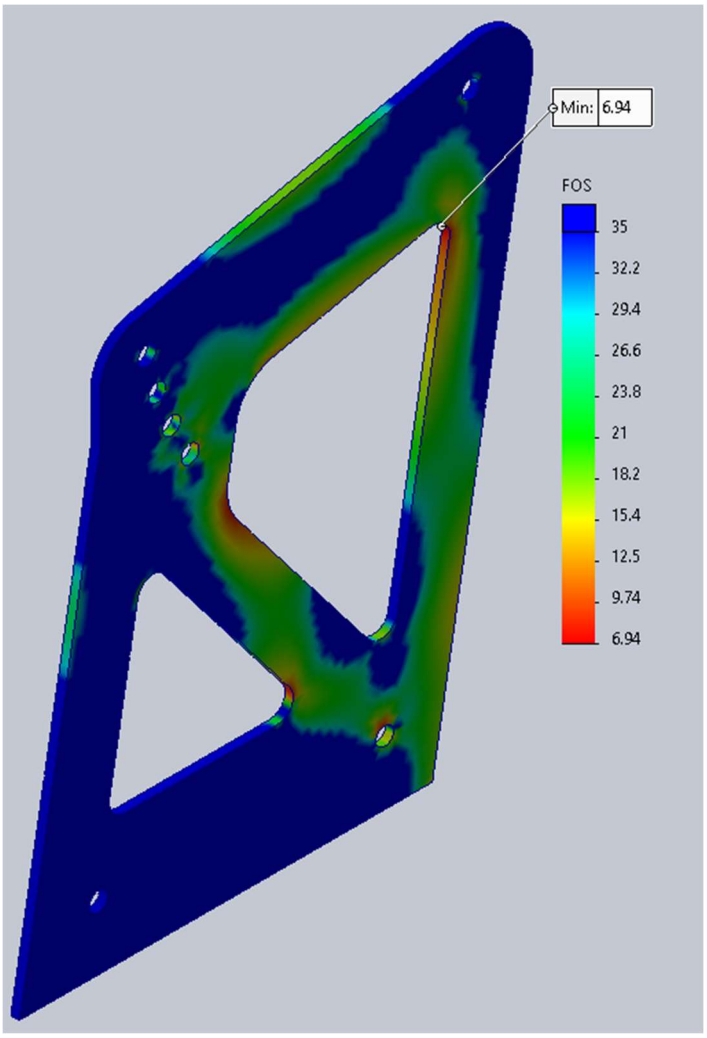

Figure D3-11: Wing vertical support 2000 Newton factor of safety plot

Bearing Stress

$F := 175\ N$ $A := 0.057177\ in^2$ $S := 3.516 \cdot 10^8\ Pa$

$$\sigma_b := \frac{F}{A} = 4.744\ MPa$$

$$FoS := \frac{S}{\sigma_b} = 74.114$$

Figure D3-11: Bearing FoS calculation

Appendix D4 – Splitter FEA

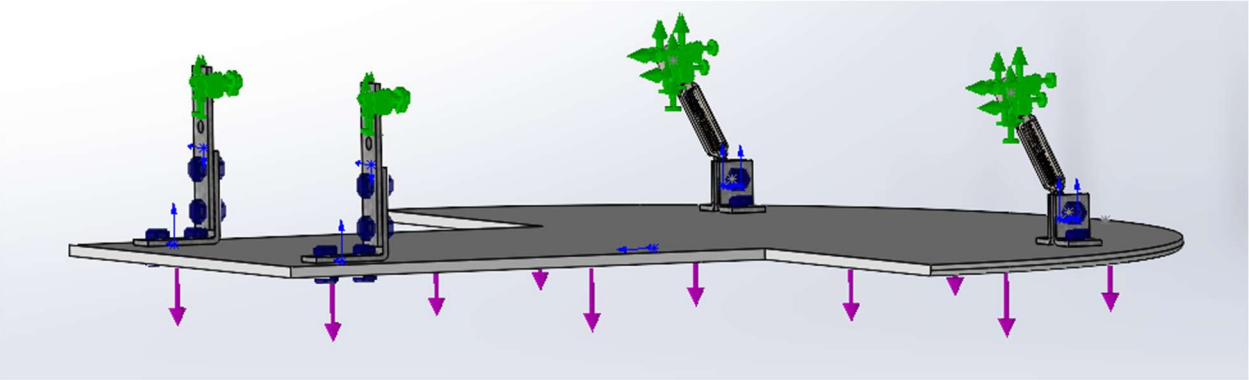

Figure D4-1: Full Splitter Configuration

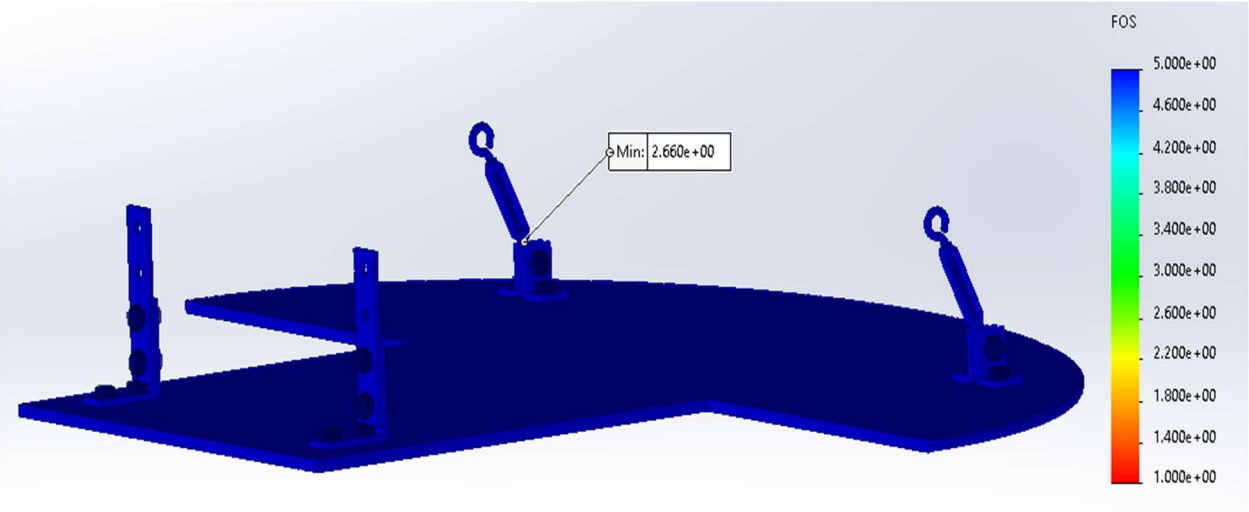

Figure D4-2: Full Splitter Configuration 200N factor of safety plot

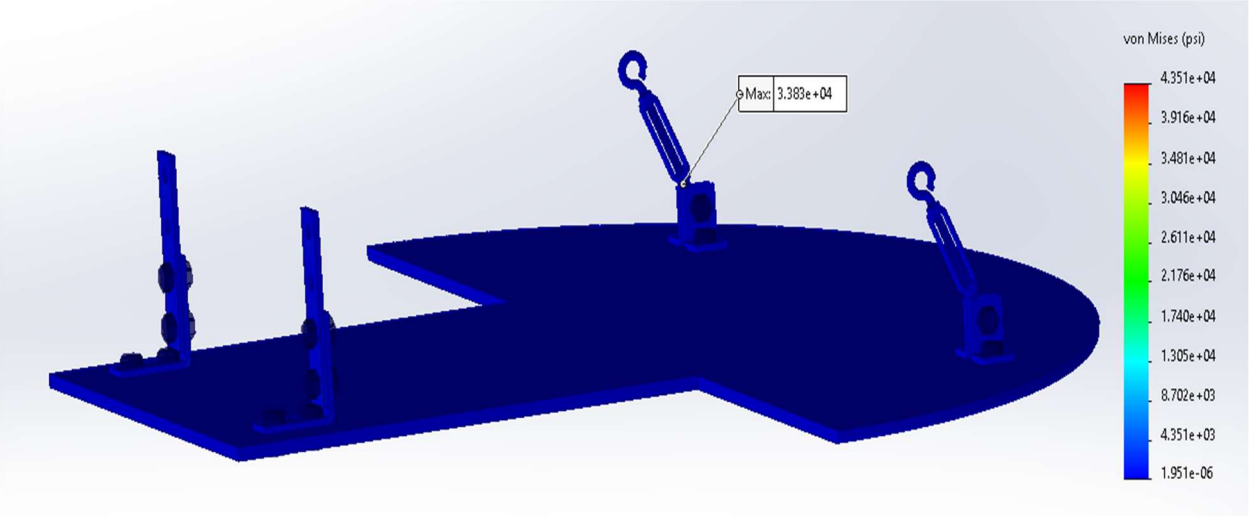

Figure D4-3: Full Splitter Configuration 200N von Mises plot

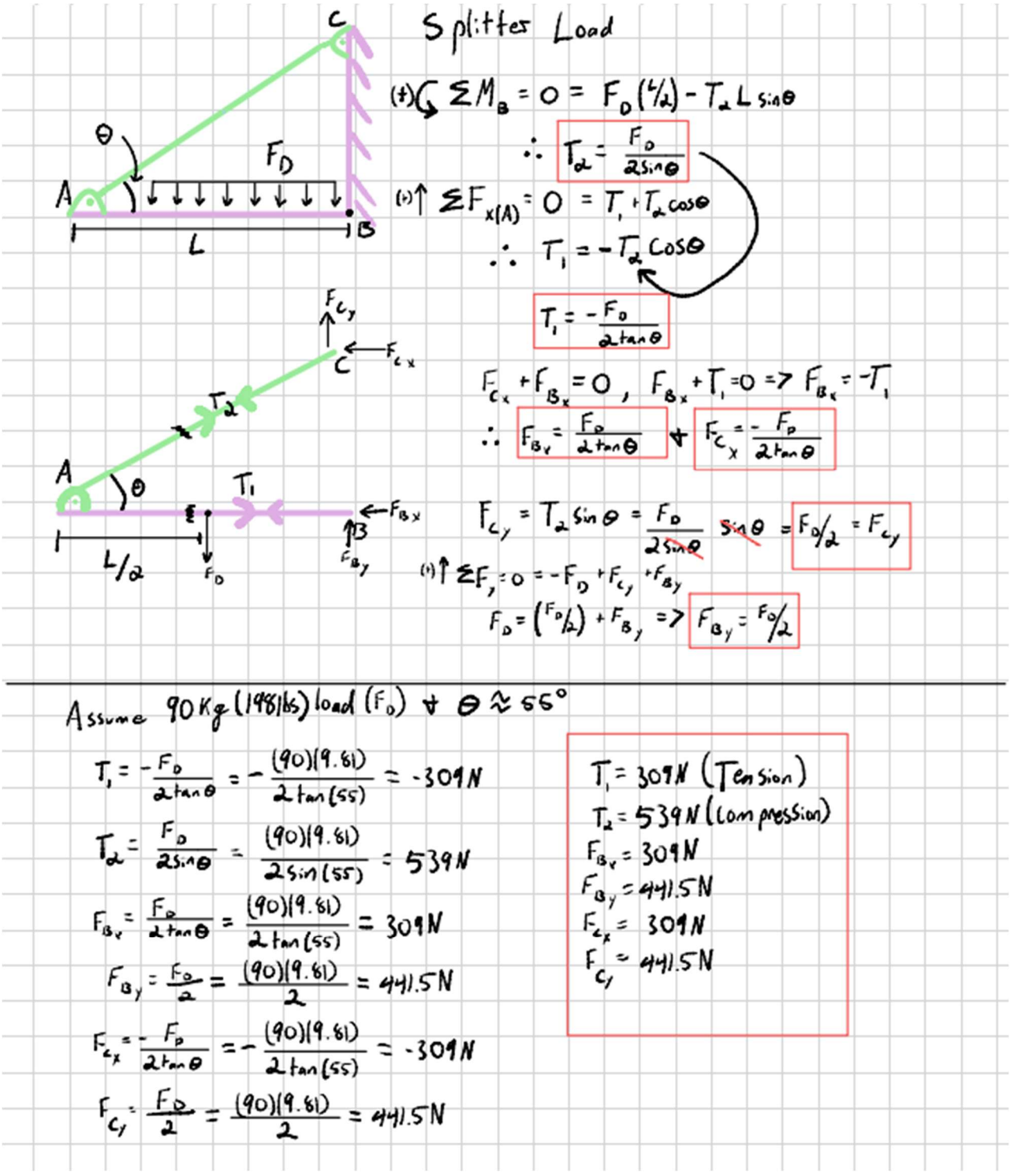

Assume 90 Kg (198 lbs) load (F_D) & $\theta \approx 55°$

$$T_1 = -\frac{F_D}{2\tan\theta} = -\frac{(90)(9.81)}{2\tan(55)} = -309N$$

$$T_2 = \frac{F_D}{2\sin\theta} = \frac{(90)(9.81)}{2\sin(55)} = 539N$$

$$F_{B_x} = \frac{F_D}{2\tan\theta} = \frac{(90)(9.81)}{2\tan(55)} = 309N$$

$$F_{B_y} = \frac{F_D}{2} = \frac{(90)(9.81)}{2} = 441.5N$$

$$F_{C_x} = -\frac{F_D}{2\tan\theta} = -\frac{(90)(9.81)}{2\tan(55)} = -309N$$

$$F_{C_y} = \frac{F_D}{2} = \frac{(90)(9.81)}{2} = 441.5N$$

$T_1 = 309N$ (Tension)
$T_2 = 539N$ (Compression)
$F_{B_x} = 309N$
$F_{B_y} = 441.5N$
$F_{C_x} = 309N$
$F_{C_y} = 441.5N$

Figure D4-4: Splitter Load Calculations

Highest likelyhood of Shear @ T_2

$$\frac{539N}{2} = 269.5N = 60.59lbf$$

Bolt dia (D) = .5 in.

Splitter thickness (t) = .5 in

Bolt Direct Shear Failure

$$\gamma_{shear} = \frac{P}{2A_{shear}} = \frac{60.59}{2\left(\frac{\pi}{4}(.5)^2\right)} = 154.29Pa$$

Far too low to Shear

Bolt Tearout Failure

head dia (D) = 1.094 in.

thread dia (d) = .5 in.

$$A_{tearout} = \pi(1.094 - .5)(.5) = .9331 in^2$$

$$\gamma_{tear} = \frac{P}{A_{tearout}} = \frac{60.59}{.9331} = 64.937 Pa$$

again, quite small

should not need to worry abt. tear out

Figure D4-5: Splitter Bolt Shear and Tear out Calculations

APPENDIX E – Aerodyanmics Test Plan

- Initial testing setup-track day 1
  - The right half of the vehicle will be used to conduct tuft testing. 2-inch-long lengths of string will be taped 3 inches apart in a grid pattern along the entire car including the aerodynamic surfaces
  - Brightly colored tape will be placed on the left side of the vehicle from rear to hood ensure the strip is level
  - A stationary camera will be placed just prior to the braking zone of the longest straight
  - A camera will be mounted within the vehicle pointed at where the wing would be placed, wide angle lens preferred
  - A radar gun or GPS speedometer will be used to find maximum speed
  - The driver will be asked to note differences felt from different testing setups
- Testing setups
  - No aero – the wing and diffuser will be removed; the splitter & air dam assembly is integral for cooling so will remain installed
  - Minimal downforce – wing and diffuser will be installed with the wing set on the shallowest angle of attack
  - Maximum downforce – wing and diffuser will be installed with the wing set on the steepest angle of attack
  - Intermediate setups – the two intermediate angle of attack options for the wing will only be used if testing time is available
- Data analysis
  - Video and visual observation of the tuft testing will be used to validate CFD streamlines
  - Still images captured from the stationary camera will be used to compare vehicle ride heights
    - Difference in ride height accompanied with knowledge of the suspension setup can be used to estimate downforce to validate CFD calculations
  - Differences in top speed will be analyzed to estimate drag
  - Any available feedback from the testing driver will be used to begin optimization plans
- Optimization testing-performed after initial testing
  - The same testing setup will be used
  - Testing will focus on tweaking both wing angle and splitter height to optimize downforce and drag
  - Whenever possible the team will discuss performance with the driver making and noting changes before another lap is performed
  - Similar data analysis techniques will be used, but with the goal of maximizing performance rather than validating the CFD simulations

- Coast down test-facilities dependent [5]
    - The vehicle will accelerate to a minimum of 60 mph before shifting to neutral and coasting until the vehicle comes to a complete stop, this declaration must be timed by the driver or a codriver
    - Optimally this will be done with the same setup in the opposite direction to account for wind and minor road grade
        - Grades above 0.02% must be measured and accounted for in calculations
    - This test will be performed with, at minimum, the no aero configuration and full downforce configuration
    - The data will be analyzed, and the different setups can be compared to calculate differences in aerodynamic drag

APPENDIX F – Roll Cage Calculations

Geometry

$L_{foot} := 45\ in$ $x_{main} := 0\ in$ $x_{front} := 24\ in$ $L_{roof} := x_{front} = 24\ in$

$L_{DB} := 45\ in$ $L_{hit} := 22\ in$ $a_{DB} := 22.5\ in$ $b_{DB} := 22.5\ in$

$L_{bay} := 24\ in$ $B_{bay} := 35\ in$

$D_{out} := 1.5\ in$ $t_{wall} := 0.120\ in$ $A := \frac{\pi}{4} \cdot \left((D_{out})^2 - (D_{out} - 2 \cdot t_{wall})^2 \right) = 0.52\ in^2$

$I := \frac{\pi}{64} \cdot \left((D_{out})^4 - (D_{out} - 2 \cdot t_{wall})^4 \right) = 0.125\ in^4$ $C := \frac{D_{out}}{2} = 0.75\ in$

Bending and axial Stresses for Roof

$W := 2000\ lbf$ $k_R := 2$ $P_R := k_R \cdot W = (4 \cdot 10^3)\ lbf$ $\alpha := 0.5$

$P_{main} := \frac{P_R}{2}$ $P_{front} := P_{main}$ $P_{roof} := P_{main}$ <-- Loads

$R_F := \frac{P_{front}}{2} \cdot \frac{x_{front}}{L_{foot}}$ $R_M := P_{main} - R_F$ $M_{roof} := P_{roof} \cdot \frac{L_{roof}}{4} = (1.2 \cdot 10^4)\ in \cdot lbf$

$\sigma_{aM} := \frac{R_M}{A}$ $\sigma_{aF} := \frac{R_F}{A}$ $\sigma_{broof} := \frac{M_{roof} \cdot C}{I} = (7.213 \cdot 10^4)\ psi$

$n_{roof} := \frac{1}{4} = 0.25$ <-- 4 members for the roof $\sigma_{roofAllow} := 75000\ psi$ <--- Yield

$\sigma_{totRoof} := \sigma_{aF} + \sigma_{aM} + \sigma_{broof}$

$FOS_{roof} := \frac{\sigma_{roofAllow}}{\sigma_{totRoof} \cdot n_{roof}} = 3.949$ <---- Close to FEA of 3

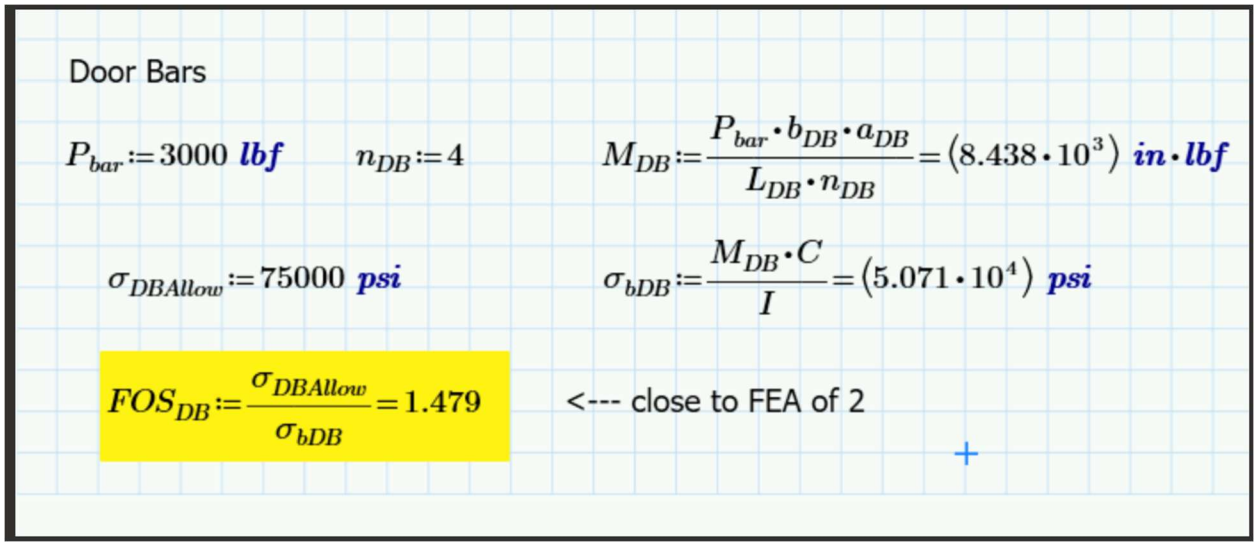

Figure F1: Splitter Bolt Shear and Tear out Calculations

References

[1] “Splitter Length and Side Fences,” Occam’s Racer, May 23, 2019. [Online]. Available: https://occamsracers.com/2019/05/23/splitter-design/

[2] Vvluvva, “2 Pack Waterproof Toggle Switch with line, 12V DC 15A/250VAC SPST 2 pin on/OFF MARINE TOGGLE switch with weatherproof boot cap cover metal and Bakelite construction for vehicles and boats: Automotive,” Amazon. [Online]. Available: https://www.amazon.com/Waterproof-Weatherproof-Bakelite-Construction-Vehicles/dp/B0FX556VKN. [Accessed: Feb. 3, 2026].

[3] Mishimoto, “Performance aluminum fan shroud kit, fits Mazda Miata 1990-1997,” Mishimoto. [Online]. Available: https://www.mishimoto.com/performance-aluminum-fan-shroud-kit-fits-mazda-miata-1990-1997.html. [Accessed: Feb. 3, 2026].

[4] rcscomponents, “JD1912 JD1914,” rcscomponents. [Online]. Available: https://www.rcscomponents.kiev.ua/datasheets/JD1912-JD1914.pdf. [Accessed: Feb. 3, 2026].

[5] C. O. Probst, Ford Fuel Injection & Electronic Engine Control: All Ford/Lincoln-Mercury Cars and Light Trucks 1988-1993. Cambridge, MA, USA: Bentley Publishers, 1993, ch. 4-5.

[6] Ford Motor Company, “EEC-IV Control Strategy: GuFB,” internal engineering documentation, Dearborn, MI, USA, 1989.

[7] Universal Technical Institute, “Ignition Timing & Performance,” student training reference guide, Avondale, AZ, USA, 2020.

[8] HP Tuners, “Ford EEC Parameters: Spark Retard for ACT,” VCM Editor support documentation. [Online]. Available: https://www.hptuners.com/help. [Accessed: Jan. 31, 2026].

[9] B. Bober, M. Andrych-Zalewska, and P. Boguś, “Influence of exhaust manifold modification on engine power,” Combustion Engines, vol. 196, no. 1, pp. 54-65, Jan. 2024, doi: 10.19206/CE-171389. [Online]. Available: https://www.researchgate.net/publication/373767136_Influence_of_exhaust_manifold_modification_on_engine_power.

[10] B. Bober, M. Andrych-Zalewska, and P. Boguś, “Influence of exhaust manifold modification on engine power,” Combustion Engines, vol. 196, no. 1, pp. 63-65, Jan. 2024, doi: 10.19206/CE-171389. [Online]. Available: https://www.researchgate.net/publication/373767136_Influence_of_exhaust_manifold_modification_on_engine_power.

[11] “Stainless steel exhaust manifold headers — Ford Mustang 5.0 V8 GT/LX/SVT (1979-1993),” vcarpart.com. [Online]. Available: https://vcarpart.com/products/stainless-steel-exhaust-manifold-headers-fit-mustang-5-0-v8-gt-lx-svt-1979-1993?variant=42609383833647. [Accessed: Jan. 29, 2026].

[12] “MatWeb - The Online Materials Information Resource,” MatWeb. [Online]. Available: https://www.matweb.com/search/DataSheet.aspx?MatGUID=10b74ebc27344380ab16b1b69f1cffbb&ckck=1.

[13] O. Use, “What is effectiveness-NTU method?,” How Engineering Works, Nov. 14, 2025. [Online]. Available: https://www.howengineeringworks.com/questions/what-is-effectiveness-ntu-method/. [Accessed: Feb. 3, 2026].

[14] T. L. Bergman, Fundamentals of Heat and Mass Transfer, WileyPLUS Blackboard Card. S.L.: John Wiley, 2019.

[15] RoyMech, “Gear Efficiency,” n.d. [Online]. Available: https://roymech.co.uk/Useful_Tables/Drive/Gears.html#efficiency. [Accessed: Feb. 3, 2026].

[16] H. Ozdes, M. Tiryakioglu, and P. D. Eason, “On estimating axial high cycle fatigue behavior by rotating beam fatigue testing: Application to A356 aluminum alloy castings,” Materials Science & Engineering A, vol. 697, pp. 95-100, 2017, doi: 10.1016/j.msea.2017.05.008.

[17] NPTEL, “Lecture 12: Helical Gears - Problems (Table 12.1 - Overload Factor K_o),” n.d. [Online]. Available: https://archive.nptel.ac.in/content/storage2/courses/112106137/pdf/2_12.pdf. [Accessed: Feb. 3, 2026].

[18] Practical Maintenance, “Fundamentals, selection, installation and maintenance of gearboxes - Part 1,” n.d. [Online]. Available: https://practicalmaintenance.net/wp-content/uploads/Fundamentals-Selection-Installation-and-Maintenance-of-Gearboxes-Gear-Drives-Part-1.pdf. [Accessed: Feb. 3, 2026].

[19] K. Newman, J. German, A. Bandivadekar, and M. D. Hall, “Benchmarking and modeling of a conventional mid-size car using ALPHA (2015-01-1140),” SAE Int., Apr. 14, 2015. [Online]. Available: https://www.epa.gov/sites/default/files/2016-10/documents/2015-01-1140_0.pdf. [Accessed: Feb. 3, 2026].

[20] E. C. Klaubert, “Highway effects on vehicle performance (Appendix B - Road Load/Driveshaft Torque and CT Engine-Braking Method),” Federal Highway Administration, Rep. FHWA-RD-00-164, Jan. 2001. [Online]. Available: https://www.fhwa.dot.gov/publications/research/infrastructure/structures/00164/pdf/appb-end.pdf. [Accessed: Feb. 3, 2026].

[21] C. O. Probst, Ford Fuel Injection & Electronic Engine Control: All Ford/Lincoln-Mercury Cars and Light Trucks 1988-1993. Cambridge, MA, USA: Bentley Publishers, 1993.

[22] “Trailer Width?,” MazdaRacers. [Online]. Available: https://mazdaracers.com/topic/4252-trailer-width/. [Accessed: Nov. 28, 2025].

[23] “Miata Engine Weight,” LocostUSA.com, Sep. 13, 2011. [Online]. Available: https://www.locostusa.com/forums/viewtopic.php?t=12804. [Accessed: Nov. 28, 2025].

[24] “Ford 302 - 5.0 Crate engine weight,” MG Engine Swaps Forum: The MG Experience, 2024. [Online]. Available: https://www.mgexp.com/forum/mg-engine-swaps-forum.40/ford-302-5-0-crate-engine-weight.1890280/. [Accessed: Nov. 28, 2025].

[25] L. Turner, You & Your Mazda MX-5/Miata. Haynes Publications, 2002.

[26] “Resources,” Aerodynamics for Students. [Online]. Available: https://www.aerodynamics4students.com/subsonic-aerofoil-and-wing-theory/flat-plate-lift.php.

[27] “What is the performance of a flat plate wing?,” Aviation Stack Exchange. [Online]. Available: https://aviation.stackexchange.com/questions/21391/what-is-the-performance-of-a-flat-plate-wing.